Estimation And Detection Theory in Visible Light Communication Systems: A Perspective on Realistic Receivers

by

Maysa Yaseen

Supervisor

Professor: Salama Ikki

Submitted to the Lakehead University
In fulfillment of the requirements for the degree of
Doctor of Philosophy
in
Electrical and Computer Engineering

May 24, 2024

Declaration of Authorship

I, Maysa Yaseen, declare that the dissertation, which I hereby submit for the degree of Doctor of Philosophy at Lakehead University, is my own work and has not previously been submitted by me for a degree at this or any other tertiary institution. This is a true copy of the thesis, including any required final revisions, as accepted by my examiners.

I understand that my thesis may be made electronically available to the public.

Abstract

VISIBLE light communications (VLC) has been proposed as a promising way for next-generation wireless communication networks to mitigate the scarcity of the radio frequency (RF) spectrum, and has consequently attracted much attention. Accordingly, this thesis investigates single-input single-output (SISO) VLC when subject to signal-dependent shot noise (SDSN). Firstly, we consider the case of fixed-location user located in an indoor environment. For instance, in a classroom setting, a teacher may utilize VLC to transmit lecture notes and supplementary materials to students' tablets or laptops, ensuring a seamless exchange of information without the need for traditional wireless networks. The topics of discussion include channel estimation and data transmission, where in the former, we introduce both least square (LS) and maximum likelihood (ML) estimators. The Cramér–Rao lower bound (CRLB) of the channel estimation error is also derived. In terms of data transmission, we propose optimal and sub-optimal receiver designs and present their bit error rate (BER) performances. In specific, we derive a closed-form expression of the BER for the sub-optimal receiver and an approximated version for the optimal one. Our analysis indicates that the performance of the CRLB demonstrates no linear relationship with the SDSN, thermal noise, or fading channel gain. On the other hand, SDSN has quite a severe effect on the channel estimation error bound, and as such, it can dramatically degrade the BER performance. Heightened performance degradation can also be explained by the joint effects of the channel estimation error and SDSN.

Secondly, we consider the case of random location of the user located in an indoor environment, such as a conference room within a corporate office where the user may move around freely during a meeting or presentation. In particular, the second part of this research estimates the channel of the considered system using ML, LS, linear minimum mean square error (LMMSE), maximum posteriori probability (MAP) and minimum

mean square error (MMSE) estimators. Furthermore, a Bayesian Cramér-Rao lower bound (BCRLB) is derived for the proposed system and it is compared to the mean square error (MSE) of the proposed estimators. The problem of the unknown SDSN factor at the receiver side is discussed and two solutions are investigated. The receiver of a VLC system under SDSN and random channel gain is designed and its BER is studied. Monte Carlo simulation results of the proposed estimators, which show the dramatic effect of the SDSN on the considered system, are provided. In particular, the presence of noise variance, as well as the SDSN factor, causes an increase in the MSE of the system, while increasing the power reinforces the system performance.

Moreover, the third part of this research explores the interplay between SDSN and another inherent noise in the light source called relative intensity noise (RIN), revealing their combined adverse effect on channel estimation accuracy in a VLC system. Towards this direction, we first derive CRLB in the presence of the SDSN and the RIN, which gives a lower estimate for the variance of an unbiased estimator. Then, we present the derivation of LS and ML channel estimators. Furthermore, we present the optimal receiver in ML sense and compare it with a simple threshold detector as a sub-optimal solution, quantifying the impact of channel estimation accuracy on both receivers. The findings presented in this part reveal that the RIN and the SDSN jointly have a significant adverse effect on the VLC channel estimation, consequently leading to a pronounced degradation in BER performance of the VLC system. In addition, we proposed optimal and sub-optimal receiver designs and present their BER. The Monte Carlo simulation results of the BER for the two presented receivers show that the optimal receiver performance excels beyond the performance of the sub-optimal receiver.

In other words, our study focuses on investigating the effects of signal-dependent noise in VLC systems. Initially, we explored how SDSN impacts VLC systems serving fixed-location

users. Subsequently, we delved into the influence of SDSN in scenarios where channel gain variability arises from the randomness of user locations. Following, we analyzed the combined impact of SDSN and RIN on the performance of VLC systems catering to fixed-location users in indoor environments. Our investigation involved the use of various channel estimation techniques, which were compared against a derived lower bound to evaluate their performance. Additionally, we designed different receivers to demonstrate how such noise affects the BER of the considered VLC systems.

Table of Contents

List of Figures

Chapter 1

Introduction

1.1 Background and Motivations

Optical communication, among the earliest forms of communication, was historically employed by utilizing fire and the reflection of sunlight. Visible light communication (VLC) is a type of wireless optical communication based on light-emitting diode (LED)/laser diode (LD) for data transmission. This technology has experienced significant growth in recent years, capturing widespread attention from researchers.

The surge in broadband services has escalated the need for communication technologies that offer both high performance and high capacity. However, radio frequency (RF) spectrum resources are limited and costly, and it is highly crowded [2]. Motivated by the revolution in solid lighting manufacturing, academic and industrial researchers have suggested VLC as an alternative to RF communication to address these limitations. Compared to RF, VLC has many advantages, including open licensing, wide spectrum, and resistance to radio interference, while being robust and providing efficient communication at short distances [3].

Channel estimation is a crucial task to ensure the robustness, error-free operation, and reliability of the VLC system. Over time, various channel estimation schemes have

been devised for RF-based wireless communication systems. However, there are notable distinctions between RF and VLC channels. VLC channel is effectively more intense due to the line-of-sight (LoS) and non-line-of-sight (NLoS) optical multipath reflections coming from the walls and ceilings that compose an indoor environment. Moreover, the position, shape, and size of the opaque physical obstacles have a severe effect on the characteristics of the VLC channel [4].

It is important to mention that VLC channels have some properties that set them apart from RF. The VLC transmitted signal should be nonnegative and have a real value since light is used for data modulation (and it is well known that a light signal cannot be negative or have a complex value). To achieve accurate channel estimation, it's crucial to consider the noise added to the signal during the transmission process. Many works have considered the constraints of the VLC channel gain [5]. However, only a few studied the effect of the SDSN in the VLC system. Taking these into careful consideration, the statistical nature of the VLC channel was modeled in [6] using a monotonic decreasing distribution with additive noise corrupting the channel. Notwithstanding that, none of the aforementioned channel estimation studies considered this statistical channel model for a VLC system since it poses major challenges to the provision of reliable data transmission. Up until now, the channel model in [6] was considered only in [7], where the performance of an indoor single-input single-output (SISO) VLC system was evaluated with imperfect channel state information (CSI) at the receiver.

On the other hand, the existence of signal-dependent noise is also a key physical characteristic that differentiates VLC from RF for certain receiving devices [8]. Typically, signal-dependent distortions are observed in high signal-to-noise ratio (SNR) VLC links that employ high-gain narrow field-of-view photon avalanche diode (APD) receivers [9]. The photodetector shot noise, which, considering the increasing number of received photons, can be approximated using a Gaussian process, is also signal dependent due to the quantum nature of the received optical energy [10, 11].

It is widely known that the optimal version of many designs no longer supports signal-dependent shot noise (SDSN), leading to a dramatic deterioration in the system performance along with increased background noises [11, 12]. Thus, the necessity of re-investigating the design structures when SDSN plays a non-negligible role is highlighted in [12], where effective modulation design techniques were proposed for both single and multi-carrier VLC systems. Meanwhile, the mutual information and its lower bound were analyzed for spatial modulation-based VLC in the presence of input-dependent noise in [13]. Following these, efficient transceiver design methods were studied in [14]. The theoretical expression of the BER was obtained in [15], and channel capacity bounds were derived in [8] for VLC systems with signal-dependent Gaussian noise. However, SDSN leads to analytical complications when it comes to deriving closed-form expressions, adding to the already existing challenges to signal processing and modulation design. Therefore, SDSN models have not been sufficiently studied in the VLC field yet.

The lack of studies on VLC systems under the joint impacts of SDSN and imperfect CSI motivates our work. This study fills in the gap by analytically evaluating the error performance of an indoor VLC system with a single light source at the transmitter side and a single photo-diode at the receiver side. We consider the monotonic decreasing distribution model for the channel gain as given in [6]. Specifically, an optimal receiver is proposed and compared to a sub-optimal one. Furthermore, we estimate VLC channel gains using different methods and compare their performance to a derived benchmark. In particular, we first consider that the location of the user is fixed, and then we study the case of random user location.

Another essential source of signal-dependent noise in optical communication systems is relative intensity noise (RIN). RIN represents the undesired fluctuations in the power of an optical signal relative to its average power. The presence of RIN can significantly impact the quality of the transmitted signal, consequently affecting the overall performance of the communication link [16].

Numerous researchers have delved into the study of RIN, exploring its origins, measurement techniques, and its impact on various optical communication systems. Specifically, in [17], researchers numerically investigated the RIN of quantum dot lasers through a rate equation, considering both spontaneous emission and carrier contributions. The study reveals that carrier noise originating from the ground and excited states significantly amplifies the RIN of the laser. While in [18], the RIN of the comb lines from a quantum-dot comb source lasers have been characterized using complementary time- and frequency-domain measurements. The time-domain results yield the average RIN over the 6 GHz measurement bandwidth, correlation time, and power spectral density. The frequency-domain results yield the RIN spectra and integrated RIN.

The effect of an asymmetric design of an external cavity semiconductor laser sensor on the sensor RIN was studied in [19]. While in [20], through numerical simulations, researchers studied the effect of RIN on the performance of low-complexity heterodyne optical coherent receivers. Furthermore, the numerical and simulation methods were used to demonstrate the impact of RIN for hybrid-cavity semiconductor lasers in [21].

Notably, the literature does not explore the impact of RIN in the presence of SDSN in VLC systems. This research gap motivated us to introduce RIN to the noises in the VLC system under consideration in this work. The joint effect of SDSN and RIN on VLC system estimation is a focal point of this thesis.

1.2 Thesis Contributions

Compared to the existing literature and motivated by the significance of the previous reasons, the contribution of this work can be summarized as follows:

1. In the first phase of this study, the performance of the SISO-VLC system is examined under the condition of a fixed user location in the presence of SDSN. The study reveals

that SDSN can degrade the Bit Error Rate (BER) performance and has a significant impact on the channel estimation error bound.

2. The Cramér–Rao lower bound (CRLB) can be used as a benchmark to evaluate the unbiased estimators' efficiency when the system under the effects of SDSN is derived. Both of the least square (LS) and maximum likelihood (ML) estimators are proposed, and their performance is compared with the derived CRLB.

3. An optimal receiver design that can properly treat the SDSN is proposed, and its performance is compared with the traditional ML one. More specifically, we derive a closed-form expression of the sub-optimal receiver BER and an approximated expression of the BER for the optimal one.

4. Additionally, the effect of imperfect CSI on the system performance is studied. In particular, the error performance in the presence of imperfect CSI has been obtained and analyzed.

5. In the second phase, we consider the case of random user location, investigating the impact of SDSN on a SISO-VLC system in the presence of a random channel.

6. We derive a Bayesian CRLB (BCRLB) for the considered random VLC channel with SDSN. Moreover, Four different estimators, namely LS, ML, maximum posterior probability (MAP), minimum mean square error (MMSE) and linear MMSE (LMMSE) are used to estimate the random VLC channel. Their mean square error (MSE) is then compared with the derived BCRLB to evaluate their performance.

7. Two different techniques are proposed to solve the problem of an unknown SDSN factor (ζ^2) at the receiver. Both of the techniques are applied to estimate the channel gain h using an LMMSE estimator. The MSE of the estimation procedure with unknown ζ^2 is compared to that of the known ζ^2 case.

8. In the third phase of this study, we investigate the joint effect of RIN and SDSN, along with the presence of thermal noise on the performance of an indoor VLC system. In our analysis, we take into account that RIN is proportional to the transmitted power and the channel gain, while SDSN is proportional to the square root of both.

9. To quantify the ultimate performance limits, we derive the Fisher information for the proposed system model, leading to the computation of the CRLB. We utilize the CRLB to compare and evaluate the performance of the derived LS and ML estimators.

10. We derive a closed-form expression for the MSE of the LS estimator in the presence of the joint RIN and SDSN effect and verify it through simulation results. In addition, we propose an optimum receiver considering the joint effects of RIN, SDSN and shot noise as well as a sub-optimal receiver neglecting RIN and SDSN.

11. We present simulation results to demonstrate the significant degradation of system performance due to the presence of RIN. In addition, the effects of SDSN and thermal noise are studied.

1.3 Thesis Organization

The rest of the report is organized as follows: Chapter 2 introduces the necessary theoretical concepts and key points of this thesis. Specifically, this chapter provides a background on the VLC system, along with the channel estimation, fisher information, and the CRLB.

The following is Chapter 3, which presents the proposed channel and VLC system for a fixed user location with SDSN. It includes the derivations of two estimators, the CRLB of the system, and two receiver designs. Additionally, this chapter introduces the simulation results for this part of the work and provides discussions on them.

Next is Chapter 4, where we address the randomness stemming from user mobility. Consequently, we introduce and discuss five channel estimators for a SISO VLC system in the presence of SDSN with a random user location. Additionally, we derive the benchmark BCRLB. We delve into a special case where the SDSN factor is unknown, presenting and comparing two different solutions. Furthermore, we propose optimal and sub-optimal receiver designs. The chapter presents and discusses simulation results for the estimators, BCRLB and BER of the receivers.

Afterward, in Chapter 5, we explore the impact of RIN jointly with SDSN. A detailed discussion of numerous cases is presented to illustrate the severe degradation of SISO-VLC system performance. To analyze the effect of RIN and SDSN on the proposed system, we derive the MSE for both the simplest and most commonly used estimators, considering the presence of both noises alongside the well-known thermal noise. Additionally, we utilize the CRLB derived in this chapter to assess the performance of the estimators. The receiver design is modified to accommodate the joint presence of the three types of noises under consideration, leading to a redesign of the receivers. The chapter concludes with the introduction of simulation results and discussions on these results, ultimately ending with conclusions.

In the concluding Chapter 6, we consolidate the core elements of our research, providing a comprehensive summary of the crucial results and conclusions derived from our study. Beyond this retrospective analysis, we pivot our attention toward the future, presenting opportunities for continued exploration and research. By delineating potential directions and highlighting areas deserving sustained attention, we adopt a holistic approach.

1.4 List of Publications

1. M. Yaseen, M. Alsmadi, A. E. Canbilen and S. S. Ikki, "Visible Light Communication With Input-Dependent Noise: Channel Estimation, Optimal Receiver Design and

Performance Analysis," *IEEE Journal of Lightwave Technology*, vol. 39, no. 23, pp. 7406-7416, Dec.1, 2021.

2. M. Yaseen, A. E. Canbilen and S. Ikki, "Channel Estimation in Visible Light Communication Systems: The Effect of Input Signal-Dependent Noise," *IEEE Transactions on Vehicular Technology*, vol. 72, no. 11, pp. 14330-14340, Nov. 2023.

3. M. Yaseen, A. E. Canbilen and S. Ikki, "Estimation of Random Channel Gain for SISO Visible Light Communications System," *IEEE Canadian Journal of Electrical and Computer Engineering*, vol. 46, no. 4, pp. 262-269, Fall 2023.

4. M. Yaseen, M. Elamassie, S. Ikki, M. Uysal, "Signal-Dependent Shot and Relative Intensity Noise in Channel Estimation of Laser Diode-based Indoor VLC Systems" , (2nd round, Revision) *IEEE Transactions on Communications*.

Chapter 2

Preliminaries and Literature Review

THIS chapter gives a general idea about the VLC system. In addition to that, the fundamentals of fisher information and CRLB are explained. The literature review is provided in the last subsection of this chapter.

2.1 Introduction to VLC

The concept of using light for communication dates back to the 19^{th} century, during a period when Alexander Graham Bell did the first wireless transmission by inventing the photophone that modulated sunlight over several hundred meters and succeeded in transmitting speech. However, these early attempts were limited by the available technology and the lack of efficient light sources. The concept of using visible light for communication gained momentum in the early 21^{st} century as advancements in LED technology made it more practical. Researchers started exploring the potential of VLC for high-speed data transmission [22].

The development in transmission technology, VLC-based transmission systems capitalize on their advantages by employing components that are both cost-effective and high-performing. This positions VLC as an increasingly competitive technology when compared

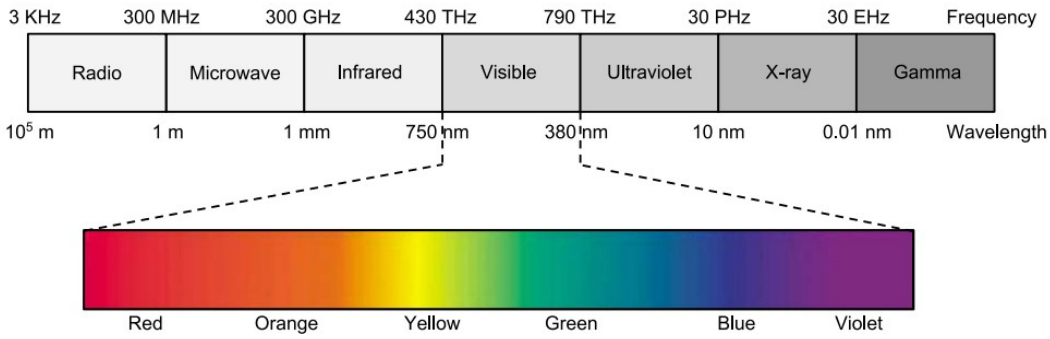

Figure 2.1: Visible light communication EM spectrum

to RF-based wireless communications. Furthermore, the widespread adoption of visible light communication in recent times can be attributed to its numerous advantages, which encompass, among other aspects, the following elements:

- **Wide spectrum:** The RF spectrum is constrained within the range of 3 kHz to 300 GHz and with the escalating demand for high-speed wireless services, there is a significant increase in congestion within the RF spectrum. On the other hand, VLC offers is at least 1000 times greater, which is from 400 THz to 780 THz as shown in Fig. 2.1 [23]. Therefore, it offers a huge, wide, unlicensed and unregulated bandwidth within the range of several THz, which solves the problem of RF spectrum crunch and allows for high data rates up to a few tens of Gbps.

- **No electromagnetic interference:** VLC is regarded as inherently immune to interference with RF signals since light does not cause interference with RF waves. Therefore, VLC is ideal to be used in RF interference-sensitive areas like hospitals, aircraft cabins, and petrochemical industries to only name a few.

- **High energy efficiency:** VLC operates using the light sources which are already present in for illumination purposes. By leveraging existing lighting infrastructure for communication, VLC eliminates the need for separate energy-consuming transmitters, reducing overall power consumption. Also, LEDs used in VLC represent the

forefront of lighting technology, offering an impressive 80% reduction in energy consumption compared to traditional lighting sources. It's noteworthy that if LEDs were to replace all conventional light sources currently in use, there could be a significant 50%reduction in global electricity consumption [24].

- **Cost-effectiveness:** Unlike other wireless communication technologies, the implementation cost of VLC is significantly lower. Only a few additional modules are added to the lighting compared to the substantial installation setup cost of an entire communication system, as seen in RF-based wireless communication. In addition, the swift progress in the light sources industry contributes to a reduction in the cost of producing VLC transceivers on a large scale.

- **Health safety:** In contrast to various other wireless communication technologies, VLC is inherently considered safe for human health. Unlike RF communications, VLC does not generate radiation, and it uses diffusive light source, distinguishing it from other optical communication technologies which use a concentrated optical power within a narrow beam. Furthermore, VLC adheres to eye and skin safety regulations.

2.2 VLC System Architecture

In this subsection, the basic system model of VLC with detailed VLC transmitter and receiver block diagrams are illustrated [25,26]. Although the VLC transmitter and receiver are physically separated, they are connected by a VLC channel. The VLC channel model is illustrated in detail in the next chapter.

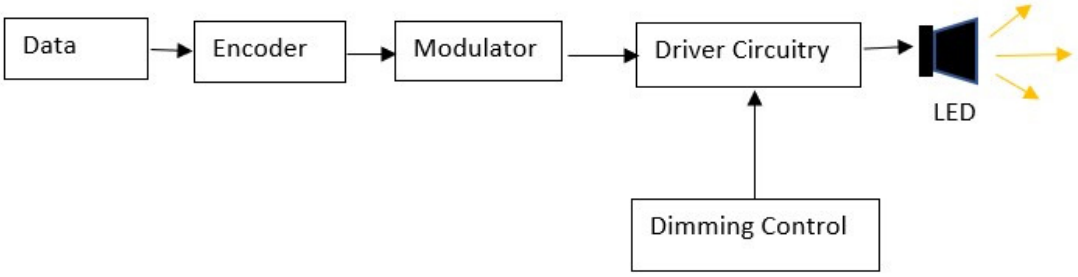

Figure 2.2: Visible light communication system transmitter

2.2.1 VLC Transmitter

As shown in Fig 2.2, the VLC transmitter compromises an encoder which transforms the data to digital form, and then this stream of data goes into the modulator. In the modulation process, the data is modulated using the intensity of the light signal which is referred to as intensity modulation (IM). Then, the modulated data and the dimming control signal are combined in the driver circuitry. The dimming control block provides the light source with a sufficient amount of current to adjust the brightness of the light source. As the brightness of the light source depends on the need of the application, for instant, in the case of public places, auditoriums, etc.., high levels of illumination are needed but in the case of offices and houses, etc.., low levels of illumination are required. Finally, this modulated data signal is fed to the light source to be transmitted.

Innovating the LEDs by the solid-state lighting (SSL) industry to replace conventional incandescent and fluorescent lamps is the main driver for VLC technology. LED has unique characteristics compared to other artificial light sources. Although LED provides high brightness, it consumes low power and has a high response besides the small size. White light is widely recognized as an accepted source of illumination, and it is commonly used for illumination in indoor and outdoor environments. Wherefore, SSL industry uses two methods to generate the white light from LEDs as shown in Fig 2.3. The first method

is using a yellowish phosphor layer to coat blue LED. In this approach, the white light is emitted by blue light generated by the LEDs which is absorbed by the phosphor layer. Consequently, the blue wavelength excites the phosphor causing it to glow white. The kind of LED manipulated by this approach is called white phosphorescent LED (WPLED). The second method is called (RGB) LEDs, it produces white light by combining three different coloureds of LEDs. Red, green and blue lights are mixed in the approach to generate the white light.

Although WPLED is preferred over RGB LED in VLC due to the lower complexity and cost because it needs only one LED, the slow response of phosphor limits the modulation bandwidth of the WPLED to a few MHz. However, some techniques can be employed to achieve high data rate‘ [27]:

- Using a blue filter at the receiver side to filter out the slow-response yellowish components.
- Using pre-equalizer at the LED driving module at the transmitter side.
- Using post-equalizer at the receiver side.
- A big raising in the data rate can be obtained by merging the three former mentioned methods.
- Implementation of more complex modulation techniques such as discrete multi-tone modulation.

2.2.2 VLC Receiver

From the block diagram of the VLC receiver shown in Fig 2.4, it can be figured out that at the receiving side of a VLC system, the received light signal is concentrated by passing through an optical concentrator. Then, the unwanted signal components generated

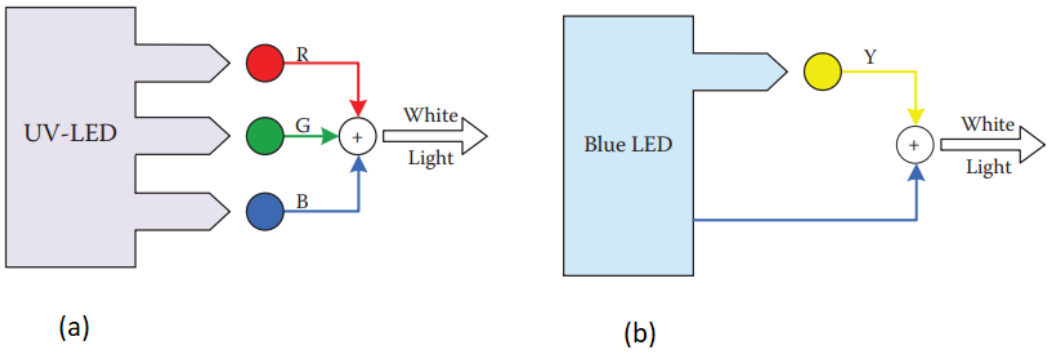

Figure 2.3: Two methods of generating white light from LEDs, (a) WPLED approach, (b) RGB LED approach.

because of reflections and refractions are filtered out using the optical filter. After the filtering process, the desired signal is passed to the photo-diode and then it is fed to a trans-impedance amplifier to convert the signal from current to voltage signal and amplify it. The first two steps at the transmitter are reversed at the receiver. Particularly, the data is demodulated and then decoded to get the original data stream.

In the VLC system, the optical can be received using a photo-diode or image/camera sensor [26, 27]. Compared to the image/camera sensor, the photo-diode provides a higher data rate and it uses simpler digital signal processing techniques for decoding the data. On the other side, the photo-diode cannot isolate the background noise, which means it is processed with the received signal, therefore, the receiver uses the photo-diode and has to employ an optical filter before the photo-diode. Additionally, field of view (FOV) is a challenging aspect in the photo-diode, because the transmitted signal should be within the FOV and it should be narrow to avoid noise. Oppositely, the image/camera sensor improved the range of the FOV to wider. This makes the image/camera sensor more suitable for long-distance mobility.

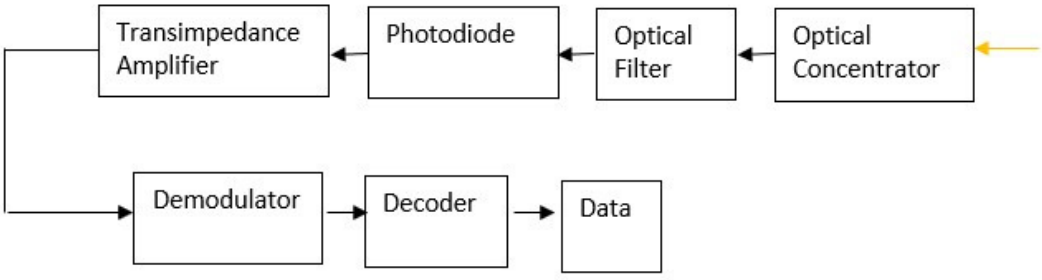

Figure 2.4: Visible light communication system receiver

2.3 Noise in VLC System

As in all communication systems, noise is a decisive factor in determining the system performance because the noise could dramatically decrease the performance of the VLC networks. The existing noise in the VLC system can be categorized into two main categories listed below [27]:

- *Independent noise:* It includes many sources such as the background noise induced by the sunlight and other artificial light sources, dark current noise caused by the passing current through the photo-diode with no optical radiation exposure and thermal noise. Thermal noise which is also known as the Johnson noise is the dominant signal-independent noise source and it is generated due to the temperature of the material of the photo-diode at the receiver side. This kind of noise doesn't depend on the input signal and it can be modelled as being additive white Gaussian noise (AWGN) which can be mathematically represented as $n \sim \mathcal{N}(0, \sigma_n^2)$, where σ_n^2 is the variance of the noise.

- *Dependent noise:* This type of noise varies with the signal being measured. In other words, the amount of noise present in a signal is dependent on the strength or level of the signal itself. Signal-dependent noise can be particularly problematic in data

acquisition and signal processing applications, as it can distort or mask important features of the signal. There are two main sources of signal-dependant noise, which are the SDSN and the RIN. In LEDs, SDSN is the dominant dependent noise, while in LDs, the RIN has a significant effect. In particular, low frequency intensity fluctuations in LEDs are much smaller than those in LDs. Therefore RIN can be neglected in LEDs. Given the importance of SDSN to our research, we extensively discuss it in the next subsection.

2.4 Signal-Dependent Shot Noise

Today, shot noise remains an important topic of research in both theoretical and experimental physics. It is used to study a wide range of physical phenomena, from the behaviour of semiconductors and quantum computers to the transmission of information in communication systems. Understanding the origin and properties of shot noise is essential for advancing our understanding of the fundamental principles that govern the behaviour of matter and energy in the universe.

2.4.1 Background and Origin

Signal-dependant shot noise, also known as Poisson noise is a type of random fluctuation or noise that arises in electrical circuits due to the discrete nature of charged particles. This phenomenon was first observed in the early 20th century, and it has since become an important topic in both theoretical and experimental physics.

The concept of shot noise was first introduced in 1918 by Walter Schottky, a German physicist who was studying the behaviour of electrons in vacuum tubes. At the time, vacuum tubes were used as amplifiers and switching devices in electronic circuits, and Schottky was interested in understanding the nature of the current flowing through them [28].

Schottky observed that the current in a vacuum tube was not constant, but instead exhibited random fluctuations that could not be explained using classical physics. Schottky theorized that these fluctuations were due to the discrete nature of electrons, which could only flow in discrete packets or "shots" of charge. Schottky's theory of shot noise was later confirmed by other physicists, including John B. Johnson and Harry Nyquist, who observed similar fluctuations in other electronic devices. In the 1920s and 1930s, shot noise became an important topic of research in the field of electronics, as engineers and physicists worked to develop more reliable and efficient electronic devices.

In the decades that followed, the study of shot noise expanded to other fields, such as solid-state physics, quantum mechanics, and information theory. Today, shot noise is used as a tool for understanding a wide range of physical phenomena, including the behaviour of semiconductors, the operation of quantum computers, and the transmission of information in communication systems. One of the most important applications of shot noise is in the field of quantum mechanics, where it plays a crucial role in the study of single-particle behaviour. By observing the fluctuations of individual particles, physicists can gain insights into the quantum nature of matter and the fundamental principles that govern the behaviour of the universe.

The magnitude of shot noise is proportional to the square root of the current, which means that the noise becomes more pronounced at higher currents. This is because the flow of electrons becomes more random and unpredictable as the number of particles in the current increases. Shot noise is not limited to electronic devices but can also arise in other physical systems where the flow of particles is discrete. For example, the movement of grains of sand or the emission of photons from a light source can also exhibit shot noise [29].

2.4.2 Theory

Shot noise arises in electronic devices due to the random nature of the behaviour of individual electrons in a current flow. The reason shot noise is described as a Poisson process is that it is caused by the random arrival of electrons, which can be modelled using a Poisson distribution. A useful analogy for understanding the discrete nature of shot noise can be visualized by imagining an hourglass lying on its side, with sand in the upper bulb. If the hourglass is then lifted slightly towards an upright position, the sand will start falling through the neck of the hourglass one grain at a time. However, the grains of sand will not arrive in the lower bulb at uniform intervals; rather, each grain will have a different inter-arrival time, resulting in great variation. This variability in the arrival time of each grain of sand is an example of shot noise in electronic devices.

The Poisson distribution is used to describe the probability of a specific number of events occurring in a given time interval, with the probability of a single event being constant and independent of the arrival of previous events. In the case of shot noise, the Poisson distribution is used to calculate the probability of a specific number of particles arriving at a given time. Another reason that shot noise can be modelled as a Poisson process is that each charge carrier's arrival is independent and random, with a constant average rate over time. The Poisson process describes this randomness in the arrival of charge carriers and the variability in the inter-arrival time between particles.

Considering that number of photons N measured by a given sensor element over a time interval t, the discrete probability distribution function (PDF) of the charge carrier counting is given as [30]

$$\Pr(N = k) = \frac{(\lambda t)^k e^{-\lambda t}}{k!}, \tag{2.1}$$

where, λ is the expected number of charge carriers per unit time interval, which is proportional to the received light signal. The other parameter λt represents the rate parameter of the Poisson pdf which corresponds to the expected incident charge carriers count. Following that the charge carrier count is a Poisson distributed, and the mean and the variance

are equal. i.e., $E[N] = Var[N] = \lambda t$. This demonstrates that SDSN is a signal-dependent noise. Moreover, the root mean square value of the shot noise current is given by [31]

$$I_{sh} = \sqrt{2qIf}, \tag{2.2}$$

where q is the charge in Coulombs, I represents the current in amperes, and f is the noise bandwidth in hertz. Again, here we can observe that the shot noise current is proportional to the square root of the signal.

A Poisson process is a random process that models the occurrence of discrete events over time, where the events occur independently of each other and at a constant rate. In contrast, a Gaussian process is a random process that models continuous functions, where any finite set of function values is jointly Gaussian distributed. At high numbers of events, the Poisson process can be approximated by a Gaussian process due to the central limit theorem, which states that the sum of a large number of independent and identically distributed random variables tends to follow a normal distribution [28].

In a Poisson process, the number of events that occur in a given time interval follows a Poisson distribution, which has a mean and variance that are equal. As the number of events increases, the variance also increases proportionally. However, when the number of events is large, the Poisson distribution can be approximated by a normal distribution with the same mean and variance. This approximation is known as the Poisson limit theorem. Therefore, at high numbers of events, the Poisson process can be modelled as a Gaussian process, where the mean and variance of the process can be estimated from the observed data. This approximation allows us to apply techniques from Gaussian process modelling, such as regression and classification, to Poisson processes. However, it is important to note that this approximation is only valid when the number of events is sufficiently large. In VLC, the signal has high intensity, which makes the approximation valid. Consequently, the SDSN can be represented as SDSN $\sim \mathcal{N}(0, \sigma^2_{sdsn})$, where $\sigma^2_{sdsn} = \zeta^2\sigma^2$, $\zeta^2 = \frac{\sigma^2_{ds}}{\sigma^2_n}$ represents the shot noise scaling factor, and σ^2 is the variance of the independent noise.

2.4.3 Signal-Dependent Shot Noise in VLC system

Shot noise can have a significant effect on the performance of VLC systems. Here are some of the effects of shot noise in VLC systems [27, 32]:

- Reduced SNR: Shot noise introduces random fluctuations in the received signal, which reduces the SNR of the signal. This can lead to errors in signal detection and degradation in the quality of the received signal.
- Limitations on detection sensitivity: Shot noise places a fundamental limit on the detection sensitivity of the receiver, as it sets a lower bound on the minimum detectable signal power.
- Interference from other sources: Shot noise from other sources in the system, such as the transmitter and the amplifier circuits, can add to the overall noise in the system and degrade the SNR further.
- Impact on modulation schemes: The effect of shot noise is more pronounced in digital modulation schemes, as the signal is binary and any errors in the signal detection can lead to significant bit errors.
- Optimization of system parameters: To minimize the effect of shot noise, the system parameters such as the receiver bandwidth, amplifier gain, and detection threshold need to be optimized.

Overall, SDSN can be a significant factor in the performance of any wireless communication system, particularly in low-power and high-frequency applications such as VLC applications. System designers need to carefully consider the impact of SDSN to ensure reliable and efficient communication.

2.5 Relative Intensity Noise

In communication systems, the degradation of signal strength due to the presence of noise signals is typically measured by the signal-to-noise ratio (SNR). It serves as a crucial indicator reflecting the transmission channel's quality and the minimum signal power detectable. RIN is one of the most important factors that causes degradation in SNR. Unlike the SDSN, RIN is proportional to the intensity, thereby limiting the SNR. In this section, the theory and the background of RIN are introduced.

2.5.1 Background and Origin

The predominant source of RIN is spontaneous emission [33,34]. Specifically, the intensity fluctuations come primarily from the spectral properties of a laser. When lasers operate beyond their lasing threshold (The definition of the lasing threshold is when the stimulated emission exceeds the spontaneous emission.), they predominantly produce stimulated emission along with a minor quantity of spontaneous emission. Spontaneous emission photons exhibit unpredictable characteristics, including wavelength, polarization, direction, and phase. These photons may coincide with the wavelength and direction of stimulated emission photons, causing fluctuations in the light source's output intensity and frequency.

In a photodetector the stimulated emission interacts with any residual spontaneous emission, effectively creating noise that can be observed electrically. Many photodetectors generate an output current that corresponds to the optical power, which is, in turn, proportional to the square of the electrical field.

Due to this nonlinear relationship between the strength of the optical field and the photodetector current, photons of varying optical frequencies generate "beat signals," akin to the processes observed in electrical nonlinear devices handling multiple signals at their input (such as the mixer in a radio) as shown in Fig 2.5, which represents an event where the two emissions interfere with each other. The level of beat noise produced in the

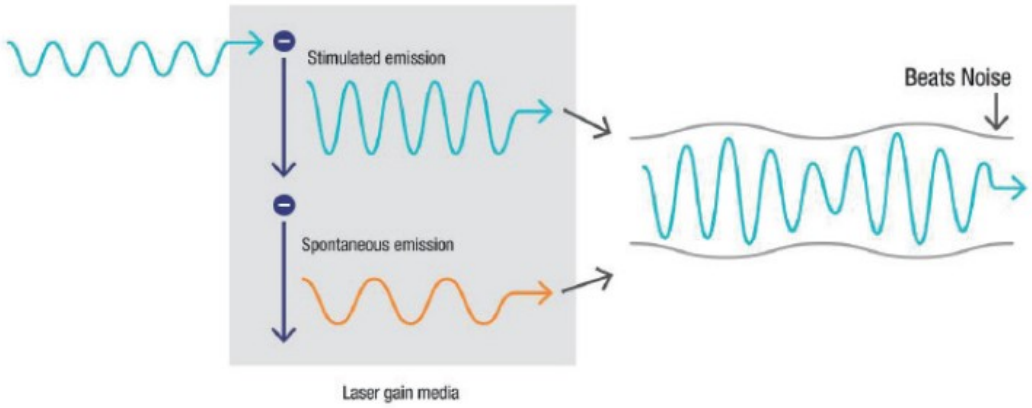

Figure 2.5: Laser intensity noise - an event where two emissions interfere with each other [1]

photodetector is contingent upon the properties of the receiver. Hence the RIN uses to describe the contributions of the laser intensity fluctuations to the electrical noise in the receiver relative to the signal power.

2.5.2 Theory

RIN refers to the fluctuations in the output intensity of a laser over time. It is expressed as a ratio relative to the average intensity and can be written as [35]

$$\frac{< \Delta P >^2}{< P_o >^2} \tag{2.3}$$

where $< \Delta P >^2$ and $< P_o >^2$ are the mean square intensity fluctuation spectral density of the light output and average light output optical power, respectively. In Fig 2.6, the left figure illustrates the ideal output intensity of a laser, biased at a d.c. level while all the parameters influencing the laser, such as temperature, are assumed to be constant. On the other hand, the right figure shows the real case, when the output intensity of the laser shows power fluctuation due to intensity noise.

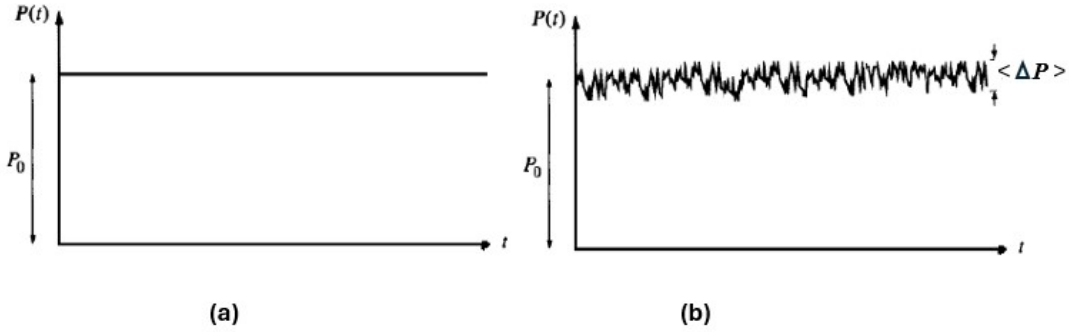

Figure 2.6: (a) is the ideal output power for a laser with DC bias, and (b) is the real laser output power having intensity noise.

2.6 Channel Estimation: Classical Approach

Channel estimation is crucial for the performance of any wireless communication system, i.e., accurate estimation is essential for follow-up equalization, demodulation, and decoding. Therefore, an accurate estimator leads to reliable communication systems [36]. CRLB, which can be used as a benchmark to evaluate the estimators' performance. The estimation approaches can be classified into the classical approach and the Bayesian approach. In this section, we will discuss the classical approach. Following that, we will delve into the Bayesian approach in the subsequent section.

The classical estimation approach, also known as frequentist estimation, is a statistical framework that focuses on estimating unknown parameters based on the analysis of observed data. In this approach, parameters are considered deterministic but unknown, and the goal is to use sample data to make inferences about these parameters.

The most common classical estimation method are LS and ML estimation methods. In addition, CRLB is a fundamental concept in classical statistics that establishes a theoretical limit on the variance of unbiased estimators for a parameter.

2.6.1 Fisher Information and Cramer Lower Bound

Suppose that θ is an unknown parameter that is to be estimated from N independent observations of x. Fisher information measures the amount of information that an observation x carries about an unknown parameter θ of a distribution that models x.

CRLB gives a lower bound for the variance of any unbiased estimators. Thus if an estimator is unbiased and has a variance equal to CRLB, it is then impossible to find an unbiased estimator that has a smaller variance.

To simplify the idea, suppose that we have only one point of pilot signal ($N = 1$) and the probability density function (pdf) of x is given as

$$f(x;\theta) = \frac{1}{\sqrt{2\pi\sigma^2}} \exp\left(-\frac{1}{2\sigma^2}(x-\theta)^2\right). \tag{2.4}$$

Assume that the regularity condition is satisfied, which means that the first moment of the partial derivative with respect to θ of the natural logarithm of the likelihood function evaluated at the true parameter value θ

$$\mathbf{E}\left\{\frac{\partial}{\partial\theta}\log f(\mathbf{x};\theta)\right\} = 0. \tag{2.5}$$

The fisher information is a way of measuring the amount of information about the unknown parameter θ that is carried by the random variable x. Mathematically, the fisher information is defined as

$$I(\theta) = \mathbf{E}\left\{\left(\frac{\partial}{\partial\theta}\ln f(x;\theta)\right)^2\right\}. \tag{2.6}$$

The CRLB is given in terms of the fisher information as

$$Var(\hat{\theta}) \geq \frac{1}{I(\theta)}, \tag{2.7}$$

where, $\hat{\theta}$ is the estimator of θ.

Therefore, the larger amount of information can be obtained from the observations, the lower CRLB.

2.6.2 Least Square Estimator

The method of least squares is about estimating parameters by minimizing the squared differences between the parameter value and the parameter estimated value. That means the LS estimator chooses the estimated value of the parameter that makes the estimated signal closest to the true value, which means it minimizes the squared error between the observed signal and its expected value. As we mentioned in the previous subsection, suppose that we have N independent observations of x. In addition to that, suppose we have a signal model

$$s[n] = \theta h[n], \tag{2.8}$$

where $n = 1, 2, \ldots N$. Thus, the square error can be measured by taking the sum of the difference between the real data points and the estimated values of them given as

$$\sum_{n=1}^{N} (x[n] - \theta h[n])^2, \tag{2.9}$$

where $h[n], \forall n = 1, 2, \ldots N$ are known. To find the LS error, the previous equation should be differentiated with respect to the unknown parameter θ and solved to get the estimated θ as

$$\hat{\theta} = \frac{\sum_{n=1}^{N} x[n]h[n]}{\sum_{n=1}^{N} h^2[n]}. \tag{2.10}$$

This method of estimation is characterized by being simple to be understood and applied. It's applicable in most cases. Indeed, LS estimation has a strong underlying theoretical foundation in statistics. Above all these advantages, it doesn't need any statistical information about the unknown parameter. The main disadvantage of the LS estimation method that is has the least accurate results especially when the data is not normally

distributed.

2.6.3 Maximum Likelihood Estimator

ML estimation is a method of estimating a parameter that maximizes a likelihood function, therefore, the point in the parameter space that maximizes the likelihood function is called the maximum likelihood estimate. Given that we have N points of data x depending on the unknown parameter θ. Since the logarithmic function is a monotonic function, the log-likelihood will have a maximum in exactly the same places where the likelihood has a maximum. Consequently, the estimated θ using the ML estimator can be found by maximizing the log-likelihood function as

$$\hat{\theta} = \underset{\theta}{\operatorname{argmin}} \log f(\boldsymbol{x}; \theta), \tag{2.11}$$

where $\boldsymbol{x}$ denotes the matrix of the N points of data. ML estimator has the advantage of simplicity and applicability. ML estimator characterize as an asymptotically efficient estimator. Therefore, it's asymptotically optimal. That means when the number of pilots $N \to \infty$, ML estimator is asymptotically unbiased and it attains the CRLB.

2.7 Channel Estimation: Bayesian Approach

The Bayesian estimation approach is a statistical framework that focuses on estimating unknown parameters by incorporating prior information about parameters and updates them based on observed data to obtain a posterior distribution. In this approach, parameters are considered random. The Bayesian approach, when applicable, can therefore improve the estimation accuracy. This is the Bayesian approach, so named because its implementation is based directly on Bayes' theorem.

The most common Bayesian estimation method are MAP, MMSE and LMSSE esti-

mation methods. Moreover BCRLB provides a bench mark to evaluate the MSE of the Bayesian estimators.

2.7.1 Bayesian Cramér–Rao Lower Bound

BCRLB is an extension of the CRLB that provides a lower bound on the variance of any unbiased estimator. The BCRLB takes into account the uncertainty in parameter estimation by incorporating the prior distribution of the parameters. BCRLB helps to assess the efficiency of Bayesian estimators by comparing their performance to the lower bound

The Bayesian information is given as [37]

$$J = \mathbf{E}\left\{I(\theta)\right\} + I_R, \tag{2.12}$$

where $I(\theta)$ denotes the Fisher information function and I_R represents the contribution of the prior information that can be calculated from

$$I_R = \mathbf{E}\left\{\left(\frac{\partial}{\partial h}\ln f_\theta(\theta)\right)^2\right\}. \tag{2.13}$$

Here, $\ln f_\theta(\theta)$ is the log-PDF of the random variable θ. Therefore, the BCRLB can be given as

$$Var_B(\hat{\theta}) \geq \frac{1}{J}, \tag{2.14}$$

where, $\mathrm{Var}_B(\hat{\theta})$ is the BCRLB of the random parameter θ, $\hat{\theta}$ is the estimator of θ.

2.7.2 Maximum Posteriori Probability Estimator

MAP estimator is a statistical technique employed for determining the most likely value of unknown parameter θ within a probabilistic model based on observed data. In particular,

it integrates prior information about the parameter with the likelihood function $f_\theta(\theta)$ of the observed data to identify the parameter value $f(\boldsymbol{x};\theta)$ that maximizes the posterior probability. Hence, the MAP estimator can be expressed as

$$\hat{\theta}_{\text{MAP}} = \arg\max_{\theta} f(\theta|\boldsymbol{x}) = \arg\max_{\theta} \ln f(\theta|\boldsymbol{x}), \tag{2.15}$$

where $f(\theta|\boldsymbol{x})$ denotes the posteriori function of the of the parameter θ given the data $\boldsymbol{x}$. From Bayes' rule, $f(\theta|\boldsymbol{x})$ can be written as

$$f(\theta|\boldsymbol{x}) = \frac{f(\boldsymbol{x}|\theta) f_\theta(\theta)}{f_{\boldsymbol{x}}(\boldsymbol{x})}, \tag{2.16}$$

where $f_\theta(\theta)$ is the prior pdf of the unknown parameter θ, which represents the prior information of the parameter. Furthermore, $f_{\boldsymbol{x}}(\boldsymbol{x})$ denotes the likelihood function of the data $\boldsymbol{x}$ given the parameter θ. While $f_x(x)$ is the pdf of the observed data x. Noting that $f_x(x)$ is constant with respect to parameter θ, the MAP estimator can be calculated by maximizing $f(\boldsymbol{x}|\theta) f_\theta(\theta)$ as follows:

$$\hat{\theta}_{\text{MAP}} = \arg\max_{\theta} f(\boldsymbol{x}|\theta) f_\theta(\theta) = \arg\max_{\theta} \ln f(\boldsymbol{x}|\theta) f_\theta(\theta). \tag{2.17}$$

2.7.3 Minimum Mean Square Error Estimator (MMSE)

The MMSE method is an estimation technique designed to reduce the anticipated value of the squared difference between the estimated parameter and the true parameter, commonly known as the estimation error. This characteristic positions it as a measure of the mean squared error in estimation. MMSE estimator can be given as

$$\hat{\theta}_{\text{MMSE}} = \arg\min_{\theta} \mathbf{E}[(\hat{\theta} - \theta)^2]. \tag{2.18}$$

In other words, the MMSE is considered the optimal estimator which minimizes the MSE of the estimation process, often referred to as the conditional mean estimator. This can be expressed as

$$\hat{\theta}_{\text{MMSE}} = \mathbf{E}\left\{\theta|\boldsymbol{x}\right\} = \int \theta f(\theta|\boldsymbol{x})\, d\theta, \tag{2.19}$$

where $f(\theta|\boldsymbol{x})$ is the posterior pdf, which can be represented according to Bayes's Rule as in (2.16).

It is worth mentioning that while the MMSE is considered as an optimal estimator, it requires complex calculations of the posterior pdf, and obtaining a closed form for the MMSE estimator may be challenging or, in some cases, not feasible.

2.7.4 Linear Minimum Mean Square Error Estimator (LMMSE)

LMMSE estimator is a special case of MMSE estimator that is designed to estimate an unknown parameter θ in a linear fashion. It is particularly applicable when the relationship between the observed data and the parameter is linear, such as

$$\hat{\theta} = \sum_{n=0}^{N-1} a_n xn + a_N, \tag{2.20}$$

where a_n and a_N are weights to be determined such that the MSE $\mathbf{E}[(\hat{\theta} - \theta)^2]$ of the estimator is minimized. Therefore, the LMMSE estimator can be given as

$$\hat{\theta} = \frac{\text{Cov}(\theta, \boldsymbol{x})}{\text{Var}(\theta)} + \mathbf{E}[\theta]. \tag{2.21}$$

One key advantage of the LMMSE estimator is it is not necessary to determine the posterior pdf of the unknown parameter θ. Unlike MMSE and MAP estimators, the LMMSE only depends on the first two moments of the parameter θ and the observed data $\boldsymbol{x}$. This

characteristic simplifies the computational requirements and offers a more straightforward implementation.

2.7.5 Final Note:

Classical estimation is commonly used for deterministic parameters, and Bayesian estimation is the preferred approach for random parameters due to the enhanced accuracy it provides. Nevertheless, classical estimation can be employed to estimate a random parameter when there is insufficient prior information available.

Chapter 3

Visible Light Communication with Input-Dependent Noise: Channel Estimation, Optimal Receiver Design and Performance Analysis

3.1 Introduction

Indoor illumination is currently undergoing a revolution due to the widespread deployment of LEDs. Unlike older illumination technologies, LEDs are capable of rapidly varying their light intensities. The change is actually too fast to be visible to the human eye, allowing data to be encoded in and transmitted through the emitted light. A photodetector (also known as a photodiode) or an image sensor (i.e. a matrix of photodiodes) can receive the modulated signals and decode the data. Therefore, LEDs can be utilized not only for illumination but also for communication. This functionality has given rise to VLC technology, where LEDs are used for high-speed data transfer ($\sim$100 Mbps in IEEE 802.15.7 standard and up to multiple Gbps in research) [38].

The use of light propagation for data transmission, whether in terrestrial or satellite applications, can be traced back decades ago. However, with the ever-increasing demand for high data rate wireless communication, VLC has recently regained considerable interest from both industry and academia [39]. VLC has many advantages, such as worldwide availability, high security and immunity to radio frequency (RF) interference [40].

Additionally, the visible light spectrum is unlicensed and still substantially unused for communication. Transitioning to this spectrum would allow for low-cost broadband communication while mitigating spectrum density in the RF. VLC systems have relatively simple and inexpensive front-end components for both transmitters and receivers that operate in the baseband. Furthermore, they do not require frequency mixers or complicated algorithms to correct hardware impairments such as phase noise and in-phase/quadrature-phase (I/Q) imbalance [41]. Without a doubt, VLC is a promising candidate for short-range wireless communication in the future technologies.

3.1.1 Related Works

The novel transmission paradigm of VLC is quite different from RF communication. The essential difference is that the transmitted signals in VLC must be real and positive. A reliable VLC system is also required to be flicker-free and satisfy specific lighting and power constraints [42]. Hence, the specifications of VLC requires re-engineering the designs across many layers, including physical layer (PHY) signal processing and modulations [43]. Considering this, advanced PHY techniques originally proposed for RF communication have been reconfigured for use in the context of VLC. For instance, the orthogonal frequency division multiplexing (OFDM) technique has been applied to VLC with certain adjustments [44–46].

Afterwards, advanced spatial modulation-based techniques were extended to VLC [47, 48]. Taking the power and lighting constraints into account, constellation designs were revised for multi-carrier VLC systems with the aim of maximizing the minimum distance

between two arbitrary constellation symbols [49, 50]. Even more, a framework was developed for LED-based VLC systems for the transmission power and rate optimization [51]. The performance of VLC systems, adopting hybrid modulation techniques, is also investigated under dynamic fading channels [52].

In comparison to RF-based wireless communications, there has been limited consideration of channel estimation for VLC. However, this is a key aspect to investigate when it comes to the synchronization, equalization and implementation of transceiver functions (e.g. precoding at the transmitter and data detection at the receiver). Although VLC channels have unique properties that attract a lot of attention during the study of channel estimation, the principles of traditional estimation technologies, such as the pilot-aided schemes, may also apply to VLC scenarios. Considering this, several techniques have been proposed to enhance the channel estimation performance of VLC systems as well as reduce their BER [53–59]. For instance, an evaluation of two channel estimation methods, the LS and MMSE algorithms, for indoor OFDM-based VLC systems was presented in [53].

Indeed, channel estimation schemes for OFDM-based VLC systems and their performance are extensively studied in the literature [55]. In addition, [57] proposes a novel neural network based methodology for the prediction of VLC channel parameters. The problem associated with finding a scheme that minimizes the noise variance under maximum and average power constraints was solved in [60]. Next, the BER performance of spatial multiplexing in a multiple-input multiple-output (MIMO) VLC system was evaluated in [61], where the channel matrix, estimated using constructed codes, was used in data detection.

Chapter Organization. The rest of the chapter is organized as follows: Section 3.2 describes the channel and system models. Next, Section 3.3 discusses the channel estimation and the Cramér–Rao lower bound. Then, Section 3.4 proposes the receiver designs and presents their performance. Section 3.5 discusses the numerical results and the chapter is concluded in section 3.6.

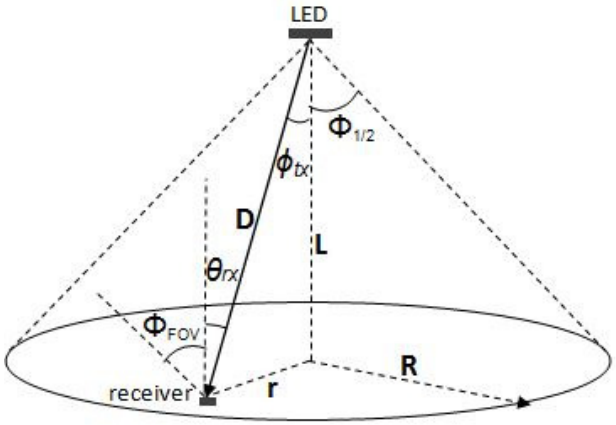

Figure 3.1: Visible light communication system model

3.2 System and Channel Models

We consider a SISO-VLC downlink transmission scenario, where an LED is mounted on the ceiling of a regular indoor environment to serve a user on the floor. The user is confined within a circular area[1] with radius R as shown in Fig. 3.1. The location of the user is assumed to be static, and a symbol-by-symbol detection is performed on the receiver side. However, an extension of this work to include a coded system would be straightforward.

Considering that thermal noise and SDSN affect the optical signal x sent from the LED, the received signal by the user can be written as

$$y = hx + \sqrt{hx}n_{\text{ds}} + n, \tag{3.1}$$

where $x = s+d$, s is the transmitted symbol and d is the bias level (DC value). $n \sim \mathcal{N}(0, \sigma_n^2)$ is the signal-independent thermal noise, where $\mathcal{N}(\mu, \sigma^2)$ represents a Gaussian distribution with mean μ and variance σ^2. The term $\sqrt{hx}n_{\text{ds}}$ is the SDSN term, where $n_{\text{ds}} \sim \mathcal{N}(0, \sigma_{ds}^2)$. We can define a new term $\zeta^2 = \frac{\sigma_{ds}^2}{\sigma_n^2}$ to represent the shot noise scaling factor. This is used to indicate the strength of the SDSN compared with the signal-independent thermal noise.

[1]We assume that all users remain inside the circle. This is a practical assumption widely made in the literature; however, it is key to note that outside this region, there is no coverage by the specified LED.

In this way, the shot noise can be represented by $n_{\text{ds}} \sim \mathcal{N}(0, \sigma_n^2 \zeta^2)$, and the term ζ^2, which can be determined by the receiver parameters, occupies practical values ranging from 1 to 10 [11, 62]. However, our analysis is valid for any value of ζ^2.

Generally, shot noise demonstrates Poisson distribution. However, it becomes congruent with Gaussian distribution at large numbers of received photons, and this is associated with the high-intensity nature of light in VLC systems [11, 48, 62–64].

The DC offset value d is added to guarantee that the VLC signal is always positive. Furthermore, h denotes the channel gain of the VLC LoS beam between the LED and the photodetector. Although there is no exact formula for calculating the channel gain h, the LoS component has been modeled in the literature depending on several factors, including the distance between the transmitter and receiver as [6, 27]

$$h = \frac{A_{pd}\eta(m+1)}{2\pi D^2} \cos^m(\phi_{tx}) T_s(\theta_{rx}) g(\theta_{rx}) \cos(\theta_{rx}), \tag{3.2}$$

where A_{pd} is the detection area of the photodetector. Here, η is the average responsivity of the receiver, D is the Euclidean distance from the transmitter to the receiver, ϕ_{tx} and θ_{rx} refer to the angle of irradiance and the angle of incidence, respectively. $T_s(\theta_{rx})$ is the gain of the receiver's optical filter, $m = \frac{-1}{\log_2(\cos(\Phi_{1/2}))}$ is the Lambertian radiation order with LED emission semi-angle $\Phi_{1/2}$. $g(\theta_{rx}) = n^2/\sin^2(\Phi_{\text{FOV}})$ denotes the gain of the optical concentrator, which depends on the reflective index n of the concentrator and the field-of-view angle Φ_{FOV}. Note that $g(\theta_{rx}) = 0$ when $\theta_{rx} > \Phi_{FOV}$.

Even though the VLC channel consists of both LoS and NLoS diffused signals caused by indoor reflectors, the weakest LoS signal is about 7 dB higher than the strongest NLoS signal in indoor environments [65], and thus, NLoS can be fairly neglected. Hence, we only consider the LoS VLC link in this work.

3.3 Channel Estimation and Cramér–Rao lower bound

In this section, we calculate the CRLB, which can be used as a benchmark to evaluate the estimators' performance in the presence of the SDSN. Then, LS and ML estimators are presented and studied.

3.3.1 Fisher Information and Cramér–Rao Lower Bound

In this part of the report, we find the Fisher information to calculate the CRLB. Let N be the number pilot symbols and $\mathbf{x} = [x_1, x_2, \cdots, x_{\mathrm{N}}]^T$ be the transmitted pilots' vector, where $(.)^T$ denotes the transpose operation. Then, the received signal vector $\mathbf{y} = [y_1, y_2, \ldots, y_{\mathrm{N}}]^T$ can be written as

$$\mathbf{y} = h\mathbf{x} + \sqrt{h}\mathrm{diag}(\mathbf{x})\mathbf{n}_{ds} + \mathbf{n}, \tag{3.3}$$

where $\mathrm{diag}(\mathbf{x})$ is an $\mathrm{N} \times \mathrm{N}$ diagonal matrix with the elements of $\mathbf{x}$ in the main diagonal, $\mathbf{n} = [n_1, n_2, \ldots, n_{\mathrm{N}}]^T$, and $\mathbf{n}_{ds} = [n_{ds1}, n_{ds2}, \ldots, n_{ds\mathrm{N}}]^T$. The elements of $\mathbf{n}$ are independent and identically distributed random variables, i.e., $\mathbf{n} \sim \mathcal{N}(0, \sigma_n^2 I_{\mathrm{N}})$ where I_{N} is the identity matrix of size N. The same for $\mathbf{n}_{ds}$, i.e., $\mathbf{n}_{ds} \sim \mathcal{N}(0, \zeta^2\sigma_n^2 I_{\mathrm{N}})$. It is worth mentioning that all the pilot symbols must have positive values, i.e., $x_i > 0$, where $i \in \{1, 2, \cdots, \mathrm{N}\}$.

The lower bound on the variance of any unbiased estimator of h can be obtained using the CRLB as follows[2]

$$\sigma_{\hat{h}}^2 \geq \frac{1}{\mathrm{J}(h)}, \tag{3.4}$$

where $\mathrm{J}(h)$ is the Fisher information of h given by

$$\mathrm{J}(h) = -\mathbf{E}\left\{\frac{\partial^2}{\partial h^2}\ln f(\mathbf{y}; h)\right\}. \tag{3.5}$$

Here, $\mathbf{E}\{\cdot\}$ denotes the expectation operator and $\ln f(\mathbf{y}; h)$ is the log-likelihood function of

[2]An estimator of a given parameter, e.g., h, is said to be unbiased if its expected value is equal to the true value of the parameter that should be estimated.

the unknown channel h. Since we assume that all the samples are independent, the joint PDF of N observations, which is also equal to the likelihood function of h, $f(\mathbf{y};h)$, can be written as

$$f(\mathbf{y};h)=\left(\prod_{i=1}^{N}\frac{1}{\sqrt{2\pi\sigma_n^2\left(1+\zeta^2hx_i\right)}}\right)\exp\left(-\frac{1}{2\sigma_n^2}\sum_{i=1}^{N}\frac{(y_i-hx_i)^2}{1+\zeta^2hx_i}\right). \tag{3.6}$$

After some tedious mathematical manipulations, which are provided in APPENDIX A, J(h) can be expressed as

$$\mathrm{J}(h)=\frac{1}{2}\sum_{i=1}^{N}\frac{(\zeta^2x_i)^2}{(1+\zeta^2hx_i)^2}+\frac{2x_i^2}{\sigma_n^2(1+\zeta^2hx_i)}. \tag{3.7}$$

Without loss of generality, and assuming that all the transmitted symbols are identical i.e., x_i=p, the Fisher information can be significantly simplified to

$$\mathrm{J}(h)=\frac{Np^2}{2\sigma_n^2}\frac{\zeta^4\sigma_n^2+2\zeta^2hp+2}{(1+\zeta^2hp)^2}. \tag{3.8}$$

Consequently, the CRLB can be expressed as

$$\mathrm{CRLB}=\frac{2\sigma_n^2}{Np^2}\frac{(1+\zeta^2hp)^2}{\zeta^4\sigma_n^2+2\zeta^2hp+2}. \tag{3.9}$$

It is observed from (3.9) that, as the number of pilots increases, the error estimation decreases. Furthermore, if $\zeta^2\to 0$, the CRLB reduces to

$$\lim_{\zeta^2\to 0}\mathrm{CRLB}=\frac{\sigma_n^2}{Np^2}. \tag{3.10}$$

This is a well-known result when there is no SDSN, and this validates the presented analysis. It is worth mentioning that the CRLB in (3.10) does not depend on the fading channel

itself. However, as $\zeta^2 \to \infty$, the CRLB in (3.9) can be expressed as

$$\lim_{\zeta^2 \to \infty} \text{CRLB} = \frac{2h^2}{N}. \tag{3.11}$$

We can see that as ζ^2 increases, the CRLB no longer depends on the transmitted power or the thermal noise. On the other hand, increasing the number of pilot symbols improves the CRLB; thus increasing the number of pilot symbols is more essential when trying to improve the CRLB than increasing the transmitted power in the presence of SDSN. Furthermore, as is evident from (3.11), as ζ increases, the CRLB starts to depend more on the fading channel h.

Remark 1: The CRLB performance does not have a linear relationship with ζ^2, σ_n^2, or h. i.e., increasing ζ^2 might increase or decrease the CRLB depending on σ_n^2 and h values.

It is worth mentioning that in the case of σ_n^2 approaches zero, i.e., $\sigma_n^2 \to 0$, after simple mathematical manipulations, the CRLB can be expressed as

$$\lim_{\sigma_n^2 \to 0} \text{CRLB} = \frac{2h^2\sigma_{ds}^2}{N(\sigma_{ds}^2 + 2hp)}. \tag{3.12}$$

As expected, when $\sigma_{ds}^2 \to 0$, the CRLB approaches zero, indicating the perfect case. It should be noted that CRLB $\propto \sigma_n^2/p^2$ and also CRLB $\propto \sigma_{ds}^2/p$, highlighting the greater severity with which dependent noise affects the CRLB in comparison with thermal noise.

3.3.2 Least Square Estimator

Using the LS estimator, we can obtain a low-complexity receiver with no prior statistical information. The estimated $\hat{h}$ can be expressed as

$$\hat{h}_{\text{LS}} = \frac{\mathbf{x}^T\mathbf{y}}{\|\mathbf{x}\|^2}. \tag{3.13}$$

The performance of the LS estimator can be evaluated by determining the MSE, which is equivalent to the variance of the estimation error. Thus, the MSE can be calculated as

$$\epsilon_{\text{LS}} = \hat{h}_{\text{LS}} - h. \tag{3.14}$$

From (3.13), $\hat{h}_{\text{LS}}$ can be simplified to

$$\hat{h}_{\text{LS}} = h + \frac{\mathbf{x}^T}{\|\mathbf{x}\|^2}\sqrt{h\text{diag}(\mathbf{x})}\mathbf{n}_{\text{ds}} + \frac{\mathbf{x}^T}{\|\mathbf{x}\|^2}\mathbf{n}. \tag{3.15}$$

Taking into consideration the fact that $\mathbf{E}\{\hat{h}_{\text{LS}}\} = h$, as seen in (3.15), we can conclude that the LS estimator is unbiased. Furthermore, by applying both (3.14) and (3.15), ϵ_{LS} can be written as

$$\epsilon_{\text{LS}} = \frac{\mathbf{x}^T}{\|\mathbf{x}\|^2}\left(\sqrt{h\text{diag}(\mathbf{x})}\mathbf{n}_{\text{ds}} + \mathbf{n}\right). \tag{3.16}$$

It is evident from (3.16) that ϵ_{LS} is a Gaussian random variable, i.e., $\epsilon_{\text{LS}} \sim \mathcal{N}(0, \sigma^2_{\epsilon_{\text{LS}}})$, where $\sigma^2_{\epsilon_{\text{LS}}}$ is inversely proportional to the pilots' SNR value and can be written as

$$\sigma^2_{\epsilon_{\text{LS}}} = \frac{\sigma_n^2 \sum_{i=1}^{N} x_i^2(1+\zeta^2 h x_i)}{\left(\sum_{i=1}^{N} x_i^2\right)^2}. \tag{3.17}$$

Now, assuming that the transmitted pilot $x_i = p$ for all i, $\sigma^2_{\epsilon_{LS}}$ can be further simplified as

$$\sigma^2_{\epsilon_{LS}} = \frac{\sigma_n^2(1+\zeta^2 hp)}{Np^2}. \tag{3.18}$$

It can be noted from (3.18) that the obtained CRLB is smaller than the $\sigma^2_{\epsilon_{LS}}$, i.e.,

$$\frac{\text{CRLB}}{\sigma^2_{\epsilon_{LS}}} = \frac{2(1+\zeta^2 hp)}{\zeta^4\sigma_n^2 + 2\zeta^2 hp + 2} = \frac{2(1+\zeta^2 hp)}{2(1+\zeta^2 hp) + \zeta^4\sigma_n^2} < 1. \tag{3.19}$$

Remark 2: The performance of the LS estimator reaches the CRLB in two cases: 1) when the transmitted energy $p \to \infty$, and 2) when $\zeta^2 \to 0$.

3.3.3 Maximum-Likelihood Estimator

The ML estimator is a technique used to gauge unknown parameters by maximizing their likelihood PDF. Through the application of this estimator, the log-likelihood of (3.6) can be given as

$$\ln f(\mathbf{y};h) = -\frac{N}{2}\ln\left(2\pi\sigma_n^2\right) - \frac{1}{2}\sum_{i=1}^{N}\left[\ln(1+\zeta^2 h x_i) + \frac{(y_i - h x_i)^2}{\sigma_n^2(1+\zeta^2 h x_i)}\right]. \tag{3.20}$$

The estimated channel in (3.20), can be determined by evaluating $\frac{\partial}{\partial h}\ln f(\mathbf{y};h) = 0$, which can be expressed as

$$-\frac{1}{2}\sum_{i=1}^{N}\frac{\zeta^2 x_i}{1+\zeta^2 h x_i} + \frac{1}{2\sigma_n^2}\sum_{i=1}^{N}\left[\frac{2x_i(y_i - h x_i)}{1+\zeta^2 h x_i} + \frac{\zeta^2 x_i (y_i - h x_i)^2}{(1+\zeta^2 h x_i)^2}\right] = 0. \tag{3.21}$$

While it is nearly impossible to manually find a closed-form expression for the roots of the above equation ($\hat{h}_{\mathrm{ML}}$), numerical tools and software, such as Matlab, can easily solve for $\hat{h}_{\mathrm{ML}}$.

In order to simplify the analysis while maintaining a degree of generality, we assume that the transmitted pilot $x_i = p$. After some mathematical manipulations, which were realized by taking into account the fact that h can never be negative, (3.21) can be expressed as the following quadratic equation

$$-h^2 + Bh + C = 0, \tag{3.22}$$

where B and C can be expressed respectively as

$$B = -\frac{2}{\zeta^2 p} - \frac{\zeta^2\sigma_n^2}{p}, \tag{3.23}$$

and

$$C = -\frac{\sigma_n^2}{p^2} + \frac{\sum_{i=1}^{N} y_i^2}{Np^2} + \frac{2\sum_{i=1}^{N} y_i}{N\zeta^2 p^2}. \tag{3.24}$$

When determining the roots of the equation, keeping in mind that the VLC channel cannot be negative, we can obtain the following result

$$\hat{h}_{\mathrm{ML}} = \frac{1}{2}B + \frac{1}{2}\sqrt{B^2 + 4C}. \tag{3.25}$$

It is clear here that the estimator is biased, i.e., $\mathbf{E}\{\hat{h}_{\mathrm{ML}}\} \neq h$. When considering the law of large numbers, however, it remains a reasonable estimator because as $N \to \infty$ and $\frac{1}{N}\sum_{i=1}^{N} y_i^2 \to \mathbf{E}\{y_i^2\} = h^2p^2 + \sigma_n^2(1 + \zeta^2 hp)$, $\frac{1}{N}\sum_{i=1}^{N} y_i \to \mathbf{E}\{y_i\} = hp$. Therefore, from (3.25) we obtain

$$\begin{aligned}
\mathbf{E}\{\hat{h}_{\mathrm{ML}}\} &= \mathbf{E}\left\{\frac{1}{2}\left[-\frac{2}{\zeta^2 p} - \frac{\zeta^2\sigma_n^2}{p}\right] + \frac{1}{2}\sqrt{\left[-\frac{2}{\zeta^2 p} - \frac{\zeta^2\sigma_n^2}{p}\right]^2 + 4\left[-\frac{\sigma_n^2}{p^2} + \frac{\sum_{i=1}^{N} y_i^2}{Np^2} + \frac{2\sum_{i=1}^{N} y_i}{N\zeta^2 p^2}\right]}\right\} \\
&\xrightarrow{N\to\infty} \frac{1}{2}\left[-\frac{2}{\zeta^2 p} - \frac{\zeta^2\sigma_n^2}{p}\right] + \frac{1}{2}\sqrt{\left[-\frac{2}{\zeta^2 p} - \frac{\zeta^2\sigma_n^2}{p}\right]^2 + 4\left[h^2 + h\left(\frac{\zeta^2\sigma_n^2}{p} + \frac{2}{\zeta^2 p}\right)\right]} \\
&\xrightarrow{N\to\infty} \frac{1}{2}\left[-\frac{2}{\zeta^2 p} - \frac{\zeta^2\sigma_n^2}{p}\right] + \frac{1}{2}\sqrt{\left(2h + \left[\frac{2}{\zeta^2 p} + \frac{\zeta^2\sigma_n^2}{p}\right]\right)^2} \\
&\xrightarrow{N\to\infty} h.
\end{aligned} \tag{3.26}$$

It should be noted here that in practice, it is seldom known in advance how large N must be in order for (3.26) to hold, however, our simulation results show that, depending on ζ^2, $N \in \{5, 20\}$ is sufficiently enough to satisfy (3.26).

For the values $h = 0.1$ and $\sigma^2 = 1$, the results are shown in Tables 3.1 and 3.2 for varying numbers of pilot symbols. It is evident from the tables that a greater number of samples is needed for the real value to converge at higher values of ζ^2. It can also be observed that the mean converges around $N = 5$, for $\zeta^2 = 1$, and $N = 25$ for $\zeta^2 = 5$, at

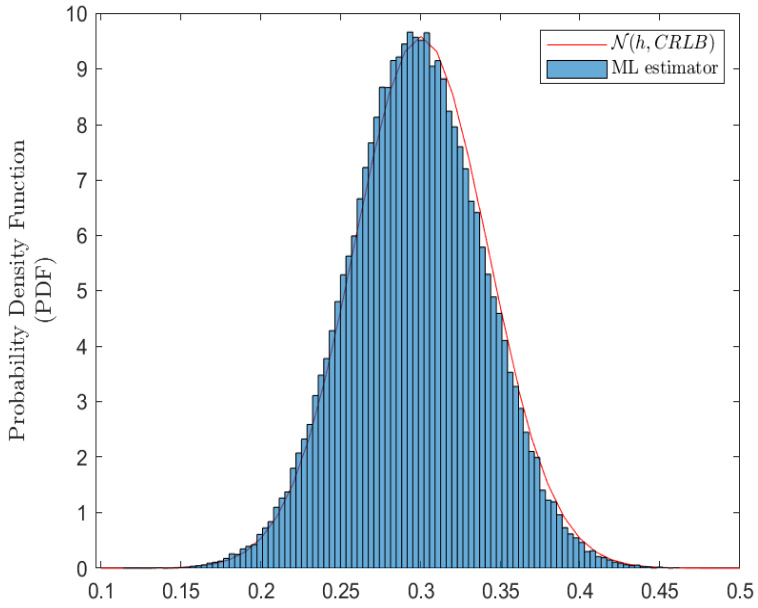

Figure 3.2: The PDF of $\mathcal{N}(h, \text{CRLB})$ and the histogram of the ML estimator when $N = 5$, ${\sigma_n}^2 = 1$ and $h = 0.3$.

different levels of power.

Unlike the LS estimator, where the estimated $\hat{h}_{\text{LS}}$ is always a Gaussian random variable, it is obvious from (3.25) that $\hat{h}_{\text{ML}}$ cannot be a Gaussian random variable so long as $\zeta \neq 0$. Thus, since the estimation is biased, the estimation error $\epsilon_{\text{ML}} = h - \hat{h}_{\text{ML}}$ cannot be a Gaussian random variable and cannot have a zero mean. As a result, the MSE does not equal the variance of the error, ϵ_{ML}, but rather it equals $\mathbf{E}\{\epsilon_{\text{ML}}^2\} - (\mathbf{E}\{\epsilon_{\text{ML}}\})^2$.

It is extremely difficult to analytically study the MSE of the ML estimation, so we must resort to some sort of approximation. The PDF, or histogram, of $\hat{h}_{\text{ML}}$ was constructed using a Monte Carlo simulation in Fig. (3.2), and this was done for $N = 5$. In the same figure, the theoretical PDF of $\mathcal{N}(h, \text{CRLB})$ is plotted. It is evident from the figure that, when superimposed, the histogram and theoretical PDF can hardly be distinguished from each other. In other words, the theoretical PDF and histogram resemble each other to an almost identical degree. Note that, for $N = 5$, the estimated PDF is slightly displaced to the left.

Table 3.1: Theoretical asymptotic and actual mean for ML estimator at different power levels, when $h = 0.1$ and $\zeta^2 = 1$.

Number of pilots, N	15 dB	20 dB	25 dB	30 dB
1	0.0866	0.0952	0.0984	0.0995
5	0.0974	0.0991	0.0997	0.0999
10	0.0987	0.0995	0.0998	0.1
15	0.0992	0.0997	0.0999	0.1
25	0.0995	0.0998	0.0999	0.1
50	0.0997	0.0999	0.1	0.1
Asymptotic value	0.1			

Table 3.2: Theoretical asymptotic and actual mean for ML estimator at different power levels, when $h = 0.1$ and $\zeta^2 = 5$.

Number of pilots, N	15 dB	20 dB	25 dB	30 dB
1	0.0805	0.0847	0.0926	0.0976
5	0.0951	0.0968	0.0986	0.0995
10	0.0974	0.0984	0.0993	0.998
15	0.0983	0.0989	0.0996	0.0998
25	0.0990	0.0993	0.0997	0.0999
50	0.0995	0.0997	0.0999	0.0999
Asymptotic value	0.1			

This can also be observed in Tables 3.1 and 3.2, where the expected value of the estimated $\hat{h}_{\text{ML}}$ is to the left of the actual value of h. However, for large values of N, the estimated PDF is expected to more closely resemble the theoretical PDF.

We can conclude from the above discussion that, with a sufficient number of pilot symbols (around $N = 5$), the ML is unbiased and, most importantly, achieves the CRLB, i.e., $\hat{h}_{\text{ML}} \sim \mathcal{N}(h, \text{CRLB})$. The ML estimator performance consequently reaches the CRLB. It is worth mentioning that the LS estimator does not achieve the CRLB with a small number of pilots, and this comparison demonstrates the superiority of ML over LS. On the other hand, LS proves to be less complex since the ML estimator requires information on σ_n^2 and ζ^2.

3.4 Receiver Designs and Performance Analysis

This section proposes two receiver designs, namely an optimal receiver and its less complex sub-optimal version. Both receivers are presented under two scenarios: perfect and imperfect channel estimation. Furthermore, the error analysis of both receivers is presented in the context of on-off-keying (OOK) modulation.

3.4.1 Receiver Designs

Considering the discussed VLC wireless communication system, the SDSN changes the PDF of the received signal. There is a consequent need to design a receiver that can support the resulting PDF. It is assumed that the M-PAM modulation scheme is applied, and that $(x_p = \pm(2b+1)\Delta + d)$ is the modulated baseband transmitted signal. Here, $b \in \{0, 1, \cdots, M-1\}$, Δ is the distance between the constellation points, and d is the DC bias level that is strategically chosen in such a way that all the constellation points have positive values.

From (3.1), the joint PDF of the received signal y, given the transmitted signal x_p, can be expressed as

$$f_{y|x_p}(y) = \frac{1}{\sqrt{2\pi\sigma_n^2(hx_p\zeta^2+1)}} \times \exp\left\{-\frac{(y-hx_p)^2}{2\sigma_n^2(hx_p\zeta^2+1)}\right\}. \tag{3.27}$$

Assuming equal probability of all transmitted symbols, i.e., $p(x_p) = \frac{1}{M}$, the ML optimal receiver can be expressed as

$$\hat{x}_{opt} = \max_{x_p, p=0,\cdots,M-1} \left\{-\ln\left(hx_p\zeta^2+1\right) - \frac{(y-hx_p)^2}{\sigma_n^2(hx_p\zeta^2+1)}\right\}. \tag{3.28}$$

Here, it can be concluded that the traditional ML receiver, which applies the minimum Euclidean distance (MED), is not the optimal receiver in the presence of SDSN since it ignores the existence of SDSN. However, the traditional sub-optimal receiver that does not

need any statistical information on shot and thermal noises can be written as

$$\hat{x}_{sub} = \min_{x_p, p=1,\cdots,M-1} \left\{ (y - hx_p)^2 \right\}. \tag{3.29}$$

It will be shown later that both receivers have a comparable error performance in some cases. The same detection formulas in (3.28) and (3.29) can be applied in the case of imperfect CSI by replacing h with $\hat{h}$.

OOK is the simplest method that can be used in VLC systems (IEEE 802.15.7). With this technique, the intensity of an optical source is directly modulated by the information sequences, which are usually binary. It is readily seen that OOK is a special case of M-PAM, where $x_0 = 0$, $x_1 = 2A$ (the DC bias $d = A$). By applying the optimal receiver derived in (3.28), the optimal receiver for the OOK can be eventually formulated as

$$\hat{x}_{opt} = \begin{cases} x_0 & \text{if} \quad \frac{\zeta^2}{2} y^2 + y < hA + \frac{\sigma_n^2}{4Ah} \left[1 + 2Ah\zeta^2\right] \ln \left[1 + 2Ah\zeta^2\right], \\ x_1 & \text{otherwise.} \end{cases} \tag{3.30}$$

Following the same logic, the sub-optimal receiver can be formulated as

$$\hat{x}_{sub} = \begin{cases} x_0 & \text{if} \ \ y \leq hA, \\ x_1 & \text{otherwise.} \end{cases} \tag{3.31}$$

In this case, the same detection formulas in (3.30) and (3.31) can be applied to the case of imperfect CSI if we replace h with $\hat{h}$. It is worth mentioning that the sub-optimal receiver is identical to the optimal one in the absence of input-dependent noise.

3.4.2 Error Analysis of Sub-Optimal Receiver

In this subsection, the error analysis of the sub-optimal receiver is discussed. Given the received signal in (3.1), and by utilizing the M-PAM modulation, (3.1) can be rewritten

as

$$y = x_p h + \omega, \tag{3.32}$$

where $\omega \sim \mathcal{N}(0, \sigma_n^2(1 + x_p h\zeta^2))$.

Perfect Estimation

The conditional probability (conditioned on the channel fading gain h) of using the sub-optimal receiver to detect x_q instead of the transmitted x_p can be written as

$$\begin{aligned} P\left(x_p, x_q|h\right) &= P\left(\left[y - hx_p\right]^2 > \left[y - hx_q\right]^2\right) = P\left(2h(x_p - x_q)\omega > h^2(x_p - x_q)^2\right) \\ &= Q\left(\sqrt{\frac{h^2(x_p - x_q)^2}{4\sigma_n^2\left(1 + hx_p\zeta^2\right)}}\right), \end{aligned} \tag{3.33}$$

where $P\left(\cdot\right)$ denotes the probability of an event. Now, the symbol error probability (SER) of the M-PAM VLC system can be represented as

$$P_s(e) = \frac{1}{M}\left(P\left(x_0, x_1\right) + P(x_{M-1}, x_{M-2}) + \sum_{i=p}^{M-1}\left[P(x_{i-1}, x_i) + P(x_{i-1}, x_{i-2})\right]\right). \tag{3.34}$$

As a special case, the BER value for OOK can be written as

$$P(e|h) = \frac{1}{2}P(x_0, x_1|h) + \frac{1}{2}P(x_1, x_0|h). \tag{3.35}$$

From (3.33), the BER in (3.35) can be expressed as

$$P(e|h) = \frac{1}{2}Q\left(\sqrt{\frac{h^2A^2}{\sigma_n^2}}\right) + \frac{1}{2}Q\left(\sqrt{\frac{h^2A^2}{\sigma_n^2(1 + 2Ah\zeta^2)}}\right). \tag{3.36}$$

It is worth mentioning that the error probability of $P(x_0, x_1|h) < P(x_1, x_0|h)$, and therefore, the error probability is nonidentical to what is seen in traditional RF systems.

Moreover, in the absence of SDSN, i.e., $\zeta = 0$, the above expression can be simplified to

$$P(e|h)_{\zeta=0} = Q\left(\sqrt{\frac{h^2A^2}{\sigma_n^2}}\right). \tag{3.37}$$

Remark 3: According to (3.36) and (3.37), we have

$$\frac{P(e|h)_{\zeta\neq 0}}{P(e|h)_{\zeta=0}} = \frac{1}{2}\left[1 + \frac{Q\left(\sqrt{\frac{h^2A^2}{\sigma_n^2[1+2Ah\zeta^2]}}\right)}{Q\left(\sqrt{\frac{h^2A^2}{\sigma_n^2}}\right)}\right] > 1, \tag{3.38}$$

which is valid because the second term in the bracket is greater than one. Hence, as expected, the BER performance when $\zeta = 0$ is better than what is seen when $\zeta \neq 0$. In other words, the SDSN deteriorates the error system performance. Furthermore, the asymptotic error performance as $\zeta \to \infty$, i.e., large values of ζ, can be written as

$$P(e|h)_{\zeta\to\infty} = \frac{1}{4} + \frac{1}{2}Q\left(\sqrt{\frac{h^2A^2}{\sigma_n^2}}\right) \approx \frac{1}{4}. \tag{3.39}$$

Imperfect Estimation

The receiver estimates the channel gain h and uses the result in the same metric that would be applied if the channel was perfectly known. Hence, the conditional probability of detecting x_q instead of the transmitted x_p can be expressed as

$$P(x_p, x_q|\hat{h}) = P\left(\left[y - \hat{h}x_p\right]^2 > \left[y - \hat{h}x_q\right]^2\right) = Q\left(\sqrt{\frac{\hat{h}^2(x_p - x_q)^2}{4\sigma_n^2\left(1 + hx_p\zeta^2\right) + 4x_p^2\sigma_\epsilon^2}}\right), \tag{3.40}$$

where ϵ denotes the channel estimation error. The SER of M-PAM can be obtained by substituting (3.40) into (3.34). Moreover, the OOK BER can be rewritten as

$$P(e|\hat{h}) = \frac{1}{2}Q\left(\sqrt{\frac{\hat{h}^2A^2}{\sigma_n^2}}\right) + \frac{1}{2}Q\left(\sqrt{\frac{\hat{h}^2A^2}{\sigma_n^2(1 + 2Ah\zeta^2) + 4A^2\sigma_\epsilon^2}}\right). \tag{3.41}$$

It is clear that the error performance degrades due to imperfect channel estimation.

3.4.3 Error Analysis of the Optimal Receiver for OOK

In this subsection, the optimal error analysis for OOK is presented for both perfect and imperfect estimation cases. The error probability of $P(x_1, x_0)$ can be written as

$$\begin{aligned} P(x_1, x_0|h) &= P\left(\frac{\zeta^2}{2}(2Ah+\omega)^2 + 2Ah + \omega < hA + \frac{\sigma_n^2}{4Ah}\gamma\ln\gamma\right) \\ &= P\left(\frac{\zeta^2}{2\sqrt{\gamma}}u^2 + u < -\frac{hA}{\sqrt{\gamma}} + \frac{\sigma_n^2}{4Ah\sqrt{\gamma}}\ln\gamma\right), \end{aligned} \tag{3.42}$$

where $\gamma = 1 + 2Ah\zeta^2$ and $u \sim \mathcal{N}(0, \sigma_n^2)$. To simplify the analysis, and for small values of $\sigma_n^2 < 0.001$, the above equation can be approximated as

$$\begin{aligned} P(x_1, x_0|h) &\approx P\left(u > \frac{hA + \frac{\zeta^2\sigma_n^2}{2} - \frac{\sigma_n^2}{4Ah}\ln(1+2Ah\zeta^2)}{\sqrt{1+2Ah\zeta^2}}\right) \\ &\approx Q\left(\sqrt{\frac{\left[hA + \frac{\zeta^2\sigma_n^2}{2} - \frac{\sigma_n^2}{4Ah}\ln(1+2Ah\zeta^2)\right]^2}{\sigma_n^2(1+2Ah\zeta^2)}}\right). \end{aligned} \tag{3.43}$$

Furthermore, the error probability $P(x_0, x_1|h)$ can be given as

$$P(x_0, x_1|h) \approx Q\left(\sqrt{\frac{\left[hA - \frac{\zeta^2\sigma_n^2}{2} + \frac{\sigma_n^2(1+2Ah\zeta^2)}{4Ah}\ln\left(1+2Ah\zeta^2\right)\right]^2}{\sigma_n^2}}\right). \tag{3.44}$$

Therefore, the overall error probability can be expressed as

$$P(e|h) \approx \frac{1}{2}Q\left(\sqrt{\frac{\left[hA+\frac{\zeta^2\sigma_n^2}{2}-\frac{\sigma_n^2}{4Ah}\ln(1+2Ah\zeta^2)\right]^2}{\sigma_n^2(1+2Ah\zeta^2)}}\right) + \frac{1}{2}Q\left(\sqrt{\frac{\left[hA-\frac{\zeta^2\sigma_n^2}{2}+\frac{\sigma_n^2(1+2Ah\zeta^2)}{4Ah}\ln\left(1+2Ah\zeta^2\right)\right]^2}{\sigma_n^2}}\right). \tag{3.45}$$

Similarly, the error probability for imperfect channel estimation can be expressed as

$$P(e|\hat{h}) \approx \frac{1}{2}Q\left(\sqrt{\frac{\left[\hat{h}A-\frac{\zeta^2\sigma_n^2}{2}+\frac{\sigma_n^2(1+2A\hat{h}\zeta^2)}{4A\hat{h}}\ln\left(1+2A\hat{h}\zeta^2\right)\right]^2}{\sigma_n^2}}\right) + \frac{1}{2}Q\left(\sqrt{\frac{\left[\hat{h}A+\frac{\zeta^2\sigma_n^2(1+2Ah\zeta^2)}{2(1+2A\hat{h}\zeta^2)}-\frac{\sigma_n^2}{4A\hat{h}}\ln(1+2A\hat{h}\zeta^2)\right]^2}{\sigma_n^2(1+2Ah\zeta^2)}}\right). \tag{3.46}$$

The SER of M-PAM can be obtained by deriving $P(x_p, x_q|h)$ and substituting it into (3.34) for perfect channel estimation. Similarly, by deriving $P(x_p, x_q|\hat{h})$ and substituting it into (3.34), we can determine the SER of M-PAM for imperfect channel estimation.

3.5 Simulation Results and Discussion

The previous section concluded that the ML estimator is biased while the LS is not. Recall that the CRLB expresses the lower bound of the variance for the unbiased estimators of a deterministic parameter.

Fig. 3.3 plots the CRLB against the LS and ML estimators' performance for one pilot when ${\sigma_n}^2 = 10^{-1}$ and $h = 10^{-2}$ at different levels of SDSN. Various observations can be made, and they can all be summarized as follows:

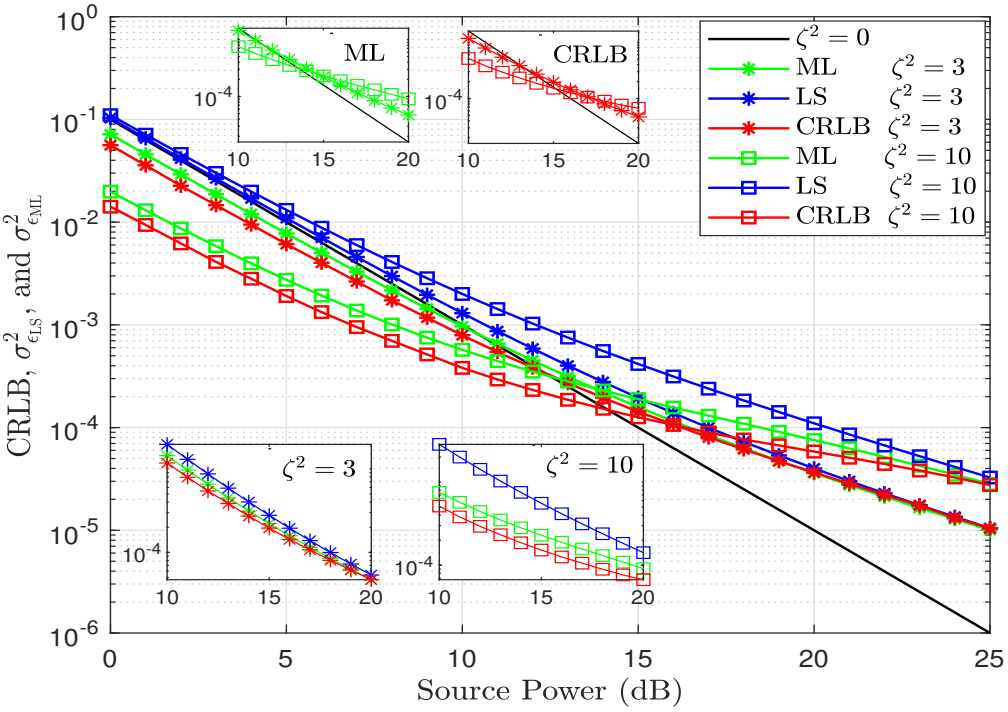

Figure 3.3: CRLB, $\sigma^2_{\epsilon_{\rm LS}}$ and $\sigma^2_{\epsilon_{\rm ML}}$ when ${\sigma_n}^2 = 10^{-1}$ and $h = 10^{-2}$.

- Both ML and LS estimators have the same performance as the CRLB when $\zeta^2 = 0$.
- The performance of the ML estimator eclipses that of the LS and CRLB when using one pilot.
- Increasing the SDSN level increases the difference between the estimators' performances. This can be clearly noticed from the subplots of $\zeta^2 = 3$ and $\zeta^2 = 10$.
- Increasing the SDSN level has a negative impact on the performance of the LS estimator.
- The relationship between the SDSN level and CRLB is non-linear, as can be concluded when looking at the CRLB subplot. Here, increasing the value of ζ^2 has a positive effect before a threshold power value and a negative effect afterwards. The same trend can be seen for the ML estimator in the ML subplot.

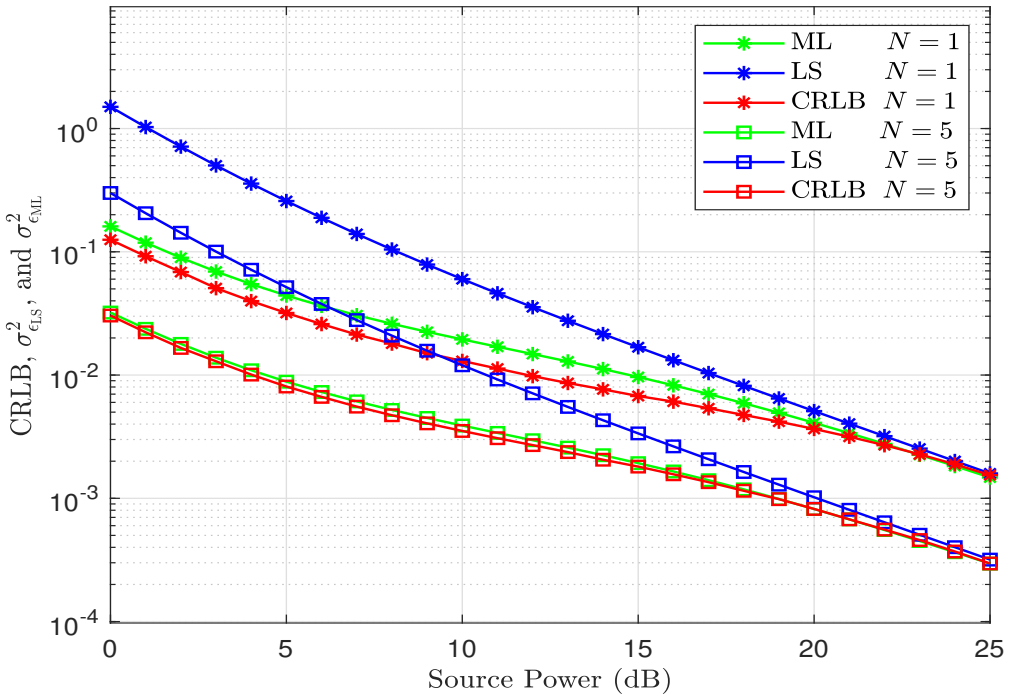

Figure 3.4: CRLB, $\sigma^2_{\epsilon_{\mathrm{LS}}}$, and $\sigma^2_{\epsilon_{\mathrm{ML}}}$ at different number of pilots when ${\sigma_n}^2 = 1$ and $h = 10^{-1}$.

- The SDSN has a notable impact on the channel estimation accuracy in the high-energy region.
- All curves approach the same performance after a certain energy value. This value shifts to the right at higher levels of SDSN.

Fig. 3.4 plots the CRLB against LS and ML estimators' performances while increasing the number of pilots. Here, ${\sigma_n}^2 = 1$, $h = 10^{-1}$ and $\zeta^2 = 5$. Two conclusions can be drawn from this figure: 1) All the remarks made when discussing the previous figure remain valid when increasing the number of pilots and 2) the performance of the ML approaches that of the CRLB when increasing the number of pilots.

This section discusses the numerical results of SISO-VLC performance in a system under the joint effects of SDSN and imperfect CSI. All results are analyzed for both the optimal and sub-optimal receivers. We assume OOK modulation technique with two transmitted

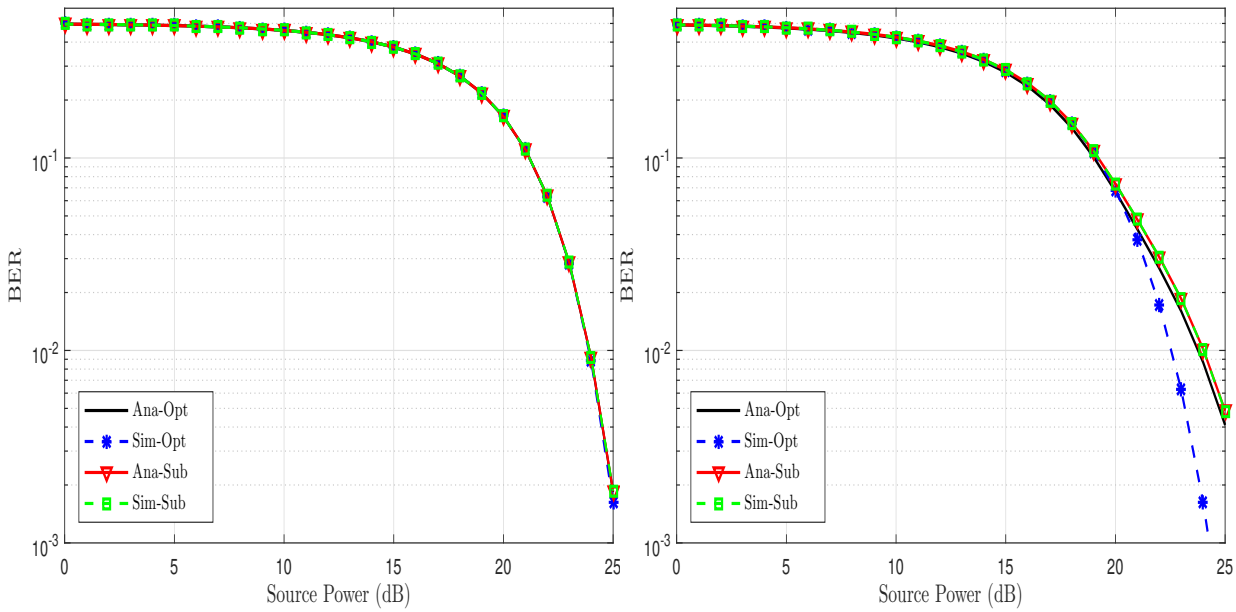

(a) ${\sigma_n}^2 = 10^{-4}$ and $h = 10^{-4}$. (b) ${\sigma_n}^2 = 10^{-2}$ and $h = 2 \times 10^{-3}$.

Figure 3.5: Analytical and simulation BER performance for the optimal and sub-optimal receivers.

signals $x_0 = 0$, $x_1 = 2A$. The simulation results are obtained using Monte Carlo simulations using at least 10^6 transmitted symbols for each figure.

Fig. 3.5 shows the analytical and simulation BER results for the optimal and sub-optimal receivers when $\zeta^2 = 5$ at different values of σ_n^2 and h. Three conclusions can be drawn from this figure: 1) In general, the optimal receiver outperforms the sub-optimal one, however, the performance difference between them shrinks as $\zeta^2 \to 0$. 2) The analytical and simulation results of the sub-optimal receiver match perfectly for all values of σ_n^2, and finally 3) The analytical and simulation results of the optimal receiver perfectly match what is seen when $\sigma_n^2 = 10^{-4}$. We can consequently deduce that our approximation in (3.45) is fairly accurate, i.e., as long as $\sigma_n^2 \leq 10^{-3}$.

Fig. 3.6 discusses the impact of ζ^2 on the performance of the optimal and sub-optimal receivers when ${\sigma_n}^2 = 10^{-3}$, $h = 5 \times 10^{-4}$ and ζ^2 is incremented along $[0, 3, 10]$. It can be observed that the BER increases as ζ^2 increases. Moreover, the result here agrees with the one in the previous figure, where the optimal receiver outperforms the sub-optimal for

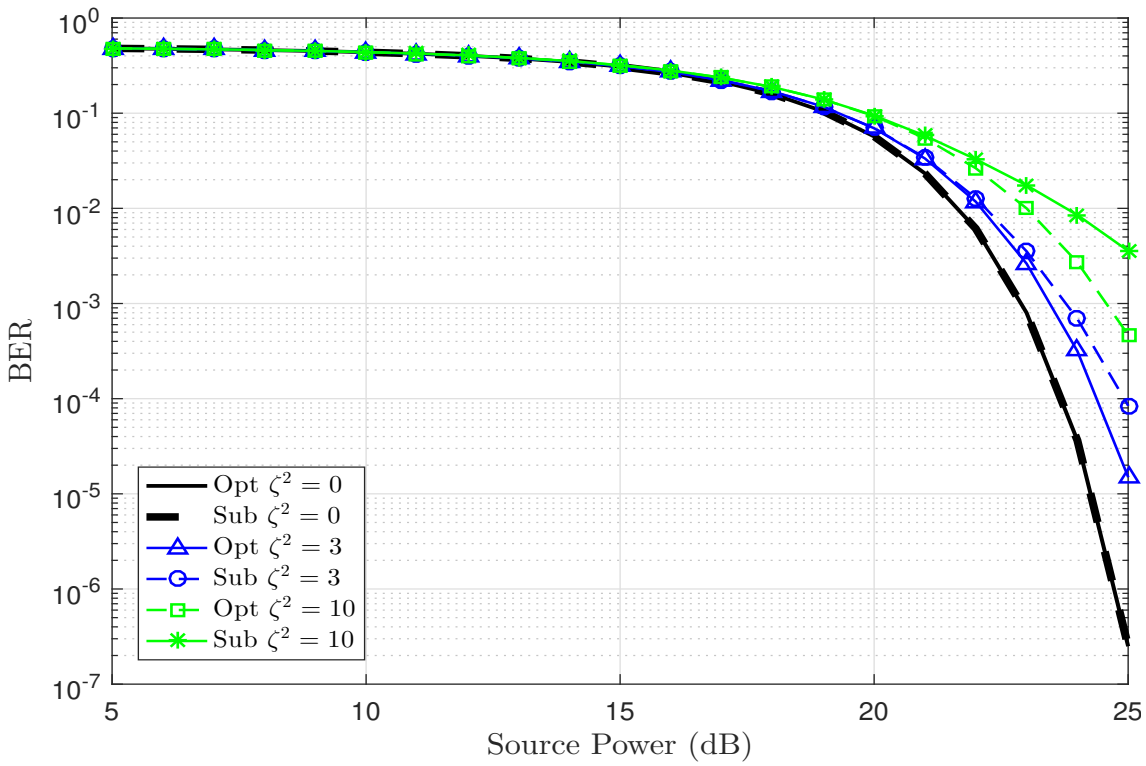

Figure 3.6: BER performance at different levels of SDSN when ${\sigma_n}^2 = 10^{-3}$ and $h = 5{\times}10^{-4}$.

all values of ζ^2. Until now, we have discussed the system performance assuming perfect CSI. In order to achieve more practical results, the joint impacts of imperfect CSI and the SDSN are analyzed in Figs. 3.7 and 3.8.

In Fig. 3.7, the effect of imperfect CSI is presented when the estimation error variance equals to the CRLB ($\sigma_\epsilon^2 = \text{CRLB}$) upon the use of one pilot. As indicated by the figure, more degradation in the performance can be noticed due to the joint effects of the channel estimation error and the SDSN. This degradation worsens at higher levels of SDSN. The effect of imperfect CSI when the estimation error variance has a fixed value of ($\sigma_\epsilon^2 = 10^{-3}$) is given in Fig. 3.8. As the figure shows, more degradation in the performance can be noticed compared to what was seen in Fig. 3.7 when the estimation error variance reached the CRLB. This confirms the importance of the estimation phase when trying to maintain the system performance. One more interesting observation related to the system performance in the high SNR region can be made: The performance of the sub-optimal receiver at

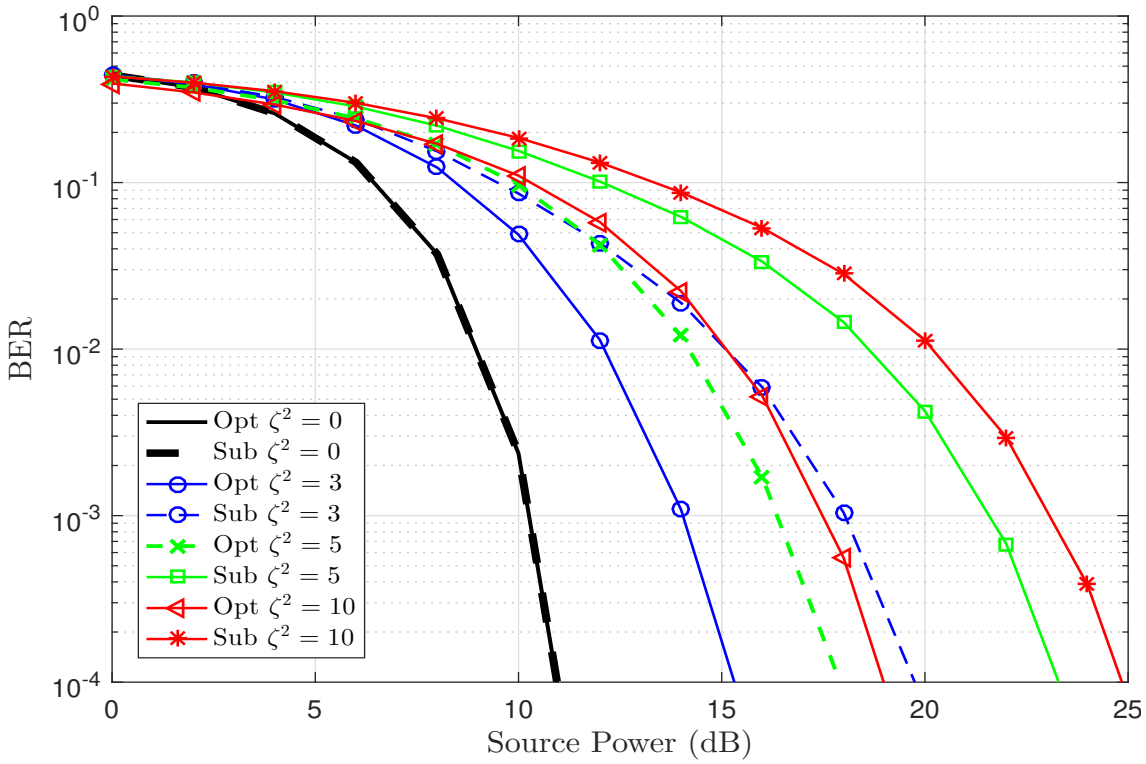

Figure 3.7: BER performance at different levels of SDSN when σ_ϵ^2 equals the CRLB with one pilot, ${\sigma_n}^2 = 10^{-1}$ and $h = 10^{-1}$.

different levels of SDSN saturates and reaches the performance of the optimal receiver when $\zeta^2 = 0$. This can be explained by noting the BER in (3.41) and (3.46), where $BER \to Q\left(\sqrt{\frac{\hat{h}^2}{4\sigma_\epsilon^2}}\right)$ as $A \to \infty$. One last conclusion that can be drawn is that the error performance of the optimal detector saturates at a lower error probability compared to the sub-optimal detector, i.e., the optimal detector saturates at BER$\approx 2 \times 10^{-4}$ while the sub-optimal saturates at $\approx 1 \times 10^{-3}$.

3.6 Conclusion

This chapter introduces an analytical framework to study the performance of SISO-VLC under the effect of SDSN in cases perfect and imperfect channel estimation. LS and ML estimators were proposed and compared to the derived CRLB. Furthermore, optimal and

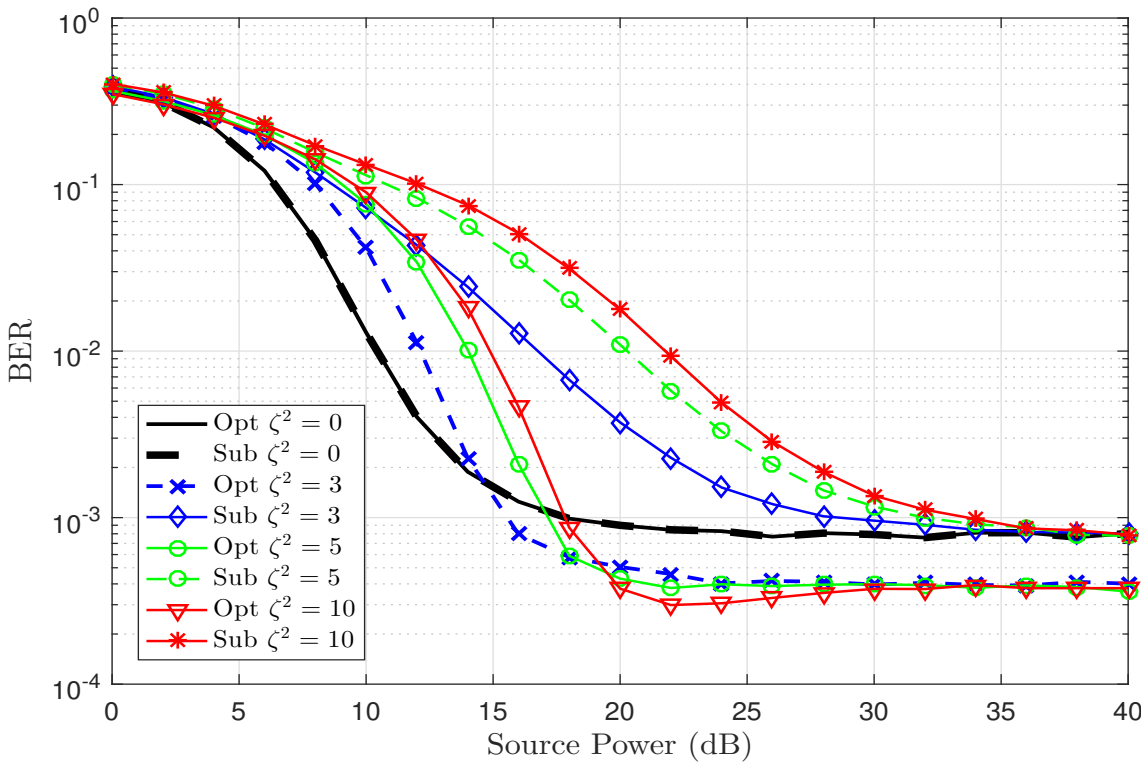

Figure 3.8: BER performance at different levels of SDSN when $\sigma_\epsilon^2 = 10^{-3}$, ${\sigma_n}^2 = 10^{-1}$ and $h = 10^{-1}$.

sub-optimal receivers were designed and compared. The analytical results corroborated by Monte Carlo simulation show the superiority of the optimal receiver design compared to the sub-optimal one in all conditions.

In addition, results demonstrated that SDSN negatively affects the system BER and the channel estimation error bound, and that it has a non linear effect on CRLB. Closed-form expressions of BER for sub-optimal detectors with OOK and M-PAM modulation techniques are derived, and an approximated BER expression for the optimal detector using OOK is presented. Deriving a closed-form expression of the BER for optimal receiver using OOK and M-PAM modulation techniques are considered for our future work.

3.7 Publications Resulted from This Chapter

- M. Yaseen, M. Alsmadi, A. E. Canbilen, and S. S. Ikki, "Visible Light Communication With Input-Dependent Noise: Channel Estimation, Optimal Receiver Design and Performance Analysis," *IEEE Journal of Lightwave Technology*, vol. 39, no. 23, pp. 7406-7416, Dec.1, 2021.

Chapter 4

Random Channel Estimation in Visible Light Communication Systems: The Effect of Input Signal-Dependent Noise

4.1 Introduction

The recent explosive growth in the number of devices connected to mobile networks, along with the accelerated development of online applications and services, have intensified the demand for ubiquitous connectivity and high capacity. As a result, there is no end to the problems faced by RF communications. VLC has been introduced as a complementary technology to address these challenging problems.

VLC exploits visible light for both illumination and data transmission. It utilizes the wide, untapped, free, and unlicensed electromagnetic (EM) spectrum from 375 nm to 782 nm [27]. In addition to a wider bandwidth, VLC boasts of many advantages over traditional RF communications. In particular, VLC does not interfere with RF systems, which makes it convenient to be used in aircraft cabins, hospitals, mines, and other EM interference-sensitive environments. Moreover, a particularly unique characteristic of visi-

ble light, namely that it cannot penetrate through walls, ensures an ideal communication environment for areas requiring high information security [66].

On the other hand, VLC has garnered significant research interest due to the use of LEDs for illumination instead of incandescent lamps. Compared to the latter, LEDs have a higher tolerance to humidity, higher power efficiency, and a smaller size. Furthermore, the use of LEDs as VLC transmitters is very cost-effective, especially when compared to using RF communications [67].

In VLC, data is modulated onto the instantaneous intensity of the released light, which is known as IM VLC [68]. At the receiving end, a photo-detector (PD) or an image sensor is used to detect the varying intensities of light, a method known as direct detection (DD) [68]. IM/DD is a simple and low-cost modulation technique; however, it requires the transmitted signal to satisfy the real and non-negative constraints. These constraints entail modifications to most modern modulation techniques used in RF systems before their application in VLC systems. In other words, a very limited number of simple modulation techniques, such as OOK, pulse position modulation (PPM), pulse amplitude modulation (PAM), and pulse width modulation (PWM), can be directly employed in VLC, but more advanced modulation schemes necessitate a few modifications before a first implementation in VLC [25].

In VLC systems, there are two main sources of noise: thermal noise and shot noise. The former occurs due to electron excitation in the conductive material of the photo diode, and is therefore independent of the signal and follows a Gaussian distribution [69].

On the other hand, shot noise is generated by the LED's transmitted signal at the receiver, and is due to an incidence of photons interacting with the photo diode. Shot noise follows a Poisson distribution and is signal-dependent. As such, it is termed SDSN. Although SDSN is Poisson-distributed, it is often modeled as Gaussian due to the large number of photons. In fact, ample lighting in VLC systems allows the shot noise to appear quite Gaussian [9, 11, 70].

SDSN has a serious deleterious impact on VLC system performance, as it dramatically reduces the ability to achieve high data rates [71–73].

4.1.1 Related Work

Although VLC is widely used in many applications due to its unique characteristics, its benefits remain untapped unless channel estimation is accurate [74]. Therefore, in order to design a reliable VLC system, an efficient estimator is a primary need. Considering that some work has been done in the literature to estimate the channels of VLC systems. For instance, in [75], the channel estimation of an OFDM-VLC system using LS and the MMSE was investigated. In [76], an adaptive statistical Bayesian MMSE technique was presented for optical OFDM-aided VLC systems, and a new mechanism called the variable statistic window (VSW), was proposed to enhance the performance of the channel estimator by exploiting the past channel information. A closed-form expression was derived for the symbol error probability (SEP) of a SISO VLC system with perfect CSI in [7]. Moreover, the SEP was derived for the imperfect CSI case, in which the system estimates the channel gain using the LS estimation technique.

The receiver structure for a wide FOV VLC system with random receiver orientation and location was presented assuming imperfect CSI in [77]. Here, the LS estimation technique was used to determine the CSI needed for receiver design. Moreover, using the designed receiver, the authors derived closed-form expressions for the SEPs. To enhance the spectral efficiency in multiple-input and single-output (MISO) optical OFDM VLC systems, a new estimation method called super training-based channel estimation was proposed in [78]. Next, a novel blind channel estimation scheme was designed in [79] with the aim of enhancing the channel estimation accuracy. In [80], an efficient and flexible de-noising convolutional neural network (FFDNet)-based channel estimation technique was investigated for MIMO VLC systems, and the results demonstrated that FFDNET provided better performance compared to the MMSE technique.

The optimization of VLC systems under the assumption of average and maximum transmit power constraints was studied in [60]. In order to mitigate the co-channel interference between the transmitters, LS channel estimation was utilized in [81] with an ML equalizer for MIMO-VLC systems, and the BER performance was investigated by considering various conditions. Furthermore, the performance of the spatial multiplexing in MIMO-VLC systems was investigated by calculating the BER in [61].

Despite the dramatic distortion effects of the SDSN on the VLC system performance, there are only a few works considering VLC systems with SDSN. In one of these studies [82], two methods were proposed to estimate the fixed (deterministic) channel of a SISO-VLC system, and CRLB was derived. The estimation performance of the proposed methods was evaluated in terms of MSE. Moreover, designs were proposed for the optimal and sub-optimal receivers, and their BER performances were also presented. In particular, we derived a closed-form expression of the BER for the sub-optimal receiver and an approximated version for the optimal one. In [11], a two-dimensional constellation diagram was designed for a VLC system with SDSN to minimize the maximum SEP. Different modulation design methods for both single- and multi-carrier VLC systems with SDSN were introduced in [12]. Additionally, two different optimization problems were solved to get the best constellations for the proposed systems. Optimal and approximated traditional log-likelihood ratio (LLR) were derived for a VLC system using Avalanche photo-diodes in [83] by considering SDSN.

To the best of the authors' knowledge, random channel estimation has not been studied in the literature for VLC systems with SDSN under the effect of imperfect CSI.

Chapter Organization: The rest of the chapter is organized as follows: The channel and system models are introduced in Section 4.2. In Section 4.3, four different estimators and the BCRLB are derived under the assumption of a known SDSN factor ζ^2, while Section 4.4 discusses the case of unknown ζ^2 at the receiver and proposes two solutions for it. Section 4.5 proposes a receiver design for the random channel gain h. Next, the

obtained numerical results are presented with insightful discussions in Section 4.6. Finally, concluding remarks are provided in Section 4.7.

4.2 System and Channel Models

We consider a SISO-VLC downlink transmission scenario, where an LED is mounted on the ceiling of a regular indoor environment to serve a user on the floor. The user is confined within a circular area[1] with radius R as shown in Fig. 4.1. The location of the user is assumed to be static, and a symbol-by-symbol detection is performed on the receiver side. However, an extension of this work to include a coded system would be straightforward.

Considering that thermal noise and SDSN affect the optical signal x sent from the LED, the received signal at the user is written as [11, 62, 84]

$$y = hx + \sqrt{hx}n_{\text{ds}} + n, \tag{4.1}$$

where $x = s + d$, while s is the transmitted symbol and d is the bias level (DC value), which is added to guarantee that the VLC signal is always positive. Without loss of generality, and assuming that 1) binary-PAM is used, 2) the input data $s \in \{-A, A\}$, and 3) the DC offset $d = A$, then the transmitted signal $x \in \{0, 2A\}$ and A can be any positive value. Additionally, $n \sim \mathcal{N}(0, \sigma_n^2)$ is the signal-independent thermal noise, and $\sqrt{hx}n_{\text{ds}}$ is the SDSN term, where $n_{\text{ds}} \sim \mathcal{N}(0, \sigma_{ds}^2)$. Here, we define a new term $\zeta^2 = \sigma_{ds}^2/\sigma_n^2$, and call it *the shot noise scaling factor*, which is used to indicate the strength of the SDSN compared with the signal-independent thermal noise. Thus, the shot noise is represented by $n_{\text{ds}} \sim \mathcal{N}(0, \sigma_n^2\zeta^2)$, and the term ζ^2, which can be determined by the receiver parameters, takes practical values ranging between 1 and 10 [11, 62]. Nevertheless, our analysis is valid for any value of ζ^2.

[1] We assume that all users remain inside the circle. This is a practical assumption widely made in the literature; however, it is key to note that outside this region, there is no coverage by the specified LED.

It is worth noting that the shot noise is generally characterized by a Poisson distribution. However, the high-intensity nature of light in VLC systems makes it congruent with a Gaussian distribution at large numbers of received photons [9, 48, 63, 64]. On the other hand, the PDF of the channel gain h can be given as [85]

$$f_h(h) = \begin{cases} \Upsilon \; h^{\frac{-2}{m+3}-1} & h_{\min} \leq h \leq h_{\max}, \\ 0 & \text{otherwise}, \end{cases} \tag{4.2}$$

where Υ can be expanded as

$$\Upsilon = \frac{2C^{\frac{2}{m+3}}((m+1)L^{(m+1)})^{\frac{2}{m+3}}}{(m+3)R^2}. \tag{4.3}$$

Here, C being a transceiver-dependent constant, L is the vertical distance from the LED to the receiver plane and m denotes the order of the Lambertian radiation pattern followed by the LED, which is given by

$$m = \frac{-1}{\log_2(\cos(\Phi_{1/2}))}, \tag{4.4}$$

where $\Phi_{1/2}$ is the LED transmitter emission semi-angle at a half-power level.

For there to be unity in the condition of the channel power [7], i.e., $\boldsymbol{E}\{h^2\} = 1$, we have

$$\left(C(m+1)L^{m+1}\right)^2 = \frac{(m+2)R^2\left(L^2\left(R^2+L^2\right)\right)^{m+2}}{\left(R^2+L^2\right)^{m+2} - L^{2(m+2)}}, \tag{4.5}$$

and the values of $h_{\min}$ and $h_{\max}$ are given in [7] as

$$h_{\min} = \frac{RL^{(m+2)}(m+2)^{1/2}}{\left(R^2+L^2\right)^{1/2}\left(\left(R^2+L^2\right)^{m+2} - L^{2(m+2)}\right)^{1/2}}, \tag{4.6}$$

$$h_{\max} = \frac{RL^{(m+2)}(m+2)^{1/2}}{L\left(\left(R^2+L^2\right)^{m+2} - L^{2(m+2)}\right)^{1/2}}. \tag{4.7}$$

Consequently, noting that $\sigma_h^2 = \boldsymbol{E}\{h^2\} - \mu_h^2$, the mean value of the random channel gain

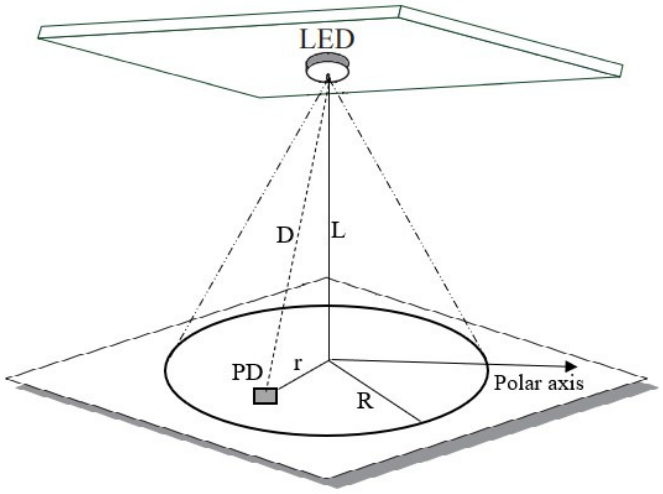

Figure 4.1: The SISO VLC system model.

h can be calculated as

$$\mu_h = \frac{(m+3)\Upsilon \times \left(RL^{(m+2)}(m+2)^{1/2}\right)^{\frac{m+1}{m+3}}}{(m+1) \times \left(\left(R^2+L^2\right)^{m+2} - L^{2(m+2)}\right)^{\frac{m+1}{2(m+3)}}} \left(\frac{1}{L^{\frac{m+1}{m+3}}} - \frac{1}{(L^2+R^2)^{\frac{m+1}{2(m+3)}}}\right). \tag{4.8}$$

4.3 Bayesian Cramér–Rao Lower Bound and Channel Estimation for Known ζ^2

In this section, considering that the factor ζ^2 is known, the BCRLB is firstly derived to get a benchmark to evaluate the performance of the presented estimators. Then, the details of the five estimators (ML, LS, MAP, LMMSE and MMSE) that are proposed to solve the random channel gain estimation problem in VLC systems are given. Furthermore, the numerical and simulation results of SISO-VLC performance are discussed in a system under the joint effects of SDSN and imperfect CSI. The results are analyzed by assuming that the factor ζ^2 is known for all considered estimators.

4.3.1 Bayesian Cramér–Rao Lower Bound (BCRLB)

Let it be assumed that a sequence of N pilot symbols, $\boldsymbol{x}$, is conveyed from the transmitter of the VLC system to the receiver in order to estimate the random channel gain, h, before the realization of data transmission. Denoting the pilot symbols as $\boldsymbol{x} = [x_1, x_2, \cdots, x_{\mathrm{N}}]^T$ and defining the various additive noises with $\boldsymbol{n} = [n_1, n_2, \ldots, n_{\mathrm{N}}]^T$, the received signal vector $\boldsymbol{y} = [y_1, y_2, \ldots, y_N]^T$ can be expressed by

$$\boldsymbol{y} = h\boldsymbol{x} + \sqrt{h\mathrm{diag}(\boldsymbol{x})}\boldsymbol{n}_{ds} + \boldsymbol{n}. \tag{4.9}$$

Note that the elements of $\boldsymbol{n}$ are independent and identically distributed (i.i.d.) Gaussian random variables with zero mean, i.e., $\boldsymbol{n} \sim \mathcal{N}(\boldsymbol{0}, \sigma_n^2 \boldsymbol{I}_N)$, where $\boldsymbol{I}_N$ is the identity matrix of size N. Now, suppose that the prior information of the channel gain PDF, $f_h(h)$, is available at the receiver, then the Bayesian information is given as [37]

$$J = \mathbf{E}\left\{I_f(h)\right\} + I_R, \tag{4.10}$$

where $I_f(h)$ denotes the Fisher information function and I_R represents the contribution of the prior information that can be calculated from

$$I_R = \mathbf{E}\left\{\left(\frac{\partial}{\partial h}\ln f_h(h)\right)^2\right\}. \tag{4.11}$$

Here, $\ln f_h(h)$ is the log-PDF of the random variable h, the first derivative with respect to h, which is obtained as

$$\frac{\partial}{\partial h}\ln f_h(h) = \left(\frac{-2}{m+3} - 1\right)\frac{1}{h}. \tag{4.12}$$

Substituting (4.12) into (4.11), I_R can be expressed by

$$I_R = \left(\frac{2}{m+3} + 1\right)^2 \mathbf{E}\left\{\frac{1}{h^2}\right\}. \tag{4.13}$$

Considering that the expected value of a random variable z can be determined by $\mathbf{E}\{g(z)\} = \int_{z_{\min}}^{z_{\max}} g(z) f_z(z) dz$, and by calculating the term $\mathbf{E}\left\{\frac{1}{h^2}\right\}$, (4.13) can be rewritten as

$$I_R = -\Upsilon \frac{(m+5)^2}{2(m+3)(m+4)} \left(h_{\max}^{(\frac{-2m-8}{m+3})} - h_{\min}^{(\frac{-2m-8}{m+3})} \right). \tag{4.14}$$

Following that, the term $\mathbf{E}\{I_f(h)\}$ in (4.10), which represents the contribution of the data, should be obtained to find the Bayesian information. Therefore, $I_f(h)$ is calculated first from

$$I_f(h) = -\mathbf{E}\left\{ \frac{\partial^2}{\partial h^2} \ln f(\boldsymbol{y}|h) \right\}, \tag{4.15}$$

where $\ln f(\boldsymbol{y}|h)$ is the log-likelihood function of the unknown channel h. Since we assume that all the samples are i.i.d., the joint PDF of N observations, which is also equal to the likelihood function of h, $f(\boldsymbol{y}|h)$, can be written as

$$f(\boldsymbol{y}|h) = \left(\prod_{i=1}^{N} \frac{1}{\sqrt{2\pi\sigma_n^2 (1+\zeta^2 h x_i)}} \right) \exp\left(-\frac{1}{2\sigma_n^2} \sum_{i=1}^{N} \frac{(y_i - h x_i)^2}{1+\zeta^2 h x_i} \right). \tag{4.16}$$

Taking the natural logarithm of $f(\boldsymbol{y}|h)$, we have

$$\ln f(\boldsymbol{y}|h) = -\frac{N}{2} \ln\left(2\pi\sigma_n^2\right) - \frac{1}{2} \sum_{i=1}^{N} \ln\left(1+\zeta^2 h x_i\right) - \frac{1}{2\sigma_n^2} \sum_{i=1}^{N} \frac{(y_i - h x_i)^2}{1+\zeta^2 h x_i}. \tag{4.17}$$

Thus, the first partial derivative of $\ln f(\boldsymbol{y}|h)$ with respect to h can be obtained as

$$\frac{\partial}{\partial h} \ln f(\boldsymbol{y}|h) = -\frac{1}{2} \sum_{i=1}^{N} \frac{\zeta^2 x_i}{1+\zeta^2 h x_i} + \frac{1}{2\sigma_n^2} \sum_{i=1}^{N} \frac{2x_i(y_i - h x_i)}{1+\zeta^2 h x_i} + \frac{\zeta^2 x_i (y_i - h x_i)^2}{(1+\zeta^2 h x_i)^2}. \tag{4.18}$$

Then, the second partial derivative is found to be

$$\begin{aligned} \frac{\partial^2}{\partial h^2} f(\boldsymbol{y}|h) = \frac{1}{2\sigma_n^2} \sum_{i=1}^{N} \frac{\sigma_n^2 (\zeta^2 x_i)^2}{(1+\zeta^2 h x_i)^2} - \Bigg[\frac{2(x_i)^2}{1+\zeta^2 h x_i} + \frac{2\zeta^2 (x_i)^2 (y_i - h x_i)}{(1+\zeta^2 h x_i)^2} + \\ \frac{2\zeta^2 (x_i)^2 (y_i - h x_i)}{(1+\zeta^2 h x_i)^2} + \frac{2(\zeta^2 x_i)^2 (y_i - h x_i)^2}{(1+\zeta^2 h x_i)^3} \Bigg]. \end{aligned} \tag{4.19}$$

Noting that $\mathbf{E}\{y_i\} = hx_i$ and $\mathbf{E}\{(y_i - hx_i)^2\} = \sigma_n^2(1+\zeta^2 hx_i)$, $I_f(h)$ in (4.10) can be written as follows

$$I_f(h) = \frac{1}{2}\sum_{i=1}^{N} \frac{(\zeta^2 x_i)^2}{(1+\zeta^2 hx_i)^2} + \frac{2x_i^2}{\sigma_n^2(1+\zeta^2 hx_i)}. \tag{4.20}$$

Without loss of generality, and assuming that $x_i = p$ $(\forall i = 1, \cdots, N)$, $\mathbf{E}\{I_f(h)\}$ can be expressed by

$$\mathbf{E}\{I_f(h)\} \frac{N\zeta^4 p^2}{2} \mathbf{E}\left\{\frac{1}{(1+\zeta^2 hp)^2}\right\} + \frac{Np^2}{\sigma_n^2}\mathbf{E}\left\{\frac{1}{(1+\zeta^2 hp)}\right\}. \tag{4.21}$$

Furthermore, utilizing (4.2), (4.21) can be rewritten as

$$\mathbf{E}\{I_f(h)\} = \frac{N\zeta^4 p^2}{2}\Upsilon \int_{h_{\min}}^{h_{\max}} \frac{h^{-(m+5)/(m+3)}}{(1+\zeta^2 hp)^2}\, dh + \frac{Np^2}{\sigma_n^2}\Upsilon \int_{h_{\min}}^{h_{\max}} \frac{h^{-(m+5)/(m+3)}}{(1+\zeta^2 hp)}\, dh. \tag{4.22}$$

After some mathematical manipulations, (4.22) can be rewritten as follows

$$\begin{aligned}\mathbf{E}\{I_f(h)\} = \Bigg[&-\frac{\Upsilon N\zeta^4 p^2}{4}(m+3)h^{\frac{-2}{(m+3)}}\, {}_2F_1\left(\frac{-2}{(m+3)}, 2; \frac{(m+1)}{(m+3)}; -ph\zeta^2\right) \\ &- \frac{\Upsilon Np^2}{2\sigma_n^2}(m+3)h^{\frac{-2}{m+3}}\, {}_2F_1\left(\frac{-2}{(m+3)}, 1; \frac{(m+1)}{(m+3)}; -ph\zeta^2\right)\Bigg]_{h_{min}}^{h_{max}}.\end{aligned} \tag{4.23}$$

Consequently, the BCRLB can be calculated from

$$\sigma_\epsilon^2 \geq \frac{1}{J}, \tag{4.24}$$

where J can be obtained by substituting (23) and (14) into (4.10).

Remark 1: The Fisher information function of the SISO-VLC system without SDSN can be obtained by substituting $\zeta = 0$ in (4.20), and thus, it can be written as follows

$$I_f(h) = \sum_{i=1}^{N} \frac{x_i^2}{\sigma_n^2}. \tag{4.25}$$

Additionally, assuming that $x_i = p$ $(\forall i = 1, \cdots, N)$, the contribution of the data, which is

defined in (4.21), turns into

$$\mathbf{E}\left\{I_f(h)\right\} = \frac{Np^2}{\sigma_n^2}. \tag{4.26}$$

Therefore, the BCRLB of the SISO-VLC system can be given in the absence of SDSN as follows

$$\sigma_\epsilon^2 \geq \left[\frac{Np^2}{\sigma_n^2} - \frac{\Upsilon(m+5)^2}{2(m+3)(m+4)}\left(h_{\max}^{(\frac{-2m-8}{m+3})} - h_{\min}^{(\frac{-2m-8}{m+3})}\right)\right]^{-1}. \tag{4.27}$$

It can be noted that the BCRLB is less than the CRLB given in [82], which is expected because of the prior information function. That is, the more information the receiver has about the channel gain, the less estimation error there will be [86].

4.3.2 Least Square (LS) Estimator

The LS estimator provides a less complex alternative to the ML estimator. In this method, no prior statistical information is needed. Instead, the estimated channel, $\hat{h}$, is expressed by

$$\hat{h}_{\text{LS}} = \frac{\boldsymbol{x}^T\boldsymbol{y}}{\|\boldsymbol{x}\|^2}. \tag{4.28}$$

In order to evaluate and compare the performance of the estimators, we calculate the MSE value, which is equivalent to the variance of the estimation error in the LS estimator. Considering that, the error of the LS estimator can be given as

$$\epsilon_{\text{LS}} = \hat{h}_{\text{LS}} - h. \tag{4.29}$$

On the other hand, $\hat{h}_{\text{LS}}$ can be expressed using (4.1) as

$$\hat{h}_{\text{LS}} = h + \frac{\boldsymbol{x}^T}{\|\boldsymbol{x}\|^2}\sqrt{h\text{diag}(\boldsymbol{x})}\boldsymbol{n}_{\text{ds}} + \frac{\boldsymbol{x}^T}{\|\boldsymbol{x}\|^2}\boldsymbol{n}. \tag{4.30}$$

Realizing that $\mathbf{E}\{\hat{h}_{\text{LS}}\} = \mu_h$ from (4.30), it can be concluded that the LS estimator is unbiased. Furthermore, utilizing both (4.29) and (4.30), ϵ_{LS} can be written as

$$\epsilon_{\text{LS}} = \frac{\boldsymbol{x}^T}{\|\boldsymbol{x}\|^2}\left(\sqrt{h\text{diag}(\boldsymbol{x})}\boldsymbol{n}_{\text{ds}} + \boldsymbol{n}\right). \tag{4.31}$$

It can be noted from (4.31) that ϵ_{LS} is a Gaussian random variable, i.e., $\epsilon_{\text{LS}} \sim \mathcal{N}(0, \sigma^2_{\epsilon_{\text{LS}}})$. Here, the variance of the estimation error, $\sigma^2_{\epsilon_{\text{LS}}}$, is inversely proportional to the pilots' SNR value, and it can be given by

$$\sigma^2_{\epsilon_{\text{LS}}} = \frac{\sigma_n^2 \sum_{i=1}^{N} x_i^2(1 + \zeta^2\mu_h x_i)}{\left(\sum_{i=1}^{N} x_i^2\right)^2}. \tag{4.32}$$

Now, assuming that the transmitted pilot $x_i = p$ for all i, $\sigma^2_{\epsilon_{LS}}$ can be simplified as follows

$$\sigma^2_{\epsilon_{\text{LS}}} = \frac{\sigma_n^2(1 + \zeta^2\mu_h p)}{Np^2}. \tag{4.33}$$

It is also worth noting that the error variance for the LS estimator, which gives the MSE, becomes $\sigma^2_{\epsilon_{LS}} = \frac{\sigma_n^2}{Np^2}$ for $\zeta^2 = 0$. This is not a surprising result, since it is traditionally well-known for the case of no SDSN. However, in the presence of the SDSN and large p, the MSE can be approximated as $\sigma^2_{\epsilon\text{LS}} = \frac{\sigma_h^2\zeta^2\mu_h}{Np}$. It is important to note the implication of this on the decay of the MSE, namely that the decay is mitigated by the presence of SDSN (i.e., proportional to $1/p$) and remains much more dramatic in its absence (proportional to $1/p^2$).

4.3.3 Maximum Likelihood (ML) Estimator

The ML estimator can be defined as finding the value of the parameter h, such that the likelihood function is maximized. Applying this estimator, the channel gain of the VLC system can be calculated by making (4.18) equal to zero and then solving it for h as follows

$$\frac{\partial}{\partial h}\ln f(\boldsymbol{y}|h) = \frac{-1}{2}\sum_{i=1}^{N}\frac{\zeta^2 x_i}{1+\zeta^2 h x_i} + \frac{1}{2\sigma_n^2}\sum_{i=1}^{N}\left[\frac{2x_i(y_i - hx_i)}{1+\zeta^2 h x_i} + \frac{\zeta^2 x_i (y_i - hx_i)^2}{(1+\zeta^2 h x_i)^2}\right] = 0 \tag{4.34}$$

If we assume that the same pilot signals are sent each time, i.e., $x_i = p$ for all i, then the estimated value of h can be found to be

$$-\hat{h}^2 + B\hat{h} + C = 0, \tag{4.35}$$

Taking into account that the channel gain h cannot be negative, $\hat{h}$ can be calculated as

$$\hat{h}_{\mathrm{ML}} = \frac{B + \sqrt{B^2 + 4C}}{2}, \tag{4.36}$$

where B and C are given by

$$B = -\frac{\sigma_n^2 \zeta^2}{p} - \frac{2}{\zeta^2 p}, \tag{4.37}$$

and

$$C = -\frac{\sigma_n^2}{p^2} + 2\frac{\sum_{i=1}^{N} y_i}{Np^2\zeta^2} + \frac{\sum_{i=1}^{N} y_i^2}{Np^2}. \tag{4.38}$$

Since it is difficult to calculate the MSE of the ML estimator analytically, the performance of the ML estimator will be studied using simulation results.

Remark 2: Please note from (4.34) that in the absence of SDSN, i.e., $\zeta^2 = 0$,

$$\frac{\partial}{\partial h}\ln f(\boldsymbol{y}|h) = \frac{1}{2\sigma_n^2}\sum_{i=1}^{N}\frac{2x_i(y_i - hx_i)}{1+\zeta^2 h x_i} = 0 \tag{4.39}$$

Assuming that $x_i = p$ $(\forall i = 1, \cdots, N)$, the channel gain can be calculated as $\hat{h}_{\mathrm{ML}} = \frac{\sum_{i=1}^{N} y_i}{Np}$, which is equal to $\hat{h}_{\mathrm{LS}}$ in (4.28). This means that in the absence of SDSN, both ML and LS have the same performance, which consequently means that the MSE of ML equals that of the LS which equals $\frac{\sigma_n^2}{Np^2}$ at $\zeta^2 = 0$.

Remark 3: Although our derived ML estimator is biased, i.e., $\mathbf{E}\{\hat{h}_{\mathrm{ML}}\} \neq \mathbf{E}\{h\}$, it is asymptotically unbiased [2] indeed. In other words, $\mathbf{E}\{\hat{h}_{\mathrm{ML}}\} = \mathbf{E}\{h\}$ at very large numbers of symbols, i.e. $N \to \infty$. Therefore, with a large number of symbols, N, the ML is unbiased and achieves the CRLB, i.e., $\hat{h}_{\mathrm{ML}} \sim \mathcal{N}(h, \mathrm{CRLB})$ [87], where CRLB equals the inverse of the Fisher information function given in (4.20). Assuming that $x_i = p$ $(\forall i = 1, \cdots, N)$, the CRLB can be written as

$$\mathrm{CRLB} = \frac{2\sigma_n^2}{Np^2} \frac{(1 + \zeta^2 hp)^2}{\zeta^4 \sigma_n^2 + 2\zeta^2 hp + 2}. \tag{4.40}$$

Channel estimation is affected by the transmitted power, noise variance σ_n^2, SDSN factor ζ^2 and the number of pilots; therefore, it is challenging to know the sufficient number of symbols to get an unbiased ML estimator.

Table 4.1 plots the values of $\mathbf{E}\{\hat{h}_{\mathrm{ML}}\}$ against the number of symbols N, is provided to study the real value of convergence for different values of ζ^2, σ_n^2 and different transmitted power levels. It can be noticed from this table that more samples are required to get an acceptable convergence level at higher ζ^2. Furthermore, with an increase in the noise variance σ_n^2, more pilots need to be sent for a satisfactory convergence. In particular, at $p = 0$ dB, $\zeta^2 = 5$, and $N = 1$, $\mathbf{E}\{\hat{h}_{\mathrm{ML}}\} = 0.648$ at $\sigma_n^2 = 0.1$, while it equals to 0.6602 at $\sigma_n^2 = 1$ at the same values of p, ζ^2 and N. It can also be proven by simulation that $\mathbf{E}\{\hat{h}_{\mathrm{ML}}\} \approx \mathbf{E}\{h\}$, while transmitting 20 symbols.

[2] An estimator of a given random parameter, e.g., h, is said to be unbiased if its expected value is equal to mean of the parameter that should be estimated.

Table 4.1: $\mathbf{E}\{\hat{h}_{\mathrm{ML}}\}$ at different number of pilots N at $\mathbf{E}\{h\} = 0.8$, different power levels, two different values of ζ^2 and two different σ_n^2 values

	$\sigma_n^2 = 0.1$					
	$\zeta^2 = 5$			$\zeta^2 = 10$		
N/p	0	10	20	0	10	20
1	0.648	0.775	0.797	0.637	0.752	0.795
5	0.767	0.795	0.799	0.760	0.791	0.799
10	0.783	0.797	0.799	0.779	0.795	0.799
20	0.792	0.798	0.799	0.789	0.797	0.799
30	0.794	0.799	0.799	0.793	0.798	0.799
	$\sigma_n^2 = 1$					
1	0.6602	0.6663	0.7756	0.7125	0.6534	0.7521
5	0.7630	0.7704	0.7953	0.7779	0.7634	0.7910
10	0.7804	0.7851	0.7976	0.7895	0.7814	0.7955
20	0.7901	0.7927	0.7988	0.7940	0.7904	0.7978
30	0.7934	0.7951	0.7991	0.7968	0.7939	0.7986

4.3.4 Linear Minimum Mean Square Error (LMMSE) Estimator

The LMMSE estimator is a linear estimator that minimizes the MSE and can be defined by $\mathbf{E}\{[\hat{h} - h]^2\}$. Considering that, the estimated channel, $\hat{h}_{\mathrm{LMMSE}}$, can be written as [87]

$$\hat{h}_{\mathrm{LMMSE}} = \frac{\sigma_h^2 \|\boldsymbol{x}\|^2 \boldsymbol{x}^T (\boldsymbol{y} - \boldsymbol{x}\mu_h)}{\sigma_h^2 \|\boldsymbol{x}\|^4 + \mu_h \zeta^2 \sigma_n^2 \boldsymbol{x}^T \mathrm{diag}(x_i)\boldsymbol{x} + \sigma_n^2 \|\boldsymbol{x}\|^2} + \mu_h, \tag{4.41}$$

where μ_h is the mean of the channel h, and σ_h^2 represents its variance that can be calculated from $\sigma_h^2 = \boldsymbol{E}\{h^2\} - (\mu_h)^2$.

Given that $\hat{h}_{\mathrm{LMMSE}} = h + \epsilon_{\mathrm{LMMSE}}$, it can be said that the estimation error $\epsilon_{\mathrm{LMMSE}}$ is a Gaussian random variable with $\epsilon_{\mathrm{LMMSE}} \sim \mathcal{N}(0, \sigma^2_{\epsilon_{\mathrm{LMMSE}}})$. Here, $\sigma^2_{\epsilon_{\mathrm{LMMSE}}}$ can be derived as

$$\sigma^2_{\epsilon_{\mathrm{LMMSE}}} = \sigma_h^2 \left[\frac{\mu_h \zeta^2 \sigma_n^2 \boldsymbol{x}^T \mathrm{diag}(x_i)\boldsymbol{x} + \sigma_n^2 \|\boldsymbol{x}\|^2}{\sigma_h^2 \|\boldsymbol{x}\|^4 + \mu_h \zeta^2 \sigma_n^2 \boldsymbol{x}^T \mathrm{diag}(x_i)\boldsymbol{x} + \sigma_n^2 \|\boldsymbol{x}\|^2} \right]. \tag{4.42}$$

Finally, assuming $x_i = p$ $(\forall i = 1, \cdots, N)$, and considering that $\boldsymbol{x}^T \text{diag}(x_i)\boldsymbol{x} = \sum_{i=1}^{N}(x_i)^3$, then (4.42) can be rewritten in a simplified form as follows

$$\sigma^2_{\epsilon_{\text{LMMSE}}} = \sigma^2_h \sigma^2_n \frac{1 + \mu_h \zeta^2 p}{\sigma^2_h N p^2 + [\mu_h \zeta^2 p + 1]\, \sigma^2_n}. \tag{4.43}$$

Remark 4: Various observations can be made from (4.43) all of which can be summarized as follows: *i)* At very low levels of transmitted power, i.e., $p \to 0$, the MSE approaches to σ^2_h, i.e., $\sigma^2_{\epsilon_{\text{LMMSE}}} \approx \sigma^2_h$. Indeed, this is obvious, since the samples are highly corrupted by the thermal noise and the MSE depends only on the prior information. *ii)* As the power increases, the MSE approximates to $\frac{\sigma^2_n \mu_h}{Np}$. In this case, the estimation does not depend on the variance of the channel gain σ^2_h. It depends on the mean of the channel gain μ_h of the prior information.

4.3.5 Maximum Posterior Probability (MAP) Estimator

It is known that a posterior function of $f(h|\boldsymbol{y})$ includes all information of the channel gain h. An estimator that finds the channel gain h maximizing the posterior function is called MAP estimator. According to this, the random channel gain h can be estimated from

$$\hat{h}_{\text{MAP}} = \arg\max_h f(h|\boldsymbol{y}) = \arg\max_h \ln f(h|\boldsymbol{y}), \tag{4.44}$$

where $f(h|\boldsymbol{y})$ can be given as

$$f(h|\boldsymbol{y}) = \frac{f(\boldsymbol{y}|h) f_h(h)}{f_{\boldsymbol{Y}(\boldsymbol{y})}}. \tag{4.45}$$

It is clear from (4.44) that the maximum value of the log-posteriori function, $\ln f(h|\boldsymbol{y})$, can be calculated in order to find $\hat{h}_{\text{MAP}}$. Thus, it is solved by using the following equation

$$\frac{\partial}{\partial h} \ln \frac{f(\boldsymbol{y}|h) f_h(h)}{f_{\boldsymbol{Y}(\boldsymbol{y})}} = 0. \tag{4.46}$$

Since $f_{\boldsymbol{Y}(\boldsymbol{y})}$ is a constant with respect to h, therefore, by substituting (4.16) and (4.2) into (4.46), we have

$$\frac{\partial}{\partial h}\Big[\frac{-N}{2}\ln\left(2\pi\sigma_n^2\right)-\frac{1}{2}\sum_{i=1}^{N}\ln\left(1+\zeta^2 h x_i\right)-\frac{1}{2\sigma_n^2}\sum_{i=1}^{N}\frac{(y_i-hx_i)^2}{1+\zeta^2 h x_i}-\frac{(m+5)}{(m+3)}\ln h-\ln f_{\boldsymbol{Y}(\boldsymbol{y})}\Big]=0. \tag{4.47}$$

Now, solving the derivation in (4.47) results in

$$-\frac{(m+5)}{(m+3)}\frac{1}{h}-\frac{1}{2}\sum_{i=1}^{N}\frac{\zeta^2 x_i}{1+\zeta^2 h x_i}+\frac{1}{2\sigma_n^2}\sum_{i=1}^{N}\left[\frac{2x_i(y_i-hx_i)}{1+\zeta^2 h x_i}+\frac{\zeta^2 x_i(y_i-hx_i)^2}{(1+\zeta^2 h x_i)^2}\right]=0. \tag{4.48}$$

Assuming that $x_i = p$ $(\forall i = 1,\ldots,N)$, the channel gain, h, can be found by solving: $h^3 + Bh^2 + Ch + D = 0$, the parameters of which are equal to

$$\begin{aligned}
B &= \frac{1}{Np}\left(N\sigma_n^2\zeta^2+\frac{2N}{\zeta^2}+2\sigma_n^2\zeta^2\frac{(m+5)}{(m+3)}\right),\\
C &= \frac{1}{p^2N}\left(N\sigma_n^2-\frac{2\sum_{i=1}^{N}y_i}{\zeta^2}-\sum_{i=1}^{N}y_i^2+4\sigma_n^2\frac{(m+5)}{(m+3)}\right),\\
D &= \frac{(m+5)}{(m+3)}\frac{2\sigma_n^2}{\zeta^2p^3N}.
\end{aligned} \tag{4.49}$$

The solution can be found numerically by taking into account that channel gain h should be real positive. It can be noticed that it is hard to find a closed form for this solution. So, the performance of the MAP estimator will be investigated by using Monte Carlo simulations.

4.3.6 Minimum Mean Square Error (MMSE) Estimator

The MMSE is an estimation method that minimizes the mean squared error, which means it is optimal in a statistical sense. The MMSE estimator is actually the expectation of the

posterior function $f(h|\boldsymbol{y})$. Therefore, the estimated channel gain is obtained as

$$\hat{h}_{\text{MMSE}} = \mathbf{E}\left\{h|\boldsymbol{y}\right\}, \tag{4.50}$$

where $f(h|\boldsymbol{y})$ is given in (4.45). Using Bayes' theorem, the MMSE estimator can also be defined as follows [87]

$$\begin{aligned}\hat{h}_{\text{MMSE}} &= \int_{h_{\min}}^{h_{\max}} \frac{h f(\boldsymbol{y}|h)\ f_h(h)}{f_{\boldsymbol{Y}(\boldsymbol{y})}}\ dh \\ &= \frac{\Upsilon}{f_{\boldsymbol{Y}(\boldsymbol{y})}(2\pi\sigma_n^2)^{N/2}} \int_{h_{\min}}^{h_{\max}} h^{\frac{-2}{m+3}} \left[\prod_{i=1}^{N} \frac{1}{\sqrt{(1+\zeta^2 h x_i)}}\right] \exp\left(-\frac{1}{2\sigma_n^2}\sum_{i=1}^{N}\frac{(y_i - h x_i)^2}{1+\zeta^2 h x_i}\right) dh.\end{aligned} \tag{4.51}$$

In case of that $x_i = p\ (\forall i = 1 \ldots N)$, $\hat{h}_{\text{MMSE}}$ is given by

$$\hat{h}_{\text{MMSE}} = \frac{\Upsilon}{f_{\boldsymbol{Y}}(\boldsymbol{y})(2\pi\sigma_n^2)^{N/2}} \int_{h_{\min}}^{h_{\max}} \frac{h^{\frac{-2}{m+3}}}{(1+\zeta^2 h p)^{\frac{N}{2}}} \exp\left(-\frac{1}{2\sigma_n^2}\sum_{i=1}^{N}\frac{(y_i - h p)^2}{1+\zeta^2 h p}\right) dh. \tag{4.52}$$

Moreover, $f_{\boldsymbol{Y}}(\boldsymbol{y})$ in (4.51) represents the marginal PDF of y, which can be given as

$$\begin{aligned} f_{\boldsymbol{Y}(\boldsymbol{y})} &= \prod_{i=1}^{N} f_{Y_i}(y_i) = \prod_{i=1}^{N} \int_{h_{\min}}^{h_{\max}} f(y_i|h) f_h(h)\ dh \\ &= \frac{\Upsilon^N}{(2\pi\sigma_n^2)^{N/2}} \prod_{i=1}^{N} \left[\int_{h_{\min}}^{h_{\max}} \frac{h^{\frac{-2}{m+3}-1}}{\sqrt{(1+\zeta^2 h x_i)}} \exp\left(\frac{-(y_i - h x_i)^2}{2\sigma_n^2(1+\zeta^2 h x_i)}\right)\ dh\right]. \end{aligned} \tag{4.53}$$

Assuming also that $x_i = p\ (\forall i = 1 \ldots N)$ here, (4.53) can be simplified as follows

$$f_{\boldsymbol{Y}(\boldsymbol{y})} = \frac{\Upsilon^N}{(2\pi\sigma_n^2)^{N/2}} \prod_{i=1}^{N} \left[\int_{h_{\min}}^{h_{\max}} \frac{h^{\frac{-2}{m+3}-1}}{\sqrt{(1+\zeta^2 h p)}} \exp\left(\frac{-(y_i - h p)^2}{2\sigma_n^2(1+\zeta^2 h p)}\right)\ dh\right]. \tag{4.54}$$

Consequently, by taking advantage of (4.52) and (4.54), the estimated channel gain $\hat{h}_{\text{MMSE}}$ can be written as

$$\hat{h}_{\text{MMSE}} = \Upsilon^{(-N+1)} \frac{\int_{h_{\min}}^{h_{\max}} \frac{h^{\frac{-2}{m+3}}}{(1+\zeta^2 hp)^{\frac{N}{2}}} \exp\left(-\frac{1}{2\sigma_n^2} \sum_{i=1}^{N} \frac{(y_i - hp)^2}{1+\zeta^2 hp}\right) dh}{\prod_{i=1}^{N} \int_{h_{\min}}^{h_{\max}} \frac{h^{\frac{-2}{m+3}-1}}{\sqrt{(1+\zeta^2 hp)}} \exp\left(\frac{-(y_i - hp)^2}{2\sigma_n^2 (1+\zeta^2 hp)}\right) dh}. \tag{4.55}$$

4.4 Channel Estimation for Two Special Cases

Considering the previous section, it is appreciable that the LS and LMMSE are the least complex estimation methods, since they are linear functions of the received samples $y(n)$, i.e., $\hat{h} = \sum_{n=0}^{N-1} \alpha(n) y(n)$, where $\alpha(n)$ is a constant that can be found from (4.28) for $\hat{h}_{LS}$, and can be calculated from (4.41) for $\hat{h}_{\text{LMMSE}}$. However, when prior statistical information is available, the LMMSE technique demonstrates a significant improvement in estimation performance as compared to the LS, even though applying LMMSE requires ζ^2 to be known at the receiver.

In this section, we consider: *i)* the case of unknown ζ^2 at the receiver side, while using the LMMSE estimator, and *ii)* joint ML estimation for both ζ^2 and h. These special cases are investigated in the following two subsections.

4.4.1 LMMSE Estimation for h under the case of Unknown ζ^2

In this section, we study the effect of ignoring the effect of ζ^2 on the performance of the LMMSE by writing $\zeta^2 = 0$ in (4.41), while assuming that μ_h and σ_h^2 are known at the receiver. In this case, the LMMSE estimator can be defined as (since ζ^2 is unknown)

$$\breve{h}_{\text{LMMSE}} = \frac{\sigma_h^2 \boldsymbol{x}^T (\boldsymbol{y} - \boldsymbol{x}\mu_h)}{\sigma_h^2 \|\boldsymbol{x}\|^2 + \sigma_n^2} + \mu_h, \tag{4.56}$$

and the MSE can be expressed by

$$\mathrm{MSE}_{\breve{h}} = \sigma_h^2 - \frac{\sigma_h^4}{\sigma_h^2 + \frac{\sigma_n^2}{Np^2}} + \frac{\sigma_h^4 \mu_h \zeta^2 \frac{\sigma_n^2}{Np}}{(\sigma_h^2 + \frac{\sigma_n^2}{Np^2})^2}. \tag{4.57}$$

It can be clearly seen from the above equation that the MSE with the knowledge of ζ^2 in (4.43) is less than MSE with unknown ζ^2.

The difference between the MSE considering ζ^2 in (4.43) and the MSE ignoring ζ^2 in (4.57) can be easily found as

$$\Delta = \frac{\sigma_h^4 \mu_h \zeta^2 \frac{\sigma_n^2}{Np}}{(\sigma_h^2 + \frac{\sigma_n^2}{Np^2})^2}. \tag{4.58}$$

Here, Δ is maximized at $p = \sqrt{\frac{3\sigma_n^2}{N\sigma_h^2}}$, and it is at this point that the difference between the two MSE curves is the largest.

Although we study the effect of ignoring SDSN on the performance of the LMMSE estimator only for simplicity, our results can be generalized for all estimators depending on ζ^2.

4.4.2 Joint ML Estimation for Unknown ζ^2 and Unknown h

In this section, we assume that the scaling factor ζ^2 and the channel gain h are both unknown. In that case, in order to estimate the channel gain h, we first estimate ζ^2 from

$$\frac{\partial}{\partial \zeta^2} \ln f(\boldsymbol{y}|h) = -\frac{1}{2} \sum_{i=1}^{N} \frac{h x_i}{1 + \zeta^2 h x_i} + \frac{1}{2\sigma_n^2} \sum_{i=1}^{N} \frac{h x_i (y_i - h x_i)^2}{(1 + \zeta^2 h x_i)^2} = 0. \tag{4.59}$$

Assuming that $x_i = p$ $(\forall i = 1, \ldots, N)$, the estimation of ζ^2 can be given for the ML estimator as

$$\hat{\zeta^2}_{\mathrm{ML}} = \frac{1}{\sigma_n^2 N h p} \sum_{i=1}^{N} (y_i - hp)^2 - \frac{1}{hp}. \tag{4.60}$$

Then, the channel gain h can be calculated by substituting (4.60) in (4.34) and solving numerically for h (because it is complex to find a solution mathematically).

4.5 Receiver Designs And Performance Analysis

One of the significant effects of the SDSN in VLC systems is the change in the PDF of the observations on $\boldsymbol{y}$, which makes proposing a new receiver design that is compatible to the modifications of the PDF an absolute must. OOK is the most common single carrier modulation (SCM) used to modulate VLC signals (IEEE 802.15.7). It is a simple modulation method, where a data bit "1" is sent by turning the LED on and a data bit "0" is sent by turning it off. Indeed, OOK can be considered a special case of M-PAM, specifically where $x = 2A$ (the DC bias $d = A$).

Consider the following two hypotheses: *i)* H_1, which is the signal present hypothesis, and *ii)* H_0, which is the noise-only hypothesis. These hypotheses can be symbolically written for N pilot symbols as

$$\begin{aligned} H_1 &: \boldsymbol{y} = h\boldsymbol{x} + \sqrt{h\text{diag}(\boldsymbol{x})}\boldsymbol{n}_{ds} + \boldsymbol{n}, \\ H_0 &: \boldsymbol{y} = \boldsymbol{n}. \end{aligned} \tag{4.61}$$

Then, we have to choose between the two hypotheses H_0 and H_1 to decide on the appropriate symbol.

The PDFs under these two hypotheses are denoted by $f(\boldsymbol{y}; h, H_1)$ and $f(\boldsymbol{y}; h, H_0)$, respectively, which can be given as follows

$$f(\boldsymbol{y}; h, H_1) = \left(\prod_{i=1}^{N} \frac{1}{\sqrt{2\pi\sigma_n^2 \left(1 + \zeta^2 h x_i\right)}} \right) \exp\left(-\frac{1}{2\sigma_n^2} \sum_{i=1}^{N} \frac{(y_i - h x_i)^2}{1 + \zeta^2 h x_i} \right) \tag{4.62}$$

$$f(\boldsymbol{y}; h, H_0) = \left(\prod_{i=1}^{N} \frac{1}{\sqrt{2\pi\sigma_n^2}} \right) \exp\left(-\frac{1}{2\sigma_n^2} \sum_{i=1}^{N} y_i^2 \right). \tag{4.63}$$

Then, the likelihood ratio can be written by

$$\Lambda(\boldsymbol{y}) = \frac{f(\boldsymbol{y}; h, H_1)}{f(\boldsymbol{y}; h, H_0)}. \tag{4.64}$$

Assuming that the probabilities of the two hypotheses are equal, i.e., $p(H_1) = p(H_0)$, an optimal ML receiver can be designed as follows

$$\Lambda(\boldsymbol{y}) = \frac{f(\boldsymbol{y}; h, H_1)}{f(\boldsymbol{y}; h, H_0)} \underset{H_0}{\overset{H_1}{\gtrless}} 1 \tag{4.65}$$

Now, keeping in mind that OOK is in effect, the ML decision rule can be defined by [82]:

$$\hat{x}_{ML} = \begin{cases} H_0 & \text{if } \frac{\zeta^2}{2} y^2 + y < hA + \frac{\sigma_n^2}{4Ah} \left[1 + 2Ah\zeta^2\right] \ln \left[1 + 2Ah\zeta^2\right], \\ H_1 & \text{otherwise.} \end{cases} \tag{4.66}$$

In the case of imperfect CSI, where the channel gain h is unknown, the ML receiver first estimates the gain h and then employs it in the same decision rule given for the perfect CSI case in (4.66), as follows

$$\hat{x}_{ML} = \begin{cases} H_0 & \text{if } \frac{\zeta^2}{2} y^2 + y < \hat{h}A + \frac{\sigma_n^2}{4A\hat{h}} \left[1 + 2A\hat{h}\zeta^2\right] \ln \left[1 + 2A\hat{h}\zeta^2\right], \\ H_1 & \text{otherwise.} \end{cases} \tag{4.67}$$

4.6 Simulation Results and Discussion

In this section, the numerical results of the SISO-VLC system performance are discussed considering both SDSN and imperfect CSI for various estimators. The provided results are obtained using Monte Carlo simulations, each of which is realized for 10^5 symbols.

Firstly, the MSE results of the proposed estimators, namely LS, ML, LMMSE, MAP, and MMSE, are given with an increasing source power in Fig. 4.2, and compared to the BCRLB for one pilot, while $\sigma_n^2 = 0.1$ and $\zeta^2 = 10$. It can be observed from Fig. 4.2

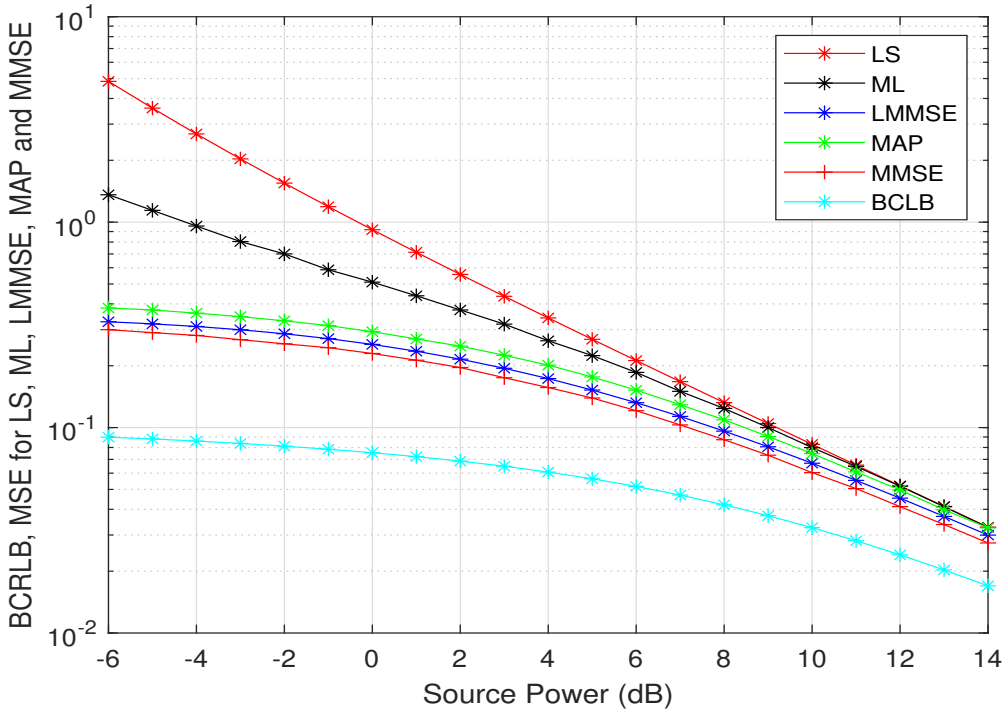

Figure 4.2: The BCRLB and the MSE values of the LS, ML, LMMSE, MAP, and MMSE estimators versus the source power for $\sigma_n^2 = 0.1$ and $\zeta^2 = 10$.

that the LS estimator has the highest MSE among all considered estimators, while on the other hand, MMSE has the lowest MSE. The differences between the MSE of the studied estimators shrink at the cost of additional power. Moreover, it can be noticed from Fig. 4.2 that the MSE values for both LS and ML increase inversely with source power. However, the BCRLB and the MSE of the other estimators (MAP, LMMSE and MMSE) approach a certain value, which provides better performance at low power levels. Consequently, it can be said that the estimators considering prior information generally have better performances than the estimators that do not.

Fig. 4.3 demonstrates the effect of increasing SDSN levels i.e., ζ^2 on the system performance. The figure plots the curves at low SDSN ($\zeta^2 = 2$) and at high SDSN ($\zeta^2 = 10$) at constant shot noise i.e. $\sigma_n^2 = 0.1$. Clearly, an increase in ζ^2 results increases the MSE of the estimators and the BCLB as well. Furthermore, it can be noticed from the figure that

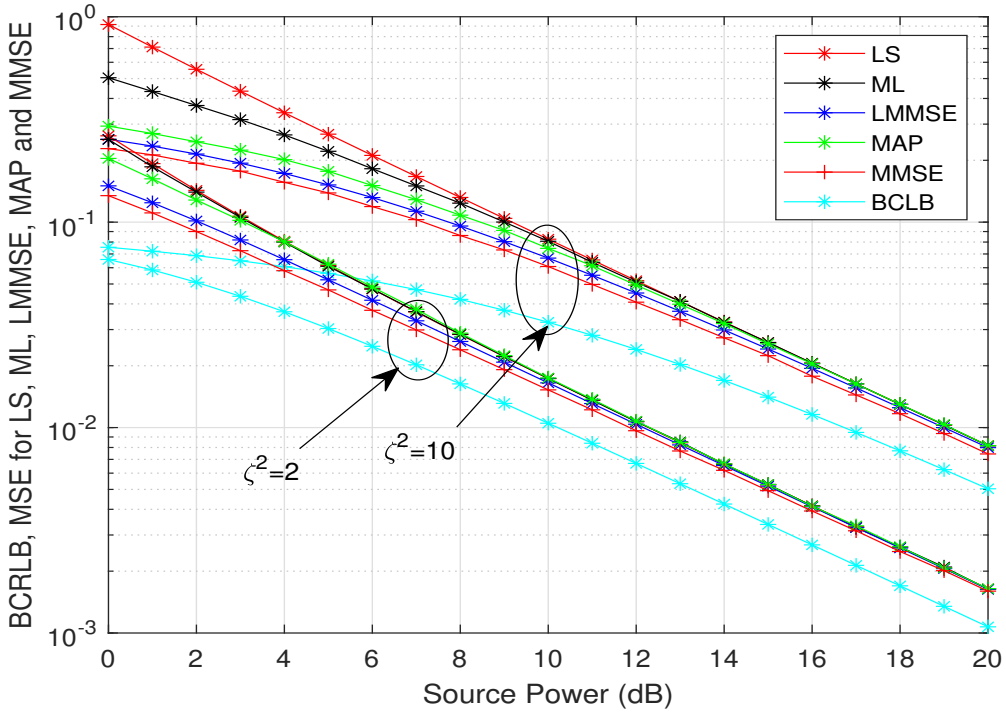

Figure 4.3: The BCRLB and the MSE values of the proposed estimators versus the source power for $\sigma_n^2 = 0.1$ at different values of ζ^2.

the curves of ML and LS approach each other as ζ^2 decreases. The gap between the two curves keeps shrinking until they have exactly the same MSE value at $\zeta^2 = 0$, as stated in Remark 2, which is consistent with the results provided in [82].

The effect of the shot noise on the estimators' performances is introduced in Fig. 4.4. It is rather clear that the MSE values of all estimators as well as the BCRLB are higher at $\sigma_n^2 = 0.1$ compared to $\sigma_n^2 = 0.01$. The implication of this is that σ_n^2 negatively affects the estimation performance of the system. Moreover, it can be observed from Fig. 4.4 that the gaps not only between the MSE values of the estimators but also between the estimators and the BCLRB widen with increasing values of σ_n^2. Consequently, the study of the system performance for different estimators provides more benefits when the shot noise level increases. Moreover, all studied estimators give similar results at high power.

Fig. 4.5 introduces the MSE of the LMMSE estimator when considering and ignoring

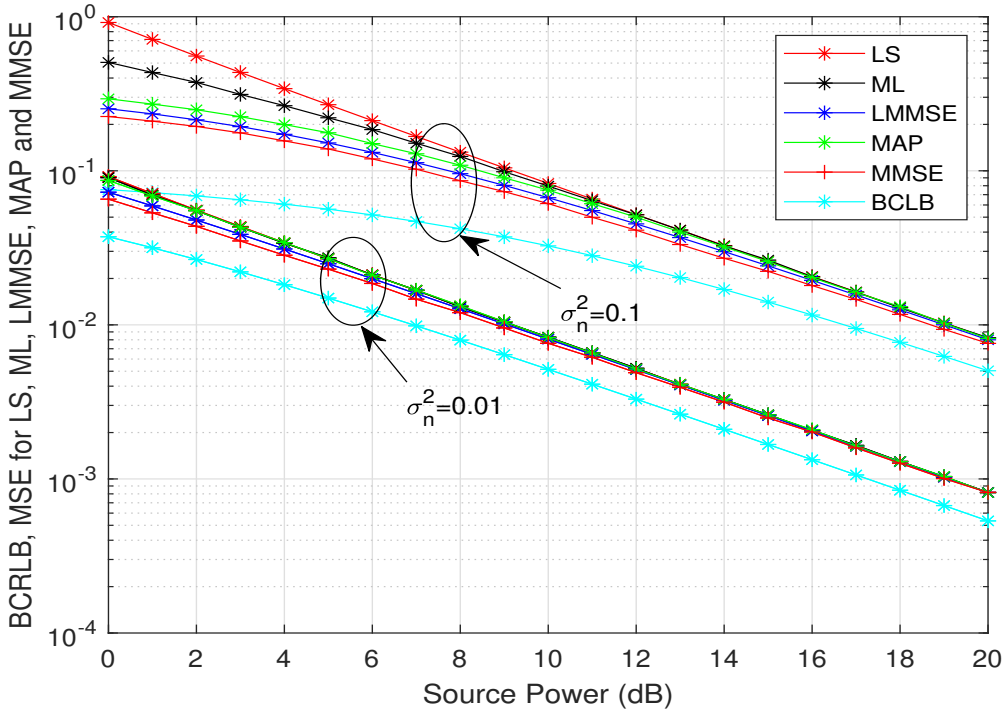

Figure 4.4: The BCRLB and the MSE values of the proposed estimators versus the source power for $\zeta^2 = 10$ at different values of σ_n^2.

the existence of SDSN. The MSE results of the LMMSE estimator that ignores the SDSN are presented by the curves named LMMSE-Ign in this figure. Interestingly, it is observed that the effect of ignoring ζ^2 has less of an impact on either very small or high values of the power. However, it has a higher impact on the region between -10 dB and 10 dB for $\sigma_n^2 = 0.1$ and between -5 dB and 15 dB $\sigma_n^2 = 1$, which causes the higher MSE seen in the figure. Indeed this depends on the value of σ_n^2.

Fig. 4.5 also illustrates that the difference between the LMMSE and LMMSE-Ign increases with ascending power until a certain value, and then decreases from there. This trend is compatible with (4.9). Returning to (4.9), it can also be noticed that the term hx is dominant at very high power values. This diminishes the effect of ζ^2, leading to minimizing the gap between the curve of MSE considering the existence of ζ^2 (LMMSE) and the curve of MSE ignoring the existence of ζ^2 (LMMSE-Ign). On the other hand, the

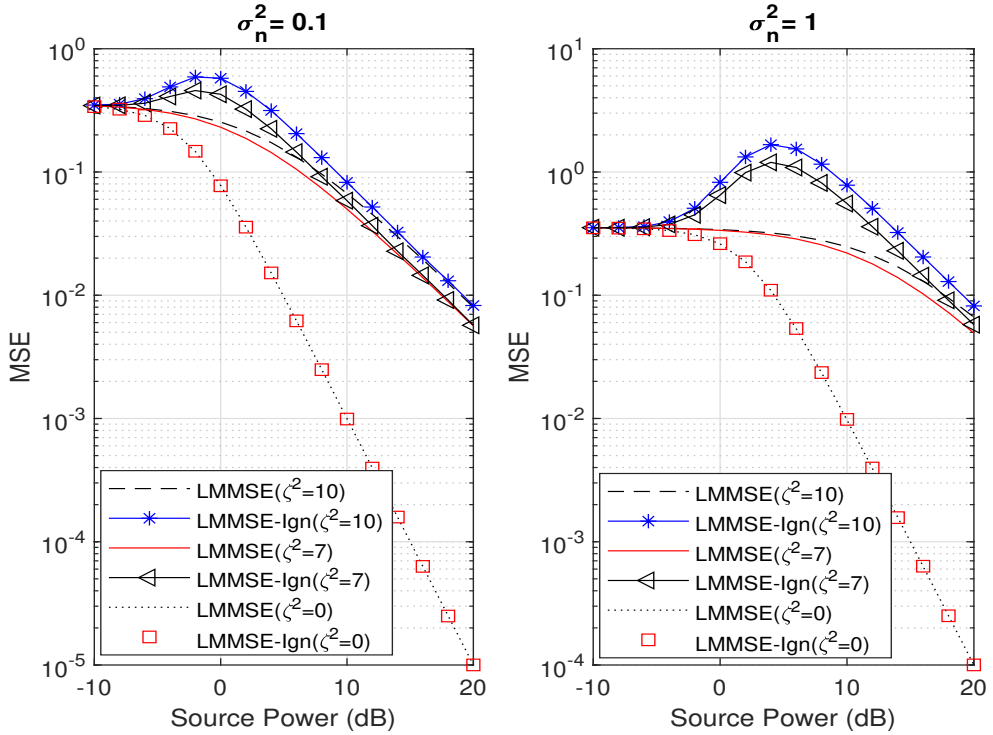

Figure 4.5: The MSE of the LMMSE and LMMSE-Ign versus the source power for $\sigma_n^2 = 0.1$ and $\sigma_n^2 = 1$ at different values of ζ^2.

shot noise n in (4.9) is the dominant term at very low power values, leading to an implicit suppression of any effect that ζ^2 may have.

A conclusion can be made that, although considering the existence of the SDSN in estimation the channel of the VLC system causes some additional complexity at the estimator as in (4.41), a hefty performance improvement can be observed. In Fig. 4.5, considering the SDSN when estimating the channel gain h (LMMSE) dropped the MSE of the system more than 80% compared to the MSE of the estimation ignoring the SDSN at $\sigma_n^2 = 1$ and $\zeta^2 = 10$. A drop of more than 55% can be obtained at $\sigma_n^2 = 0.1$ and $\zeta^2 = 10$. This enhancement increases with two factors, namely ζ^2 and σ_n^2. It is worth noting that the curves of the LMMSE and LMMSE-Ign are exactly matched at $\zeta^2 = 0$ as expected from the theoretical analysis. Fig. 4.6 compares two curves. The first one is the MSE of estimating the channel gain h using the ML estimator. In this technique, the unknown ζ^2 is estimated

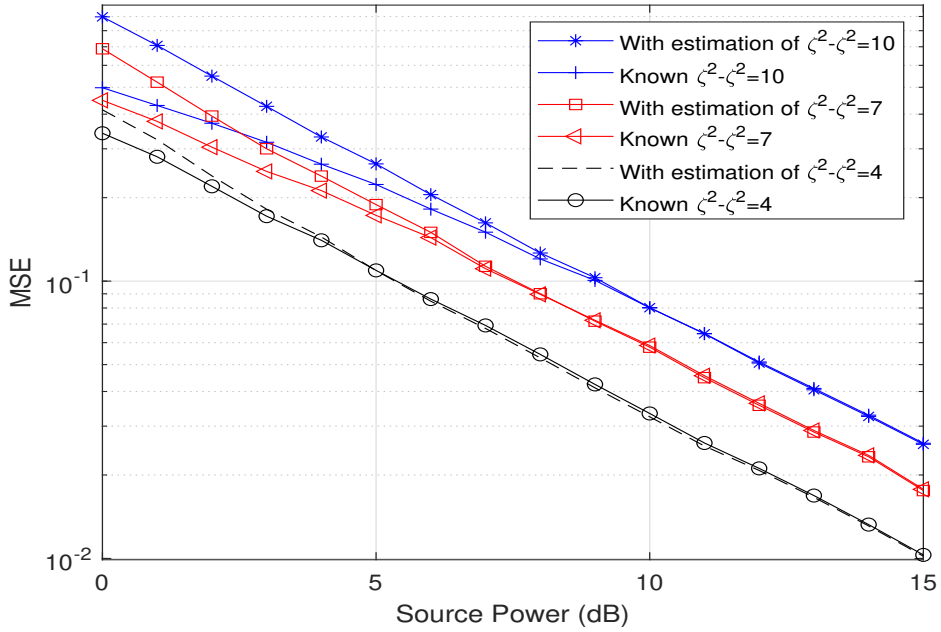

Figure 4.6: The MSE of the ML estimator for both estimated and known ζ^2 cases at the receiver versus the source power, while $\sigma_n^2 = 0.1$.

and then used to estimate h at different power values and different levels of SDSN (ζ^2). The second curve is the MSE of the estimated h when the parameter ζ^2 is known at the receiver side. It is illustrated that good results can be achieved by estimating ζ^2 when the ζ^2 is unknown to the receiver. Over and above, it can be noted that the gap between the two MSE curves shrinks as power increases. An opposite effect can be observed by the presence of SDSN (ζ^2) i.e. the gap widens as ζ^2 increases.

The BER performance of the ML receiver using the OOK modulation technique is given in Fig. 4.7. Naturally, the SDSN dramatically reduces the performance of the receiver. Besides that, the increasing noise variance, σ_n^2, increases the BER of the designed receiver. Furthermore, the effect of ζ increases with the increment of power, as seen from Fig. 4.7. The difference between the curves of BER at different values of ζ becomes larger when the transmitted power level increases. In addition to that, ζ^2 has a more significant effect at $\sigma_n^2 = 0.001$ than at $\sigma_n^2 = 0.01$.

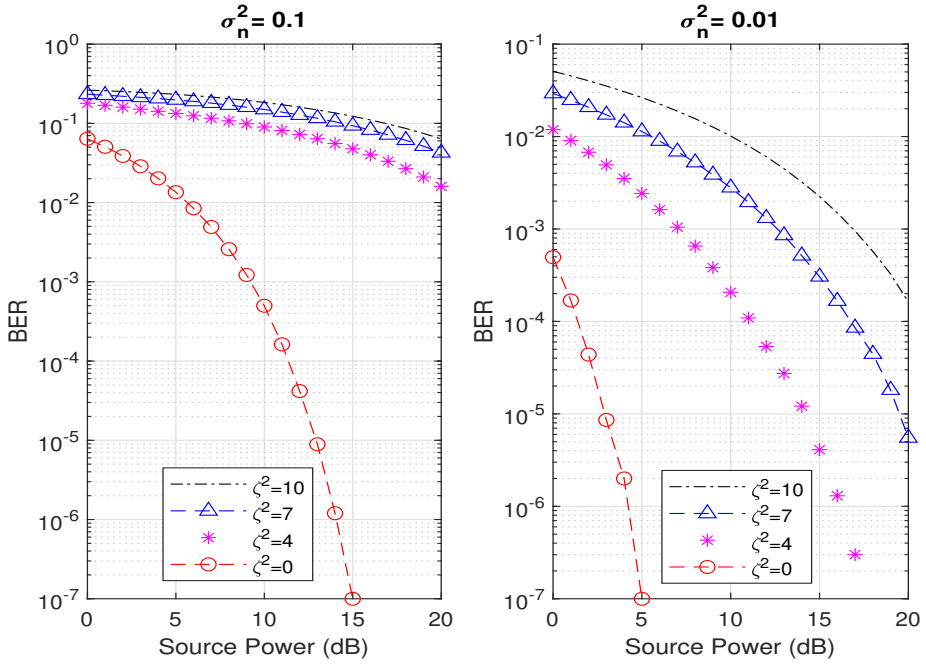

Figure 4.7: BER performance of OOK modulation for ML receiver versus the transmitted power in dB at different values of ζ^2 and σ_n^2.

4.7 Conclusion

In this chapter, we study the estimation of SISO-VLC random channels affected by the SDSN in both the cases of known and unknown intensities of SDSN i.e. the parameter ζ^2. Different estimators are utilized in the proposed system and a BCRLB is derived to serve as a benchmark for the MSE of all estimators. The obtained results comparing the MSE of the estimators show that the MMSE has the smallest MSE values among all proposed estimators. LMMSE is the runner-up, which has an MSE that is bigger than that of the MMSE estimator and less than that of the MSE of the MAP estimator. ML has a higher MSE than that of the MAP but is lower than that of the LS estimator. Finally, the LS estimator has the worst performance. Noting that the SDSN level is measured by both values of ζ^2 and σ_n^2, the investigation of the SDSN effect on the performance of the system in this chapter demonstrates that at a higher level of SDSN, higher MSE is seen upon estimation. σ_n^2. In particular, the system performs better at small values of ζ^2 and σ_n^2.

A special condition, where the receiver does not know the value of ζ^2, is studied, and the receiver estimates the channel h while ignoring the existence of the SDSN. Another solution for dealing with the unknown ζ^2 using an ML estimator is presented in this work. We present comparisons between the results of our proposed methods with the results of a case with known parameters for the user. These comparisons show the validity of the introduced solutions. It can be concluded that the VLC with accurate estimators can be a promising alternative to RF communications.

In addition, a design for the receiver of the VLC system with the effect of SDSN and the random channel gain h is suggested and the BER of the proposed receiver is studied. The results expounded that the existence of SDSN negatively affects the BER of the system, which can be observed by noting the raised BER with the increase in ζ^2.

4.8 Publications Resulted from This Chapter

- M. Yaseen, A. E. Canbilen and S. Ikki, "Channel Estimation in Visible Light Communication Systems: The Effect of Input Signal-Dependent Noise," *IEEE Transactions on Vehicular Technology*, vol. 72, no. 11, pp. 14330-14340, Nov. 2023.

- M. Yaseen, A. E. Canbilen and S. Ikki, "Estimation of Random Channel Gain for SISO Visible Light Communications System," *IEEE Canadian Journal of Electrical and Computer Engineering*, vol. 46, no. 4, pp. 262-269, Fall 2023.

Chapter 5

Signal-Dependent Shot and Relative Intensity Noise in Channel Estimation of Indoor VLC Systems

5.1 Introduction

Recently, the use of wireless connectivity has been increasing day by day. In particular, Ericsson's projection indicates that the monthly usage of a smartphone will approach 35 GB by the end of 2026 [88]. Conventional RF communications cannot meet the ever-growing demand for global connectivity due to the constrained RF spectrum, resulting in what is called a spectrum crunch. This issue has garnered tremendous attention from researchers, who are diligently investigating new technologies to address it. VLC is an emerging technology that researchers have introduced to tackle the spectrum crunch in RF communications. VLC utilizes a vast unlicensed spectrum in the range of 430 to 790 THz, offering high data rates, particularly suitable for indoor applications where the majority of users are located.

VLC offers several notable advantages. Firstly, VLC possesses inherent immunity to

RF signal interference and distinguishes itself by not disrupting the critical functions of highly sensitive electronic systems. As a result, VLC readily integrates into environments with RF restrictions, including settings such as aircraft, healthcare facilities, public street lighting systems, nuclear facilities, and more. Furthermore, in contrast to RF signals, visible light cannot penetrate walls, further enhancing the advantages of VLC, including robust physical layer security and the potential for a high-frequency reuse factor [89]. One key attribute of VLC is its safety for human health, as VLC is compliant with safety regulations for both the eyes and the skin [90].

Approximately 80% of mobile data users have been reported to be located in indoor environments [91], where the typical range for the distance between the transmitter and the receiver is 1 to 5 meters, and indoor illuminance levels typically range from 300 to 500 lx. Commercial LEDs have been used as the optical front end of the transmitter in indoor VLC systems, resulting in remarkable outcomes. Data rates exceeding few Gbits/s have been achieved in VLC systems by employing LEDs [92–95]. However, achieving such high data rates requires advanced modulation techniques to address the limited modulation bandwidth of LEDs. This matter entails the reliance on intricate transmitter-driving circuitry or the integration of frequency domain equalization at the receiving end, subsequently leading to the escalation of the overall computational complexity.

Micro-LEDs have been proposed as an alternative solution to overcome the limited bandwidth of the LEDs [96–99]. Despite achieving high-speed VLC systems using Micro-LEDs, the limited output power leads to inadequate distance and coverage area. Furthermore, increasing the densities of the injected carrier leads to the droop problem of efficiency [100].

Semiconductor LDs can operate at high current intensities without experiencing efficiency droop. Consequently, they have emerged as a compelling choice to replace LEDs in high data-rate VLC systems [101]. Compared to LEDs, LDs can achieve higher modulation bandwidths, larger communication distances, and much higher efficiencies at higher input

power densities [102].

While LDs are commonly used in outdoor communication settings due to their narrow beam widths, it has been demonstrated that they can also be effectively applied in indoor communication applications, yielding outstanding results. The mixing of lights from semiconductor LDs that emit red, green, and blue colors to create a Lambertian source suitable for indoor lighting was investigated in [103, 104]. A hybrid LD-LED approach was used to create an indoor lighting source that is conducive to illumination [105, 106].

The vertical-cavity surface-emitting laser (VCSEL) has been proposed as a promising device to replace LEDs in high-speed communications. VCSEL is a specific configuration of a semiconductor LD in which the laser beam is emitted vertically or perpendicularly from the top surface of the diode. This type of LD semiconductor is characterized by outstanding features, including high-speed modulation, exceptional power conversion efficiency, affordability, and compact [107, 108]. Recent research has shown that VCSEL can be used effectively in indoor communications [109, 110].

Despite numerous advantages, LDs suffer from two main sources of noise, which can be classified as signal-independent noise and signal-dependent noise. The primary source of signal-independent noise is thermal noise, which originates from electron excitation in the conductive material of the photodiode. The level of thermal noise increases as the operating temperature of the receiver electronics increases and decreases with an increase in resistance. Therefore, it is independent of the input signal and follows a Gaussian distribution [111].

The second noise type varies with the input signal strength and it includes two main sources which are the SDSN and the relative RIN [112–114]. The SDSN is generated at the receiver by the discrete nature of electrons or photons of the transmitted signal from the LD [115]. Even though SDSN originally adheres to a Poisson distribution, it is usually treated as Gaussian due to the substantial number of photons involved in VLC signal. [9]. It is worth noting that the SDSN is positively proportional to the square root

of the transmitted power signal.

While the RIN is directly proportional to the transmitted VLC signal, which is attributed to the source of the RIN, it is generated due to fluctuations in the intensity of a laser or optical signal relative to its average power [116]. Therefore, RIN is a signal-dependent noise, and it follows the Gaussian distribution [117, 118]. The fluctuations in the signal intensity caused by RIN lead to errors during the signal detection process, consequently resulting in an increased BER. Additionally, RIN degrades SNR, which in turn reduces overall system performance [119–121].

5.1.1 Related Works

In VLC systems, the primary principle involves using light signals to transmit data from the transmitter to the receiver. The transmitter typically includes an LD that encodes data into visible light signals through IM. This modulation technique doesn't require phase information for communication. The receiver consists of a photosensitive element, typically a photodiode (PD) or an image sensor, which captures the transmitted light signals and converts them into electrical signals using DD techniques.

The new transmission model sets VLC apart from RF communications, with VLC requiring transmitted signals to be real and non-negative [122]. These specifications lead to substantial changes in the designs of VLC systems, especially in the physical layer and modulation techniques, compared to RF systems.

With regard to modulation techniques, a very small number of simple modulation techniques, such as OOK, PPM, PAM, and PWM, can be directly employed in VLC [122, 123]. While a significant amount of work has been done to adjust the more advanced modulation schemes prior to their deployment in VLC, such as OFDM [124] and its variants [125–133].

Channel estimation is a critical component in the design of reliable VLC systems, and extensive research has been conducted in this area. In [134], the widely used LS channel

estimation scheme was adapted for VLC. In [135], an algorithm based on LS was proposed for channel estimation in an OFDM-based multiuser MISO VLC system, optimizing pilot sequences and tones to minimize the MSE of the channel estimator. The authors of [136] investigated the performance of five different channel gain estimation techniques for SISO-VLC systems, including LS, ML, MAP, LMMSE, and MMSE. Additionally, in [77], the authors introduced a receiver configuration for a wide FOV VLC system. This design considered random variations in receiver orientation and placement while accounting for imperfect CSI. They employed the LS estimation scheme to obtain the required CSI for receiver design.

The impact of SDSN in VLC systems has been considered in only a few sporadic research works. In [137], the authors studied two estimation methods used to estimate the fixed (deterministic) channel of a SISO-VLC system, deriving a benchmark for the MSE of the estimators. On the other hand, the performance of five different estimation techniques in VLC systems was investigated in [138]. Additionally, in [139], the authors explored the effect of SDSN on the estimation error bounds for distance estimation in both synchronous and asynchronous VLC systems. To the best of the authors' knowledge, no research has investigated the effect of RIN on the channel estimation of VLC systems. Furthermore, no literature review has examined the joint impact of RIN and SDSN in VLC systems. These gaps in existing research motivated the authors to pursue this chapter.

Chapter Organization. The rest of the chapter is organized as follows: In Section 5.2, we provide the channel and the system models of an indoor VLC system under consideration. In Section 5.3, we present the derivations of the Fisher information, CRLB, MSE of the LS estimator, and MSE of the ML estimator. In Section 5.4, we introduce the receiver designs and analyze their performances. Section 5.5 presents the numerical results with a detailed discussion. Finally, the conclusions are drawn in Section 5.6.

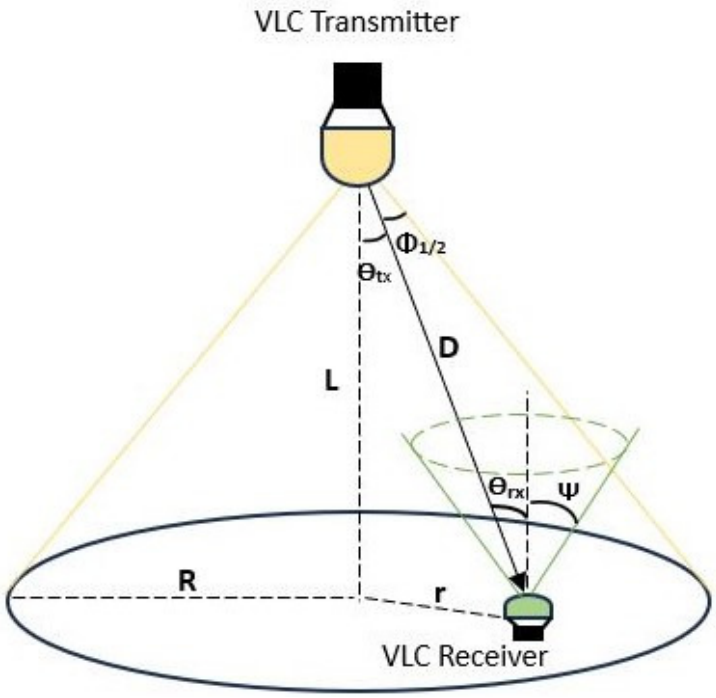

Figure 5.1: Visible light communication system model

5.2 System and Channel Models

As illustrated in Fig. 5.1, we consider an indoor VLC downlink transmission scenario, where a single LD-based lighting source serves as the wireless transmitter and the VLC receiver is in the form of a photodetector.

We assume that IM/DD is employed. Let $x = s + d$ denotes the transmitted signal, where s is the transmitted symbol and d is the bias level (DC value), which is added to guarantee that the VLC signal is always positive. Under the assumption of OOK modulation, the input data takes values of $s \in \{-A, A\}$ with the DC offset value of $d = A$. Therefore, the transmitted signal takes values of $x \in \{0, 2A\}$.

The received signal can be written as

$$y = hx + \sqrt{hx}n_{\text{ds}} + hxn_R + n, \tag{5.1}$$

where $n \sim \mathcal{N}(0, \sigma_n^2)$ is the signal-independent thermal noise. The term $\sqrt{hx}n_{\text{ds}}$ is the SDSN term, where $n_{\text{ds}} \sim \mathcal{N}(0, \sigma_{ds}^2)$. The term n_R denotes the RIN with the Gaussian distribution i.e., $n_R \sim \mathcal{N}(0, \sigma_R^2)$.

In (1), h denotes the channel coefficient of the VLC line-of-sight (LoS) link between the LD-based lighting source and the photodetector. Although there is no exact formula to calculate h, it has been modeled in literature as [6, 27, 140]

$$h = \begin{cases} \frac{A_{pd}\eta(m+1)}{2\pi D^2} \cos^m(\phi_{tx}) T_s(\theta_{rx}) g(\theta_{rx}) \cos(\theta_{rx}) & 0 \leq \theta_{rx} \leq \Psi \\ 0 & \Psi < \theta_{rx}, \end{cases} \tag{5.2}$$

where A_{pd} is the detection area of the photodetector at the receiver, η is the average receiver responsivity, and D is the Euclidean distance from transmitter to receiver. Here, ϕ_{tx} and θ_{rx} refer to the angle of irradiance and angle of incidence, respectively. $T_s(\theta_{rx})$ is the gain of the receiver's optical filter, $m = \frac{-1}{\log_2(\cos(\Phi_{1/2}))}$ is the Lambertian radiation order with lighting source emission semi-angle $\Phi_{1/2}$. $g(\theta_{rx})$ is the gain of the optical concentrator and given as

$$g(\theta_{rx}) = \begin{cases} \Upsilon \frac{n^2}{\sin^2(\Psi)} & 0 \leq \theta_{rx} \leq \Psi, \\ 0 & \Psi < \theta_{rx}, \end{cases} \tag{5.3}$$

which depends on the reflective index n of the concentrator and the FOV angle Ψ.

5.3 Cramér–Rao lower bound

In this section, we calculate the CRLB in the presence of the SDSN and the RIN. This bound gives a lower estimate for the variance of an unbiased estimator. Then, we present the derivation of LS and ML estimators as channel estimators.

5.3.1 Fisher Information and Cramér–Rao Lower Bound

In this section, we derive the Fisher information to calculate the CRLB.
Let $\mathbf{x} = [x_1, x_2, \cdots, x_N]^T$ denote the transmitted pilots' vector where N is the number of pilot symbols. The received signal vector $\mathbf{y} = [y_1, y_2, \ldots, y_N]^T$ can be written as

$$\mathbf{y} = h\mathbf{x} + \sqrt{h}\mathrm{diag}(\mathbf{x})\mathbf{n}_{ds} + h\mathrm{diag}(\mathbf{x})\mathbf{n}_R + \mathbf{n}, \tag{5.4}$$

where $\mathrm{diag}(\mathbf{x})$ is an $N \times N$ diagonal matrix with the elements of $\mathbf{x}$ in the main diagonal, $\mathbf{n} = [n_1, n_2, \ldots, n_N]^T$, $\mathbf{n}_{ds} = [n_{ds1}, n_{ds2}, \ldots, n_{dsN}]^T$ and $\mathbf{n}_R = [n_{R1}, n_{R2}, \ldots, n_{RN}]^T$. The elements of $\mathbf{n}$ are independent and identically distributed Gaussian random variables, i.e., $\mathbf{n} \sim \mathcal{N}(0, \sigma_n^2 I_N)$. Similarly, we have $\mathbf{n}_{ds} \sim \mathcal{N}(0, \sigma_R^2 I_N)$ and $\mathbf{n}_R \sim \mathcal{N}(0, \sigma_R^2 I_N)$.

The lower bound on the variance of any unbiased estimator of h can be obtained using the CRLB as[1]

$$\sigma_{\hat{h}}^2 \geq \frac{1}{\mathrm{J}(h)}, \tag{5.5}$$

where $\mathrm{J}(h)$ is the Fisher information of h given by

$$\mathrm{J}(h) = -\mathbf{E}\left\{\frac{\partial^2}{\partial h^2}\ln f(\mathbf{y}; h)\right\}. \tag{5.6}$$

Here, $\ln f(\mathbf{y}; h)$ is the log-likelihood function of the unknown channel h. Since all the samples are independent, the joint probability density function (PDF) of N observations can be written as

$$f(\mathbf{y}; h) = \exp\left(\frac{-1}{2}\sum_{i=1}^{N}\frac{(y_i - hx_i)^2}{\sigma_n^2 + \sigma_{\mathrm{ds}}^2 hx_i + \sigma_R^2 h^2 x_i^2}\right)\prod_{i=1}^{N}\frac{1}{\sqrt{2\pi\left(\sigma_n^2 + \sigma_{\mathrm{ds}}^2 hx_i + \sigma_R^2 h^2 x_i^2\right)}}. \tag{5.7}$$

After some tedious mathematical manipulations (see APPENDIX B), $\mathrm{J}(h)$ can be expressed

[1] An estimator of a given parameter, e.g., h, is said to be unbiased if its expected value is equal to the true value of the parameter that should be estimated.

as

$$\mathrm{J}(h) = \frac{1}{2}\sum_{i=1}^{N}\left[\frac{2x_i^2(1+\sigma_R^2)}{\sigma_n^2+\sigma_{ds}^2 hx_i+\sigma_R^2h^2x_i^2}+\frac{(x_i\sigma_{ds}^2+2hx_i^2\sigma_R^2)^2}{(\sigma_n^2+\sigma_{ds}^2hx_i+\sigma_R^2h^2x_i^2)^2}\right]. \tag{5.8}$$

Under the assumption that all the transmitted pilot symbols are identical i.e., x_i=p, the Fisher information can be simplified to

$$\mathrm{J}(h) = \frac{Np^2}{2}\frac{2(1+\sigma_R^2)(\sigma_n^2+\sigma_{ds}^2hp+\sigma_R^2h^2p^2)+(\sigma_{ds}^2+2hp\sigma_R^2)^2}{(\sigma_n^2+\sigma_{ds}^2hp+\sigma_R^2h^2p^2)^2}. \tag{5.9}$$

Consequently, the CRLB can be expressed as

$$\mathrm{CRLB} = \frac{2}{Np^2}\frac{(\sigma_n^2+\sigma_{ds}^2hp+\sigma_R^2h^2p^2)^2}{2(1+\sigma_R^2)(\sigma_n^2+\sigma_{ds}^2hp+\sigma_R^2h^2p^2)+(\sigma_{ds}^2+2hp\sigma_R^2)^2}. \tag{5.10}$$

For sufficiently high levels of transmitted power, the CRLB approaches the saturation value of $\frac{2}{N}\frac{h^2\sigma_R^2}{2+6\sigma_R^2}$, which is independent of p.

Special Case 1: In the case of negligible level of RIN, i.e., $\sigma_R^2 \to 0$ [141], the CRLB reduces to

$$\lim_{\sigma_R^2\to 0}\mathrm{CRLB} \to \frac{2}{Np^2}\frac{(\sigma_n^2+\sigma_{ds}^2hp)^2}{2(\sigma_n^2+\sigma_{ds}^2hp)+(\sigma_{ds}^2)^2}, \tag{5.11}$$

which coincides with the CRLB derived in [82].

At high power p without the RIN, the CRLB can be approximated to

$$\mathrm{CRLB} \to \frac{1}{N}\frac{h\sigma_{ds}^2}{p}. \tag{5.12}$$

On the opposite side, at a high level of the RIN, the CRLB can be approximated as

$$\lim_{\sigma_R^2\to\infty}\mathrm{CRLB} \to \frac{h^2}{3N}. \tag{5.13}$$

It is interesting to note that the CRLB no longer hinges on the transmitted power or the noise level. Instead, it is contingent upon the channel gain and the number of pilots.

Notably, increasing the number of pilots enhances the CRLB, in contrast to the impact of power, where no improvement in the CRLB is observed.

Special Case 2: In the case of very low SDSN level, i.e., $\sigma_{ds}^2 \to 0$ [142,143], the CRLB reduces to

$$\lim_{\sigma_{ds}^2 \to 0} \text{CRLB} \to \frac{2}{Np^2} \frac{(\sigma_n^2 + \sigma_R^2 h^2 p^2)^2}{2(1+\sigma_R^2)(\sigma_n^2 + \sigma_R^2 h^2 p^2) + (2hp\sigma_R^2)^2}. \tag{5.14}$$

At high power p without the SDSN, the CRLB can be approximated to

$$\lim_{p \to \infty} \text{CRLB} \to \frac{2}{N} \frac{h^2 \sigma_R^2}{2 + 6\sigma_R^2}, \tag{5.15}$$

which is the same result obtained when both SDSN and RIN do exist. Oppositely, at a high level of the SDSN, the CRLB can be approximated as

$$\lim_{\sigma_{ds}^2 \to \infty} \text{CRLB} \to \frac{2h}{Np}, \tag{5.16}$$

which does not depend on the noise but it depends on the power and the channel gain h.

Special Case 3: When both RIN and SDSN noises are negligible compared to the thermal noise, i.e., $\sigma_R^2 \to 0$ and $\sigma_{ds}^2 \to 0$ [142], CRLB is approximated as

$$\lim_{\sigma_{ds}^2 \to 0, \sigma_R^2 \to 0} \text{CRLB} \to \frac{\sigma_n^2}{Np^2}, \tag{5.17}$$

which is widely used in the analysis of RF wireless systems [144].

If the SDSN and the RIN are excessive, the CRLB can be approximated as

$$\lim_{\sigma_{ds}^2 \to \infty, \sigma_R^2 \to \infty} \text{CRLB} \to \frac{h^2}{3N}. \tag{5.18}$$

It is worth mentioning that the same result is obtained when only RIN is very high, emphasizing the dominant effect of RIN versus SDSN.

Special Case 4: When the thermal noise n is negligible compared to RIN and

SDSN [143], the CRLB can be approximated as

$$\lim_{\sigma_n^2 \to 0} \text{CRLB} \to \frac{2}{Np^2} \frac{(\sigma_{ds}^2 hp + \sigma_R^2 h^2 p^2)^2}{2(1+\sigma_R^2)(\sigma_{ds}^2 hp + \sigma_R^2 h^2 p^2) + (\sigma_{ds}^2 + 2hp\sigma_R^2)^2}. \tag{5.19}$$

At high power p with negligible value of thermal noise n, the CRLB can be approximated to

$$\text{CRLB} \to \frac{2}{N} \frac{\sigma_R^2 h^2 p}{2 + 6\sigma_R^2}. \tag{5.20}$$

This aligns with the result obtained in (5.15). Consequently, the presence of RIN dominates the occurrence of SDSN in scenarios characterized by high power. In contrast, under conditions of high thermal noise n, the CRB can be approximated as

$$\lim_{\sigma_n^2 \to \infty} \text{CRLB} \to \frac{2}{Np^2} \cdot \frac{\sigma_n^2}{2(1+\sigma_R^2)}. \tag{5.21}$$

It is observed that even under conditions of very high thermal noise, RIN continues to impact the CRLB, which is not the case for SDSN.

Examining (5.10), (5.11), (5.14), and (5.17) reveals that at high power, the CRLB is inversely proportional to p in the presence of SDSN and thermal noise n. However, it becomes inversely proportional to p^2 when both RIN and SDSN are absent. Conversely, in the presence of RIN and high transmitted power, the CRLB saturates. This saturation occurs whether SDSN is present or not, signifying the dominance of RIN over SDSN. Furthermore, it can be noted that increasing transmitted power significantly reduces the CRLB when only thermal noise is present. However, when both thermal noise and SDSN are present, the reduction in the CRLB is smaller. Meanwhile, RIN prevents any further reduction in the CRLB even with increased transmitted power.

5.3.2 Least Square Estimator

For the LS estimator, the estimated $\hat{h}$ can be expressed as

$$\hat{h}_{\text{LS}} = \frac{\mathbf{x}^T\mathbf{y}}{\|\mathbf{x}\|^2}. \tag{5.22}$$

Replacing (5.4) in (5.22), we obtain

$$\hat{h}_{\text{LS}} = h + \frac{\mathbf{x}^T}{\|\mathbf{x}\|^2}\sqrt{h\text{diag}(\mathbf{x})}\mathbf{n}_{\text{ds}} + \frac{\mathbf{x}^T}{\|\mathbf{x}\|^2}h\text{diag}(\mathbf{x})\mathbf{n}_R + \frac{\mathbf{x}^T}{\|\mathbf{x}\|^2}\mathbf{n}. \tag{5.23}$$

The performance of the LS estimator can be evaluated by determining the MSE, which is equivalent to the variance of the estimation error. Thus, the MSE can be calculated as

$$\epsilon_{\text{LS}} = \hat{h}_{\text{LS}} - h. \tag{5.24}$$

It can be readily checked that the LS estimator is unbiased, i.e., $\mathbf{E}\{\hat{h}_{\text{LS}}\} = h$. Therefore, ϵ_{LS} can be written as

$$\epsilon_{\text{LS}} = \frac{\mathbf{x}^T}{\|\mathbf{x}\|^2}\left(\sqrt{h\text{diag}(\mathbf{x})}\mathbf{n}_{\text{ds}} + \mathbf{n}_R + \mathbf{n}\right). \tag{5.25}$$

It is evident from (5.25) that ϵ_{LS} is a Gaussian random variable, i.e., $\epsilon_{\text{LS}} \sim \mathcal{N}(0, \sigma^2_{\epsilon_{\text{LS}}})$, where $\sigma^2_{\epsilon_{\text{LS}}}$ is inversely proportional to the pilots' SNR value and can be written as

$$\sigma^2_{\epsilon_{\text{LS}}} = \frac{\sum_{i=1}^{N} x_i^2(\sigma_n^2 + \sigma_{ds}^2 h x_i + \sigma_R^2 h^2 x_i^2)}{\left(\sum_{i=1}^{N} x_i^2\right)^2}. \tag{5.26}$$

For $x_i = p$, $\sigma^2_{\epsilon_{LS}}$ can be further simplified as

$$\sigma^2_{\epsilon_{LS}} = \frac{\sigma_n^2 + \sigma_{ds}^2 hp + \sigma_R^2 h^2 p^2}{Np^2}. \tag{5.27}$$

From (5.27), it is observed that increasing the power leads the $\sigma^2_{\epsilon_{LS}}$ to a saturation level

while increasing the number of the pilots decreases the error variance $\sigma^2_{\epsilon_{LS}}$ effectively enhancing the LS estimator performance.

5.3.3 Maximum-Likelihood Estimator

The ML estimator is based on the maximization of likelihood PDF. In our case, the log-likelihood of (5.7) is given as

$$\ln f(\mathbf{y};h) = -\frac{N}{2}\ln(2\pi) - \frac{1}{2}\sum_{i=1}^{N}\ln\left(\sigma_n^2 + \sigma_{ds}^2 h x_i + \sigma_R^2 h^2 x_i^2\right) - \frac{1}{2}\sum_{i=1}^{N}\frac{(y_i - h x_i)^2}{\sigma_n^2 + \sigma_{ds}^2 h x_i + \sigma_R^2 h^2 x_i^2}. \tag{5.28}$$

The estimated channel can be determined by evaluating $\frac{\partial}{\partial h}\ln f(\mathbf{y};h) = 0$, i.e.,

$$\frac{\partial}{\partial h}\ln f(\mathbf{y};h) = -\frac{1}{2}\sum_{i=1}^{N}\left[\frac{\sigma_{ds}^2 x_i + 2\sigma_R^2 h x_i^2}{\sigma_n^2 + \sigma_{ds}^2 h x_i + \sigma_R^2 h^2 x_i^2} - \frac{2x_i(y_i - h x_i)}{\sigma_n^2 + \sigma_{ds}^2 h x_i + \sigma_R^2 h^2 x_i^2} - \frac{(\sigma_{ds}^2 x_i + 2\sigma_R^2 h x_i^2)(y_i - h x_i)^2}{(\sigma_n^2 + \sigma_{ds}^2 h x_i + \sigma_R^2 h^2 x_i^2)^2}\right] = 0. \tag{5.29}$$

Under the assumption that the transmitted pilots are identical, i.e. $x_i = p$, (5.29) can be expressed in the form of a cubic equation as

$$Ah^3 + Bh^2 + Ch + D = 0, \tag{5.30}$$

where A, B, C and D are respectively given by

$$A = 2Np^4\sigma_R^4, \tag{5.31}$$

$$B = 3N\sigma_{ds}^2\sigma_R^2p^3 + N\sigma_{ds}^2p^3 + 2p^3\sigma_R^2\sum_{i=1}^{N} y_i, \tag{5.32}$$

$$C = N\sigma_{ds}^4p^2 + 2N\sigma_R^2\sigma_n^2p^2 + 2Np^2\sigma_n^2 - 2\sigma_R^2p^2\sum_{i=1}^{N} y_i^2, \tag{5.33}$$

$$D = N\sigma_{ds}^2p\sigma_n^2 - 2p\sigma_n^2\sum_{i=1}^{N} y_i - \sigma_{ds}^2p\sum_{i=1}^{N} y_i^2. \tag{5.34}$$

It is difficult, if not impossible, to manually find a closed-form expression for the roots of (5.30). However, numerical tools and software can be used to yield a solution

In the absence of RIN and SDSN, i.e., $\sigma_R^2 = 0$ and $\sigma_{ds}^2 = 0$, we have

$$\frac{\partial}{\partial h}\ln f(\boldsymbol{y}|h) = \frac{1}{2\sigma_n^2}\sum_{i=1}^{N} 2x_i(y_i - hx_i) = 0\cdot \tag{5.35}$$

The estimated channel gain can be now calculated as $\hat{h}_{\mathrm{ML}} = \frac{\sum_{i=1}^{N} y_i}{Np}$, which is equal to $\hat{h}_{\mathrm{LS}}$ in (5.22). This yields the well-known result in the literature that both ML and LS have the same performance in the presence of only additive thermal noise.

Remark: One of the key properties of the ML estimator is that it becomes asymptotically unbiased, meaning that as the transmitted pilots size increases, the ML estimator approaches the true parameter value it is estimating. By means of clarification, $\mathbf{E}\{\hat{h}_{\mathrm{ML}}\} = h$ at very large numbers of symbols, i.e. $N \to \infty$. [145]. Table 5.1 proves that the proposed ML estimator in this work satisfies this property. From the table, it can be concluded that at a higher value of σ_R^2 more pilots are needed to be transmitted to converge the real value of the channel gain. Taking a closer examination of the table, at $p = 20$ dB, $N = 1$, $\sigma_{ds}^2 = 0.1$ and $\sigma_R^2 = 0.1$, the $\mathbf{E}\{\hat{h}_{\mathrm{ML}}\} = 1.3038$, while at the same level of transmitted power, number of pilots, SDSN level but $\sigma_R^2 = 0.10$, $\mathbf{E}\{\hat{h}_{\mathrm{ML}}\} = 1.1044$ In the same way,

Table 5.1: Theoretical asymptotic and actual mean for ML estimator at different power levels, when $h = 1$ and $\sigma_n^2 = 0.1$ at different power levels, two different values of σ_R^2 and two different σ_{ds}^2 values.

	$\sigma_R^2 = 0.1$					
	$\sigma_{ds}^2 = 0.1$			$\sigma_{ds}^2 = 0.01$		
Np	0	10	20	0	10	20
1	1.5268	1.3185	1.3038	1.4434	1.3053	1.3024
5	1.2356	1.1424	1.1358	1.1983	1.1365	1.1352
10	1.1666	1.1007	1.0961	1.1402	1.0965	1.0956
30	1.0962	1.0581	1.0555	1.0810	1.0557	1.0552
50	1.0745	1.0450	1.0430	1.0627	1.0432	1.0428
	$\sigma_R^2 = 0.01$					
1	1.4546	1.1441	1.1044	1.3455	1.1090	1.1000
5	1.2033	1.0644	1.0467	1.1545	1.0487	1.0447
10	1.1438	1.0456	1.0330	1.1093	1.0345	1.0316
30	1.0830	1.0263	1.0191	1.0631	1.0199	1.0183
50	1.0643	1.0204	1.0148	1.0489	1.0154	1.0141

the increment in σ_{ds}^2 obstructs the ML estimator from being unbiased. Practically, it is hard to predict the number of pilots needed to satisfy the unbiased property of the ML estimator. Generally, for our proposed model, it can be observed that $N = 50$ is enough for the $\mathbf{E}\{\hat{h}_{\mathrm{ML}}\}$ to reach the real value of the channel gain.

5.4 Receiver Design and Error Rate Performance

Based on the ML decision rule, the optimal receiver takes the form of the well-known Euclidean distance decoder in the presence of additive white Gaussian noise that models the thermal noise. In the following, we derive the ML detector in the presence of RIN and SDSN in addition to the thermal noise.

From (5.1), the joint PDF of the received signal y, given the transmitted signal $x_p, \forall p =$

$0, 1$ can be expressed as

$$f_{y|x_p}(y) = \frac{1}{\sqrt{2\pi(\sigma_n^2 + \sigma_{ds}^2 h x_p + h^2 x_p^2 \sigma_R^2)}} \exp\left\{ -\frac{(y - h x_p)^2}{2(\sigma_n^2 + \sigma_{ds}^2 h x_p + h^2 x_p^2 \sigma_R^2)} \right\}. \tag{5.36}$$

Assuming equal probability of both transmitted symbols, i.e., $p(x_p) = \frac{1}{2}$, the optimal receiver in ML sense can be expressed as

$$\hat{x} = \max_{x_p, p=0,1} \left\{ -\ln\left(\sigma_n^2 + h x_p \sigma_{ds}^2 + h^2 x_p^2 \sigma_R^2\right) - \frac{(y - h x_p)^2}{(\sigma_n^2 + h x_p \sigma_{ds}^2 + h^2 x_p^2 \sigma_R^2)} \right\}. \tag{5.37}$$

Therefore, we have the following two hypotheses: *i)* H_1, which is the signal present hypothesis, where $x_1 = 2A$ and *ii)* H_0, which is the signal absent hypothesis, where $x_0 = 0$. These two hypotheses can be expressed as

$$\begin{aligned} H_1 &: y = 2hA + \sqrt{2Ah} n_{ds} + 2Ah n_R + n, \\ H_0 &: y = n. \end{aligned} \tag{5.38}$$

Using (5.36), the PDFs under these two hypotheses can be written as

$$\begin{aligned} f(y; h, H_1) &= \left(\frac{1}{\sqrt{2\pi(\sigma_n^2 + 2Ah\sigma_{ds}^2 + 4A^2h^2\sigma_R^2)}} \right) \exp\left(-\frac{1}{2} \frac{(y - 2Ah)^2}{\sigma_n^2 + 2Ah\sigma_{ds}^2 + 4A^2h^2\sigma_R^2} \right). \\ f(y; h, H_0) &= \left(\frac{1}{\sqrt{2\pi\sigma_n^2}} \right) \exp\left(-\frac{y^2}{2\sigma_n^2} \right). \end{aligned} \tag{5.39}$$

Based on the likelihood ratio, the optimal ML receiver takes the form of [146]

$$\Lambda(\boldsymbol{y}) = \frac{f(\boldsymbol{y}; h, H_1)}{f(\boldsymbol{y}; h, H_0)} \underset{H_0}{\overset{H_1}{\gtrless}} 1 \,. \tag{5.40}$$

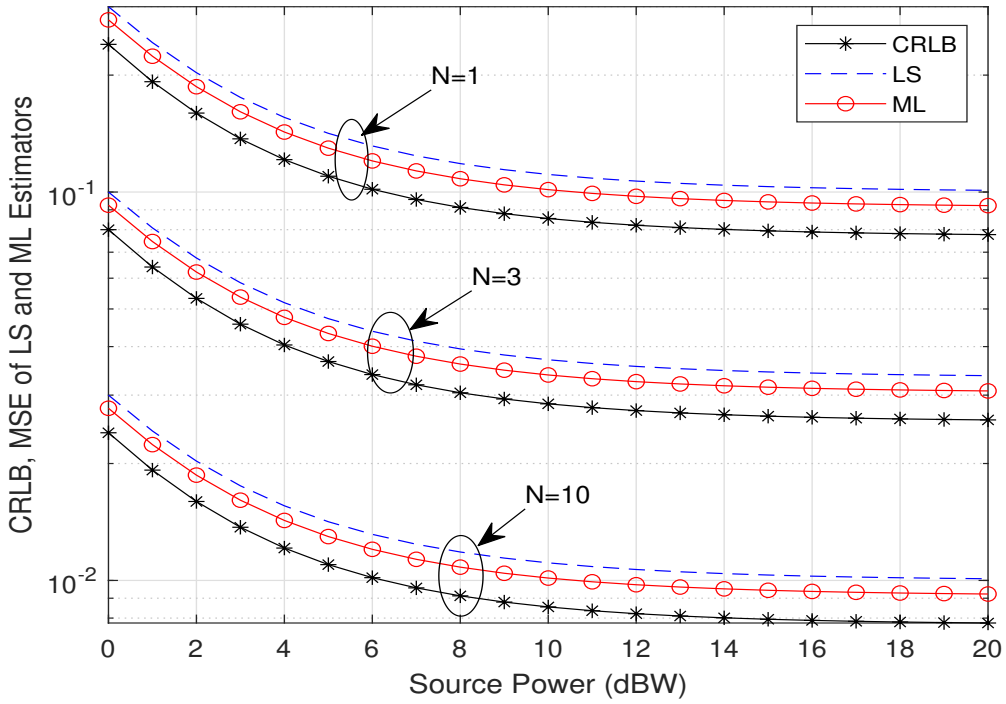

Figure 5.2: The CRLB and the MSE values of the LS and the ML estimators versus the source power at different numbers of transmitted pilots for $\sigma_n^2 = 0.1$, $\sigma_{ds}^2 = 0.1$ and $\sigma_R^2 = 0.1$ and $h = 1$.

Replacing (5.39) in (5.40), the ML decision rule is found as

$$\hat{x}_{ML} = \begin{cases} H_0 & \text{if } (2Ah\sigma_{ds}^2 + 4Ah^2\sigma_R^2)y^2 + 4Ah\sigma_n^2 y < 4A^2h^2\sigma_n^2 \\ & +\sigma_n^2 F(\ln F - ln\sigma_n^2), \\ H_1 & \text{otherwise,} \end{cases} \tag{5.41}$$

where $F = \sigma_n^2 + 2Ah\sigma_{ds}^2 + 4A^2h^2\sigma_R^2$.

In the case of imperfect CSI, where the channel gain h is unknown, the receiver first estimates the gain h and then employs it in the same decision rule given for the perfect

CSI case in (5.41), as follows

$$\hat{x}_{ML} = \begin{cases} H_0 & \text{if } (2A\hat{h}\sigma_{ds}^2 + 4Ah^2\sigma_R^2)y^2 + 4A\hat{h}\sigma_n^2 y < 4A\hat{h}^2\hat{h}^2\sigma_n^2 + \sigma_n^2 G(\ln G - ln\sigma_n^2), \\ H_1 & \text{otherwise,} \end{cases} \tag{5.42}$$

where $G = \sigma_n^2 + 2A\hat{h}\sigma_{ds}^2 + 4A^2\hat{h}^2\sigma_R^2$.

As a simpler solution, we now consider a receiver that does not need prior information about the channel.

Under this condition, (5.42) reduces to

$$\hat{x}_{sub} = \begin{cases} H_0 & \text{if } \ y \leq \hat{h}A, \\ H_1 & \text{otherwise,} \end{cases} \tag{5.43}$$

which is basically a threshold detector, and we refer to it as a sub-optimal receiver.

Error analysis of ML decision rule in (5.42) becomes challenging due to the non-Gaussian nature of the term y^2 in equations (5.41) and (5.42). Therefore, we resort to examining the error probability through numerical simulation, as presented in the upcoming simulation results section. On the other hand, the error analysis of the threshold detector can be calculated in closed form. In particular, we first write (5.1) as

$$y = x_p h + \omega, \tag{5.44}$$

where $\omega \sim \mathcal{N}(0, (\sigma_n^2 + x_p h\sigma_{ds}^2 + x_p^2 h^2\sigma_R^2))$. Then the conditional probability (conditioned on the channel coefficient h) of detecting x_q instead of the transmitted x_p can be written

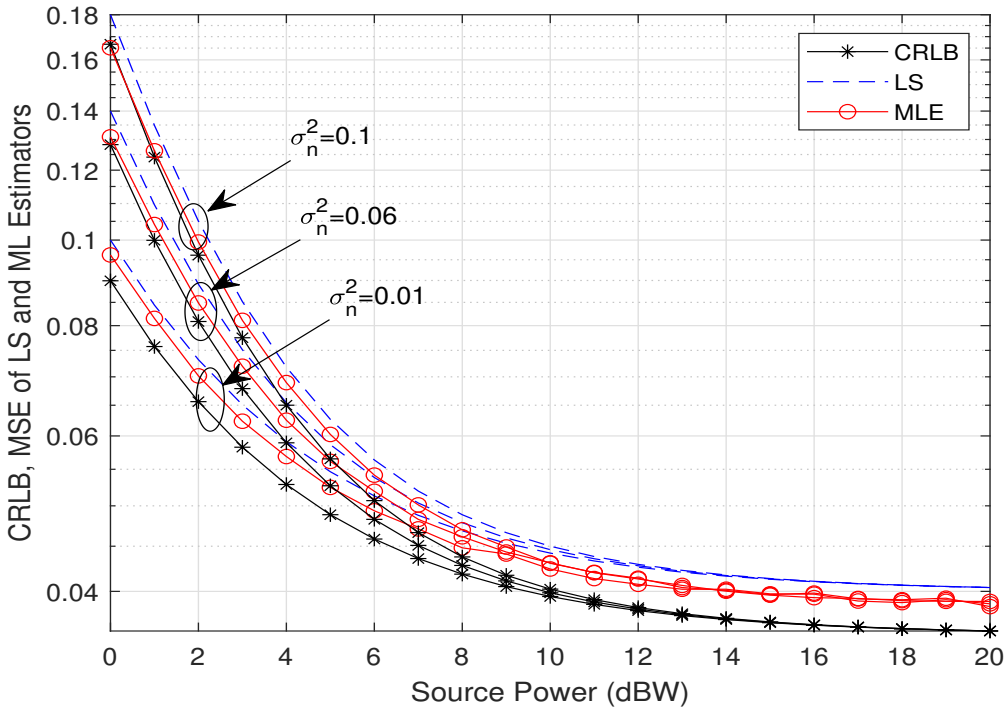

Figure 5.3: The CRLB and the MSE values of the LS and the ML estimators versus the source power at different values of the thermal noise variance σ_n^2 for the same value of $\sigma_R^2 = 0.01$, $\sigma_{ds}^2 = 0.01$, $h = 1$ and $N = 1$.

as

$$P\left(x_p, x_q|h\right) = P\left(\left[y - hx_p\right]^2 > \left[y - hx_q\right]^2\right) = P\left(2h(x_p - x_q)\omega > h^2(x_p - x_q)^2\right)$$
$$= Q\left(\sqrt{\frac{h^2(x_p - x_q)^2}{4\left(\sigma_n^2 + hx_p\sigma_{ds}^2 + h^2x_p^2\sigma_R^2\right)}}\right), \tag{5.45}$$

where $P\left(\cdot\right)$ denotes the probability of an event. Substituting in (5.45) by x_0 and x_1, the BER can be expressed as

$$P(e|h) = \frac{1}{2}P(x_0, x_1|h) + \frac{1}{2}P(x_1, x_0|h)$$
$$= \frac{1}{2}Q\left(\sqrt{\frac{h^2A^2}{\sigma_n^2}}\right) + \frac{1}{2}Q\left(\sqrt{\frac{h^2A^2}{\sigma_n^2 + 2Ah\sigma_{ds}^2 + 4A^2h^2\sigma_R^2}}\right). \tag{5.46}$$

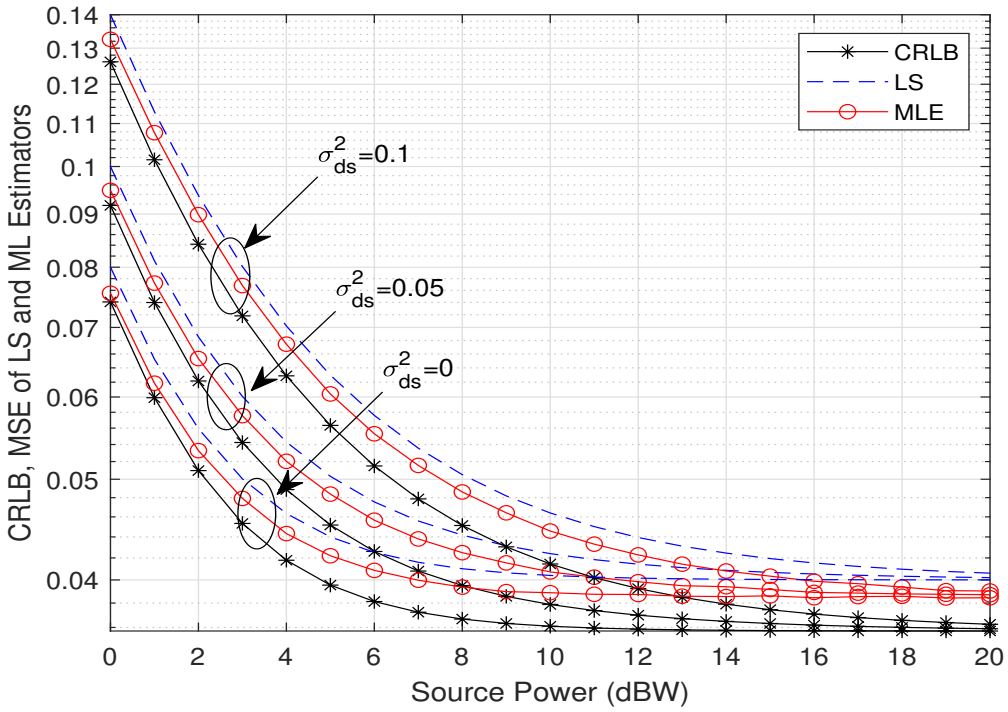

Figure 5.4: The CRLB and the MSE values of the LS and the ML estimators versus the source power at different values of the signal-dependent noise variance σ^2_{ds} for $\sigma^2_n = 0.01$, $\sigma^2_R = 0.01$, $h = 1$ and $N = 1$.

In the absence of SDSN and RIN, i.e., $\sigma^2_{ds} = 0$ and $\sigma^2_R = 0$, the above expression can be simplified to the well-known formula of

$$P(e|h)_{\zeta=0} = Q\left(\sqrt{\frac{h^2A^2}{\sigma^2_n}}\right). \tag{5.47}$$

Remark: According to (5.46) and (5.47), we have

$$\frac{P(e|h)_{\sigma^2_{ds}\neq 0,\sigma^2_R\neq 0}}{P(e|h)_{\sigma^2_{ds}=0,\sigma^2_R=0}} = \frac{1}{2}\left[1 + \frac{Q\left(\sqrt{\frac{h^2A^2}{\sigma^2_n+2Ah\sigma^2_{ds}+4A^2h^2\sigma^2_R}}\right)}{Q\left(\sqrt{\frac{h^2A^2}{\sigma^2_n}}\right)}\right] > 1, \tag{5.48}$$

which is valid because the second term in the bracket is greater than one. Hence, as expected, the BER performance when $\sigma^2_R = 0$ and $\sigma^2_{ds} = 0$ is better than what is seen

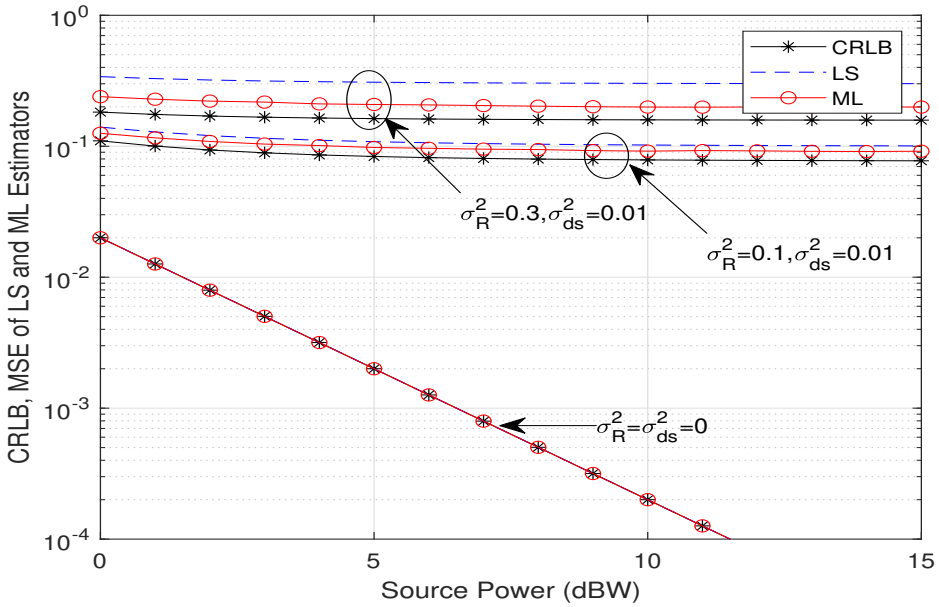

Figure 5.5: The CRLB and the MSE values of the LS and the ML estimators versus the source power at different values of the signal-dependent noise variance σ_R^2 for $\sigma_n^2 = 0.01$, $h = 1$ and $N = 1$.

when $\sigma_R^2 \neq 0$ and $\sigma_{ds}^2 \neq 0$. In other words, the signal-dependent noise (SDSN and RIN) degrades the error system performance. Furthermore, the asymptotic error performance as $\sigma_{ds}^2 \to \infty, \sigma_R^2 \to \infty$, can be written as

$$P(e|h)_{\sigma_{ds}^2 \to \infty, \sigma_R^2 \to \infty} = \frac{1}{4} + \frac{1}{2} Q\left(\sqrt{\frac{h^2 A^2}{\sigma_n^2}}\right) \approx \frac{1}{4}. \tag{5.49}$$

5.5 Numerical Results

In this section, we present numerical results to support the theoretical results obtained in the previous sections.

In Fig. 5.2, we compare the MSE of the LS and ML estimators with the CRLB. The curves are plotted under conditions of $\sigma_n^2 = 0.1$, $\sigma_{ds}^2 = 0.1$, $\sigma_R^2 = 0.1$, and $h = 1$, as the number of transmitted pilots N increases from 1 to 3 and then to 10. Several observa-

tions can be drawn from this figure. Firstly, the ML estimator consistently outperforms the LS estimator. Secondly, at low and medium transmitted power levels, increasing the transmitted power p improves the system performance. Conversely, at high transmitted power, an error floor emerges due to RIN, which is power-dependent. Thirdly, with all other factors held constant, increasing the number of pilots substantially reduces the MSE of both ML and LS estimators, along with a decrease in the CRLB. In conclusion, while increasing transmitted power ceases to enhance the system performance in the high-power regime, increasing the number of pilots continues to enhance system performance at all transmitted power levels.

In Fig. 5.3, we investigate the impact of thermal noise. Keeping all other parameters constant, namely, the RIN variance $\sigma_R^2 = 0.01$, SDSN variance $\sigma_{ds}^2 = 0.01$, shot noise variance $\sigma_n^2 = 0.01$, and channel gain $h = 1$, increasing the thermal noise variance σ_n^2 results in an increase in the MSE of the considered estimators and the CRLB, consequently degrading the overall system performance. However, this effect diminishes with an increase in source power due to the dominance of RIN. Specifically, as depicted in the figure, all curves with different σ_n^2 values converge at $p = 10$ dBW, indicating the termination of the thermal noise effect.

In Fig. 5.4, three groups of curves are compared, illustrating the MSE for both LS and ML estimators, along with the CRLB. These curves are plotted as the SDSN variance σ_{ds}^2 increases from 0 to 0.05 and then to 0.1. Notably, the MSE for both estimators and the CRLB increases with higher values of σ_{ds}^2. While the impact of SDSN noise is pronounced at lower power levels, its influence diminishes at higher power levels. Specifically, the effect of the noise becomes negligible at 20 dBW, as expected due to the dominance of RIN. The analysis reveals that the RIN effect persists at higher transmitted power levels compared to the power level at which the thermal noise impact is negligible, as seen in Fig. **??**. This observation can be attributed to the direct proportionality of SDSN to the square root of power p, while thermal noise does not depend on power.

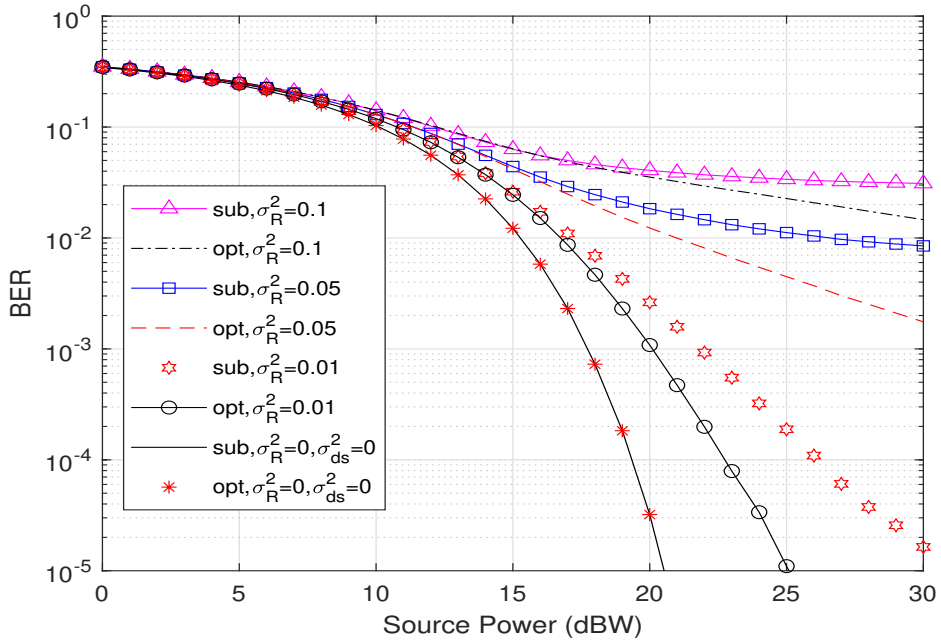

Figure 5.6: BER performance versus the source power at different levels of the RIN when $\sigma_n^2 = 0.01$, $\sigma_{ds}^2 = 0.01$, $h = 0.4$ and $N = 1$.

In Fig. 5.5, we investigate the effect of RIN. The MSE of the LS and ML estimators are compared with the CRLB at various RIN variance values. Additionally, these curves are contrasted with the case of a receiver where only thermal noise is present. The comparison reveals that RIN significantly degrades the performance of both estimators. It is noteworthy that in the case where only thermal noise is present, performance continuously improves with increasing power. Conversely, in the presence of RIN, the MSE of the estimators reaches a threshold value at relatively high power levels. Specifically, SDSN mitigates the system enhancement caused by the power rise due to its proportionality to the square root of power, while RIN leads to a saturation level at high power due to its direct proportionality to power. Consequently, when both RIN and SDSN are present, the MSE of channel estimators rapidly reaches a threshold level.

In Fig. 5.6, we present the BER performance of the VLC system based on the optimal receiver in (5.42) and sub-optimal receiver in (5.43). We assume $\sigma_n^2 = 0.01$, $\sigma_{ds}^2 = 0.01$,

$h = 4 \times 10^{-1}$, $N = 1$, while we consider different levels of RIN, i.e., σ_R^2 is increased along [0.01, 0.05, 0.1]. As a benchmark, the BER is also plotted for $\sigma_R^2 = 0$ and $\sigma_{ds}^2 = 0$. The results illustrate that the optimal receiver outperforms the threshold detector as expected, and the performance gap widens as transmitted power increases. It is also observed that the BER increases with the increase of the RIN variance. The BER curves exhibit error floors as the power level increases, and it becomes apparent that the curves approach these error floors more rapidly with an elevated value of σ_R^2, while all other parameters remain constant. In Fig. 5.7, a similar comparison is provided for various SDSN variances. The curves in the figure reveal a substantial adverse impact on the VLC system under examination due to SDSN. This detrimental effect becomes increasingly noticeable as the value of SDSN variance escalates. Furthermore, the findings presented in this figure align with those in the earlier figure, demonstrating that the optimal receiver outperforms the threshold detector for all σ_{ds}^2 values. The performances of both receivers typically exhibit a close match in the scenario when both σ_R^2 and σ_{ds}^2 equal zero.

5.6 Conclusions

In this chapter, we considered a VLC system that uses LD-empowered luminary as the wireless transmitter. While LDs provide much higher bandwidth in comparison to LEDs commonly used in VLC systems, LDs suffer from SDSN and RIN. To demonstrate the effect of these noise sources on the channel estimation performance, we calculated the CRLB in the presence of the SDSN and the RIN. The MSE of the LS and ML estimators for the channel gain were analyzed and compared against the derived CRLB. Furthermore, we presented the optimal receiver in ML sense and compared it with a simple threshold detector as a sub-optimal solution. Our results quantified the combined impact of RIN and SDSN on the channel estimation, revealing that RIN is the dominant noise source, particularly at higher levels of transmitted power. Therefore, considering these types of noise in designing communication systems can enhance the performance of the systems.

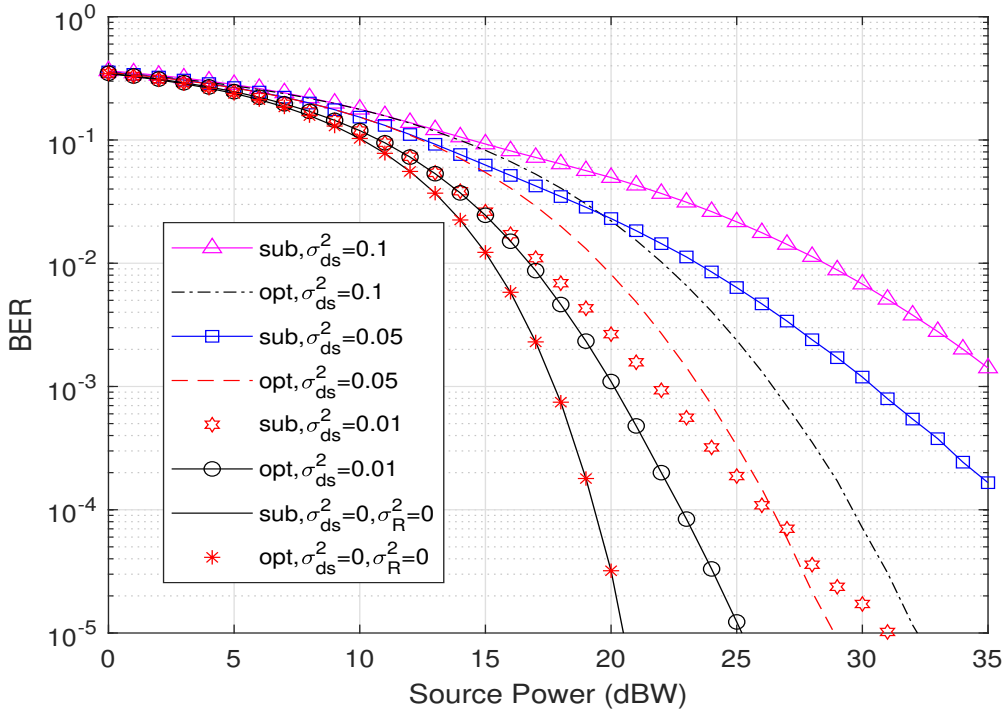

Figure 5.7: BER performance versus the source power at different values of the SDSN noise variance when $\sigma_n^2 = 0.01$, $\sigma_R^2 = 0.01$, $h = 0.4$ and $N = 1$.

5.7 Publications Resulted from This Chapter

- M. Yaseen, M. Elamassie, S. Ikki, M. Uysal, "Signal-Dependent Shot and Relative Intensity Noise in Channel Estimation of Laser Diode-based Indoor VLC Systems" , (2nd round, Revision) *IEEE Transactions on Communications*.

Chapter 6

Conclusions and Future Work

6.1 Conclusions

"In this research, we present a comprehensive study of the input signal-dependent noise in VLC systems. The study comprises three main phases. The first phase examines the effect of SDSN in VLC systems under the scenario of fixed-location users. The second phase investigates the impact of SDSN when considering a model of random user locations. In the third phase, we explore the presence of RIN and SDSN in SISO VLC systems with fixed-location users. The findings of our research, as presented in this thesis, can be summarized as follows:

- Chapter 3 proposed a SISO-VLC downlink transmission scenario wherein an LED, positioned on the ceiling of a typical indoor setting, serves a user fixedly located on the floor. The research focused on channel estimation, considering the impact of SDSN and thermal noise on the received signal at the user end. The derived CRLB served as a benchmark, demonstrating a non-linear relationship with SDSN. The SDSN level's influence on the CRLB depended on other components of the system model.

- Continuing in Chapter 3, the LS and ML estimators were derived to estimate the channel gain of our considered system model with the effect of SDSN, and their performances were compared with the CRLB. Performance comparisons of LS, ML, and CRLB indicated higher MSE for LS than ML, while the CRLB outperformed both. The SDSN level increment magnified the performance gap between the estimators and the CRLB.

- In the context of data transmission, we presented optimal and sub-optimal receiver designs and evaluated their BER performances in Chapter 3. Specifically, we introduced a closed-form expression for the BER of the sub-optimal receiver and provided an approximated version for the optimal one. The findings in this part of the research underscored the substantial influence of SDSN on BER when compared to a scenario with no SDSN.

- In Chapter 4, we expanded upon our research from Chapter 3 by examining the influence of SDSN on the SISO-VLC downlink transmission system model for a random user location scenario, implying that the channel gain is also random. Consequently, we derived the BCRLB, serving as the lower bound for unbiased MSE estimators. The outcomes indicated a rise in the BCRLB with an increase in the SDSN level.

- Furthermore, to estimate the channel gain of our introduced system model in Chapter 4, we derived five different estimators, namely, LS, ML, MAP, LMMSE, and MMSE. The comparison results showed the superiority of the MMSE estimator among other estimators. In addition, it showed that the estimators uses prior information and generally have better performances than the estimators do not depend on channel gain prior information. However, all estimators suffered negatively from SDSN.

- In Chapter 4, we examined a scenario wherein the receiver had no information about the SDSN factor. Two solutions were put forth and thoroughly examined. Compar-

isons between these two solutions and the case where the SDSN factor was known validated the effectiveness of the proposed solutions.

- Finally, in Chapter 4, the receiver of a VLC system operating under SDSN and random channel gain was formulated, and its BER was examined. The results elucidated that the presence of SDSN has an adverse impact on the system's BER, as evidenced by an observed increase in BER with the rising SDSN level.

- In Chapter 5, we explored the combined influence of SDSN and RIN on channel estimation in SISO VLC system for a fixed location user. To establish a benchmark for comparing the MSE of other estimators, we initially presented a derivation of the CRLB in the presence of both SDSN and RIN. Subsequently, LS and ML estimators were formulated and juxtaposed against the CRLB. Our findings provided a quantitative assessment of the cumulative impact of RIN and SDSN on channel estimation, highlighting RIN as the predominant noise source, especially at higher levels of transmitted power.

- Continuing in Chapter 5, both simulation and analytical outcomes pertaining to the MSE of estimators and the CRLB underscored the pronounced impact of the simultaneous existence of SDSN and RIN. Furthermore, the results indicated that the performances of the estimators and the CRLB could be improved by increasing the transmitted power up to a specific threshold, beyond which the curves reached a saturation level. It is noteworthy that augmenting the number of pilots proved effective in diminishing both the MSE and the CRLB in all instances.

- Finally, Chapter 5 introduced the designs of both optimal and sub-optimal receivers, considering the combined influence of RIN and SDSN. The outcomes demonstrated the superior performance of the optimal receiver. Additionally, the simulation results unveiled a significant detrimental effect on the VLC system being studied, arising from the simultaneous presence of SDSN and RIN.

6.2 Future Work

VLC has been applied in various fields, and there are limited studies on the impact of signal-dependent noise on the performance of VLC systems [11, 14, 62]. Consequently, there are several issues related to signal-dependent noise that still need exploration in different VLC systems. In this thesis, we initially focused on the channel estimation of a SISO VLC system with a fixed-location user in the presence of SDSN. Subsequently, we investigated the channel estimation of the same SISO VLC system, considering the randomness of the user's location. Following that, we examined the joint impact of SDSN and RIN on the channel estimation of the fixed-user SISO VLC system.

The following are suggested open research topics:

1. Explore the combined influence of SDSN and RIN on the channel estimation in a SISO-VLC system with a user's location characterized by randomness.

2. Investigate the channel estimation of a VLC system for a user with a random orientation and fixed location, considering the impact of SDSN.

3. Examine the channel estimation of a VLC system for a user with a random orientation and fixed location, taking into account the effects of both SDSN and RIN.

4. Delve into the channel estimation of a SISO VLC system, considering the joint impact of a user's random location and orientation in the presence of SDSN.

5. Study the channel estimation of a SISO VLC system, taking into account the joint impact of a user's random location and orientation in the presence of both SDSN and RIN.

6. Investigate the estimation of channel gains of a MIMO VLC system scenario with correlated channel gains.

7. Explore the application of the Kalman filter technique to enhance channel estimation in VLC systems.

8. Examine channel estimation in VLC systems using machine learning methods, including both supervised and unsupervised approaches.

9. Investigate channel estimation of outdoor VLC systems.

10. Conduct a study on the channel estimation of underwater VLC systems.

APPENDICES

APPENDIX A

Derivation of CRLB of SISO VLC System with SDSN

THIS appendix shows the derivation of the result given in (3.7). The CRLB of the variance of the estimated variable h can be obtained as the Fisher Information inverse of h which is given as

$$\mathrm{J}(h) = -\mathbf{E}\left\{\frac{\partial^2}{\partial h^2}\ln f(\mathbf{y};h)\right\}, \tag{1}$$

where $\mathbf{E}\{\cdot\}$ is the expectation operator and $\ln f(\mathbf{y};h)$ is the log-likelihood function of the unknown channel h. Assuming that all samples are independent, the joint PDF of N observations, which is also equal to the likelihood function of h, can be written as

$$f(\mathbf{y};h) = \left(\prod_{i=1}^{N}\frac{1}{\sqrt{2\pi\sigma_n^2\left(1+\zeta^2 h x_i\right)}}\right) e^{-\frac{1}{2\sigma_n^2}\sum_{i=1}^{N}\frac{(y_i-hx_i)^2}{1+\zeta^2 h x_i}}. \tag{2}$$

Taking the natural logarithm, we have

$$\ln f(\mathbf{y};h) = -\frac{N}{2}\ln\left(2\pi\sigma_n^2\right) - \frac{1}{2}\sum_{i=1}^{N}\ln\left(1+\zeta^2 h x_i\right) - \frac{1}{2\sigma_n^2}\sum_{i=1}^{N}\frac{(y_i-hx_i)^2}{1+\zeta^2 h x_i}.$$

The first partial derivative with respect to h can be obtained as

$$\frac{\partial}{\partial h}\ln f(\mathbf{y};h) = -\frac{1}{2}\sum_{i=1}^{N}\frac{\zeta^2 x_i}{1+\zeta^2 h x_i} + \frac{1}{2\sigma_n^2}\sum_{i=1}^{N}\frac{2x_i(y_i-hx_i)}{1+\zeta^2 h x_i} + \frac{\zeta^2 x_i (y_i-hx_i)^2}{(1+\zeta^2 h x_i)^2}. \tag{3}$$

Then, the second partial derivative can be obtained as

$$\begin{aligned}\frac{\partial^2}{\partial h^2}\ln f(\mathbf{y};h) =& \frac{1}{2}\sum_{i=1}^{N}\frac{(\zeta^2 x_i)^2}{(1+\zeta^2 h x_i)^2} - \frac{1}{2\sigma_n^2}\left[\frac{2(x_i)^2}{1+\zeta^2 h x_i}\right. \\ &\left. + \frac{2\zeta^2(x_i)^2(y_i-hx_i)}{(1+\zeta^2 h x_i)^2} + \frac{2\zeta^2(x_i)^2(y_i-hx_i)}{(1+\zeta^2 h x_i)^2} + \frac{2(\zeta^2 x_i)^2(y_i-hx_i)^2}{(1+\zeta^2 h x_i)^3}\right].\end{aligned} \tag{4}$$

Furthermore, (4) can be simplified to

$$\begin{aligned}\frac{\partial^2}{\partial h^2} f(\mathbf{y};h) =& \frac{1}{2\sigma_n^2}\sum_{i=1}^{N}\frac{\sigma_n^2(\zeta^2 x_i)^2}{(1+\zeta^2 h x_i)^2} - \left[\frac{2(x_i)^2}{1+\zeta^2 h x_i} + \frac{2\zeta^2(x_i)^2(y_i-hx_i)}{(1+\zeta^2 h x_i)^2} + \right. \\ &\left. \frac{2\zeta^2(x_i)^2(y_i-hx_i)}{(1+\zeta^2 h x_i)^2} + \frac{2(\zeta^2 x_i)^2(y_i-hx_i)^2}{(1+\zeta^2 h x_i)^3}\right].\end{aligned} \tag{5}$$

Finally, by taking the expectation (note that $\mathbf{E}\{y_i\} = hx_i$ and $\mathbf{E}\{(y_i - hx_i)^2\} = \sigma_n^2(1 + \zeta^2 h x_i)$), the Fisher Information can be written as

$$\mathrm{J}(h) = \frac{1}{2}\sum_{i=1}^{N}\frac{(\zeta^2 x_i)^2}{(1+\zeta^2 h x_i)^2} + \frac{2x_i^2}{\sigma_n^2(1+\zeta^2 h x_i)}, \tag{6}$$

which concludes the proof of (3.7).

APPENDIX B

Derivation of CRLB of SISO VLC System With the Joint Effect of RIN and SDSN

THIS appendix presents the derivation of (5.8). The CRLB of the variance of the estimated variable h can be obtained as its Fisher information inverse of h given as

$$\mathrm{J}(h) = -\mathbf{E}\left\{\frac{\partial^2}{\partial h^2}\ln f(\mathbf{y};h)\right\}, \tag{7}$$

where $\ln f(\mathbf{y};h)$ is the log-likelihood function of the unknown channel h. Assuming that all samples are independent, the joint PDF of N observations, which is also equal to the likelihood function of h, can be written as

$$f(\mathbf{y};h) = \prod_{i=1}^{N} \frac{1}{\sqrt{2\pi\left(\sigma_n^2 + \sigma_{\mathrm{ds}}^2 h x_i + \sigma_R^2 h^2 x_i^2\right)}} \exp\left(-\frac{1}{2}\sum_{i=1}^{N}\frac{(y_i - h x_i)^2}{\sigma_n^2 + \sigma_{\mathrm{ds}}^2 h x_i + \sigma_R^2 h^2 x_i^2}\right). \tag{8}$$

Taking the natural logarithm, we have

$$\ln f(\mathbf{y};h) = -\frac{N}{2}\ln(2\pi) - \frac{1}{2}\sum_{i=1}^{N}\ln\left(\sigma_n^2+\sigma_{ds}^2 hx_i+\sigma_R^2h^2x_i^2\right) - \frac{1}{2}\sum_{i=1}^{N}\frac{(y_i-hx_i)^2}{\sigma_n^2+\sigma_{ds}^2hx_i+\sigma_R^2h^2x_i^2}. \tag{9}$$

The first partial derivative with respect to h can be obtained as

$$\begin{aligned}\frac{\partial}{\partial h}\ln f(\mathbf{y};h) = -\frac{1}{2}\sum_{i=1}^{N}\Bigg[&\frac{\sigma_{ds}^2x_i+2\sigma_R^2hx_i^2}{\sigma_n^2+\sigma_{ds}^2hx_i+\sigma_R^2h^2x_i^2}\\ &-\frac{2x_i(y_i-hx_i)}{\sigma_n^2+\sigma_{ds}^2hx_i+\sigma_R^2h^2x_i^2} - \frac{(\sigma_{ds}^2x_i+2\sigma_R^2hx_i^2)(y_i-hx_i)^2}{(\sigma_n^2+\sigma_{ds}^2hx_i+\sigma_R^2h^2x_i^2)^2}\Bigg].\end{aligned} \tag{10}$$

Then, the second partial derivative can be obtained as

$$\begin{aligned}\frac{\partial^2}{\partial h^2}\ln f(\mathbf{y};h) = -\frac{1}{2}\sum_{i=1}^{N}\Bigg[&\frac{2\sigma_R^2x_i^2}{\sigma_n^2+\sigma_{ds}^2hx_i+\sigma_R^2h^2x_i^2} - \frac{(\sigma_{ds}^2x_i+2\sigma_R^2hx_i^2)^2}{(\sigma_n^2+\sigma_{ds}^2hx_i+\sigma_R^2h^2x_i^2)^2}\\ &+\frac{2x_i^2}{\sigma_n^2+\sigma_{ds}^2hx_i+\sigma_R^2h^2x_i^2} + \frac{2x_i(\sigma_{ds}^2x_i+2\sigma_R^2hx_i^2)(y_i-hx_i)}{(\sigma_n^2+\sigma_{ds}^2hx_i+\sigma_R^2h^2x_i^2)^2} + \frac{2\sigma_{ds}^2x_i^2(y_i-hx_i)}{(\sigma_n^2+\sigma_{ds}^2hx_i+\sigma_R^2h^2x_i^2)^2}\\ &+\frac{2\sigma_{ds}^2x_i(\sigma_{ds}^2x_i+2\sigma_R^2hx_i^2)^2)(y_i-hx_i)^2}{(\sigma_n^2+\sigma_{ds}^2hx_i+\sigma_R^2h^2x_i^2)^3} - \frac{2x_i^2\sigma_R^2(y_i-hx_i)^2-4hx_i^3\sigma_r^2(y_i-hx_i)}{(\sigma_n^2+\sigma_{ds}^2hx_i+\sigma_R^2h^2x_i^2)^2}\\ &+\frac{4hx_i^2\sigma_R^2(x_i\sigma_{ds}^2+2hx_i^2\sigma_R^2)(y_i-hx_i)^2}{(\sigma_n^2+\sigma_{ds}^2hx_i+\sigma_R^2h^2x_i^2)^3}\Bigg].\end{aligned} \tag{11}$$

(11) can be further simplified to

$$\begin{aligned}\frac{\partial^2}{\partial h^2}f(\mathbf{y};h) = -\frac{1}{2}\sum_{i=1}^{N}\Bigg[&\frac{x_i^2(1+\sigma_R^2)}{\sigma_n^2+\sigma_{ds}^2hx_i+\sigma_R^2h^2x_i^2}\\ &-\frac{(\sigma_{ds}^2x_i+2\sigma_R^2hx_i^2)(\sigma_{ds}^2x_i+2hx_i^2\sigma_R^2-2x_i(y_i-hx_i))}{(\sigma_n^2+\sigma_{ds}^2hx_i+\sigma_R^2h^2x_i^2)^2}\\ &-\frac{(y_i-hx_i)(2x_i^2\sigma_R^2y_i-6hx_i^3\sigma_R^2-\sigma_{ds}^2x_i^2)}{(\sigma_n^2+\sigma_{ds}^2hx_i+\sigma_R^2h^2x_i^2)^2}\\ &+\frac{2(x_i\sigma_{ds}^2+2hx_i\sigma_R^2)^2(y_i-hx_i)^2(\sigma_{ds}^2x_i+2hx_i^2\sigma_R^2)}{(\sigma_n^2+\sigma_{ds}^2hx_i+\sigma_R^2h^2x_i^2)^3}\Bigg].\end{aligned} \tag{12}$$

Finally, by taking the expectation (note that $\mathbf{E}\{y_i\} = hx_i$ and $\mathbf{E}\{(y_i - hx_i)^2\} = \sigma_n^2 + hx_i\sigma_{ds}^2 + h^2x_i^2\sigma_R^2$), Fisher information can be written as

$$\mathrm{J}(h) = \frac{1}{2}\sum_{i=1}^{N}\left[\frac{2x_i^2(1+\sigma_R^2)}{\sigma_n^2 + \sigma_{ds}^2 hx_i + \sigma_R^2 h^2 x_i^2} + \frac{(x_i\sigma_{ds}^2 + 2hx_i^2\sigma_R^2)^2}{(\sigma_n^2 + \sigma_{ds}^2 hx_i + \sigma_R^2 h^2 x_i^2)^2}\right], \tag{13}$$

which yields (5.8).

Bibliography

[1] Q. Photonics. (2022) Relative intensity noise (rin) application note. Accessed on: March 9, 2024. [Online]. Available: https://cdn.quantifiphotonics.com/20220527144951/QP_AppNote_RIN_v1.1.pdf

[2] J. Shi, Y. Liu, Z. Luo, Z. Li, C. Shen, J. Zhang, G. Wang, and N. Chi, "Simplified neural network with physics-informed module in mimo visible light communication systems," *Journal of Lightwave Technology*, vol. 42, no. 1, pp. 57–68, 2024.

[3] E. X. et al., "Gan-based series hybrid led array: A dual-function light source with illumination and high-speed visible light communication capabilities," *Journal of Lightwave Technology*, vol. 42, no. 1, pp. 243–250, 2024.

[4] I. B. K. Y. U. M. H. Rahman, M. Z. Chowdhury and Y. M. Jang, "Channel estimation for indoor massive mimo visible light communication with deep residual convolutional blind denoising network," *IEEE Transactions on Cognitive Communications and Networking*, vol. 9, no. 3, pp. 683–694, 2023.

[5] L. L. S. W. Ho, A. A. Saed and C. W. Sung, "Coding and bounds for channel estimation in visible light communications and positioning," *IEEE Journal on Selected Areas in Communications*, vol. 36, no. 1, pp. 34–44, 2018.

[6] L. Yin, W. O. Popoola, X. Wu, and H. Haas, "Performance evaluation of non-orthogonal multiple access in visible light communication," *IEEE Trans. Commun.*, vol. 64, no. 12, pp. 5162–5175, Dec. 2016.

[7] S. Mohapatra, G. Satapathy, S. P. Dash, and P. R. Sahu, "Performance analysis of visible light communication system with imperfect CSI," *IEEE Commun. Lett.*, vol. 24, no. 12, pp. 2844–2848, Dec. 2020.

[8] Q. Gao, K. Qaraqe, and E. Serpedin, "Rotated color shift keying for visible light communications with signal-dependent noise," *IEEE Commun. Lett.*, vol. 24, no. 4, pp. 844–848, Apr. 2020.

[9] Q. Gao, K. Qaraqe, and E. Serpedin, "Improving the modulation designs for visible light communications with signal-dependent noise," *IEEE Commun. Mag.*, vol. 58, no. 5, pp. 26–32, 2020.

[10] M. Safari, "Efficient optical wireless communication in the presence of signal-dependent noise," in *2015 IEEE Int. Conf. Communn Workshop (ICCW)*, 2015, pp. 1387–1391.

[11] H. Chen and Z. Xu, "A two-dimensional constellation design method for visible light communications with signal-dependent shot noise," *IEEE Commun. Lett.*, vol. 22, no. 9, pp. 1786–1789, Sept. 2018.

[12] Q. Gao, S. Hu, C. Gong, and Z. Xu, "Modulation designs for visible light communications with signal-dependent noise," *J. Lightw. Technol.*, vol. 34, no. 23, pp. 5516–5525, Dec. 2016.

[13] J. Wang, Z. Yang, Y. Wang, and M. Chen, "On the performance of spatial modulation-based optical wireless communications," *IEEE Photon. Technol. Lett.*, vol. 28, no. 19, pp. 2094–2097, 2016.

[14] Q. Gao, C. Gong, and Z. Xu, "Joint transceiver and offset design for visible light communications with input-dependent shot noise," *IEEE Trans. Wireless Commun.*, vol. 16, no. 5, pp. 2736–2747, May 2017.

[15] S. H. Lin, C. Liu, X. Bao, and J. Y. Wang, "Indoor visible light communications: performance evaluation and optimization," *J. Wireless Commun. Netw.*, vol. 228, pp. 1–12, 2018.

[16] K. Petermann, *Laser Diode Modulation and Noise*, 1st ed. USA: Springer, 1988.

[17] J. Duan, X. G. Wang, Y. G. Zhou, C. Wang, and F. Grillot, "Carrier-noise-enhanced relative intensity noise of quantum dot lasers," *IEEE J. Quantum Electron.*, vol. 54, no. 6, pp. 1–7, 2018.

[18] J. C. Cartledge and M. O'Sullivan, "Time- and frequency-domain characterization of the relative intensity noise of a quantum-dot frequency comb source laser," *IEEE Journal of Selected Topics in Quantum Electronics*, vol. 25, no. 6, pp. 1–9, 2019.

[19] B. W. J. C. Shrestha, S. Blom and H. H. Hillmer, "Investigation of relative intensity noise in asymmetric external cavity semiconductor laser sensors: Influence of dual-line spectral separation and linewidth enhancement factor," *IEEE Sens. J.*, vol. 15, no. 11, pp. 6619–6624, 2015.

[20] W. Y. et al., "Performance of kramers–kronig receivers in the presence of local oscillator relative intensity noise," *EEE J. Lightw. Technol.*, vol. 37, no. 13, pp. 3035–3043, 2019.

[21] J. C. L. et al., "Relative intensity noise and linewidth for hybrid-cavity semiconductor lasers," *EEE J. Lightw. Technol.*, vol. 40, no. 7, pp. 2087–2096, 2022.

[22] Z. Wang, Q. Wang, W. Huang, and Z. Xu, *Visible Light Communications: Modulation and Signal Processing*, 1st ed. Hoboken, NJ, USA: Wiley-IEEE Press, Nov. 2017.

[23] P. H. P. H. Pathak, X. Feng and P. Mohapatra, "Visible light communication, networking, and sensing: A survey, potential and challenges," *IEEE Communications Surveys Tutorials*, vol. 17, no. 4, pp. 2047–2077, 2015.

[24] H. V. D. . T. Tan, X. W. Sun and S. P. DenBaars, "Advances in the led materials and architectures for energy-saving solid-state lighting toward "lighting revolution"," *IEEE Photonics Journal*, vol. 4, no. 2, pp. 613–619, 2012.

[25] S. Vappangi, V. V. Mani, and M. Sellathurai, *Visible Light Communication: Comprehensive Theory and Applications with MATLAB*, 1st ed. CRC Press, Aug. 2021.

[26] Z. Ghassemlooy, L. Alves, S. Zvanovec, and M. Khalighi, *Visible Light Communications Theory and Applications*, 1st ed. CRC Press, Dec. 2019.

[27] Z. Ghassemlooy, W. Popoola, and S. Rajbhandari, *Optical wireless communications: system and channel modeling with MATLAB*, 1st ed. CRC Press, May 2017.

[28] J. Crawford, *Advanced phase-lock techniques.* New York, NY, U.S.A.: Artech House, 2007.

[29] F. Bonani and G. Ghione, *Noise in Semiconductor Devices, Modeling and Simulation.* New York, NY, U.S.A.: Springer, 2001.

[30] S. Hasinoff, *Photon, Poisson Noise.* In: Ikeuchi, K. (eds) Computer Vision.: Springer. Boston, MA, 2014.

[31] C. D. Motchenbacher and J. A. Connelly, *Low-Noise Electronic System Design*, 1st ed. New York, NY, U.S.A.: Wiley-Interscience, Aug. 1993.

[32] S. Vappangi, V. Mani, and M. Sellathurai, *Visible Light Communication: A Comprehensive Theory and Applications with MATLAB*, 1st ed. CRC Press, Aug. 2021.

[33] L. A. Coldren, S. W. Corzine, and M. L. Mašanović, *Diode Lasers and Photonic Integrated Circuits*, 1st ed. New York, USA: John Wiley Sons, Feb. 2012.

[34] M. Sibley, *Optical Communications: Components and Systems*, 3rd ed. Switzerland: Springer, 2020.

[35] K. Lau and A. Yariv, "Ultra-high speed semiconductor lasers," *IEEE Journal of Quantum Electronics*, vol. 21, no. 2, pp. 121–138, 1985.

[36] T. Wang, A. Hussain, Y. Cao, and S. Gulomjon, "An improved channel estimation technique for IEEE 802.11p standard in vehicular communications," *Sensors*, vol. 19, no. 1, p. 98, Jan. 2019.

[37] H. V. Trees, K. Bell, and Z. Tian, *Detection Estimation and Modulation Theory, Detection, Estimation, and Filtering Theory*, 2nd ed. Wiley-IEEE Press, Apr. 2013.

[38] P. H. Pathak, X. Feng, P. Hu, and P. Mohapatra, "Visible light communication, networking, and sensing: A survey, potential and challenges," *IEEE Commun. Surveys Tuts*, vol. 17, no. 4, pp. 2047–2077, 2015.

[39] S. Ma, H. Li, Y. He, R. Yang, S. Lu, W. Cao, and S. Li, "Capacity bounds and interference management for interference channel in visible light communication networks," *IEEE Trans. Wireless Commun.*, vol. 18, no. 1, pp. 182–193, 2019.

[40] J. Wang, J. Wang, B. Zhu, M. Lin, Y. Wu, Y. Wang, and M. Chen, "Improvement of BER performance by tilting receiver plane for indoor visible light communications with input-dependent noise," in *2017 IEEE Int. Conf. Commun. (ICC)*, 2017, pp. 1–6.

[41] A. Jovicic, J. Li, and T. Richardson, "Visible light communication: opportunities, challenges and the path to market," *IEEE Commun. Mag.*, vol. 51, no. 12, pp. 26–32, 2013.

[42] R. Wang, Q. Gao, J. You, E. Liu, P. Wang, Z. Xu, and Y. Hua, "Linear transceiver designs for MIMO indoor visible light communications under lighting constraints," *IEEE Trans. Commun.*, vol. 65, no. 6, pp. 2494–2508, 2017.

[43] Z. Wang, Q. Wang, and Z. Xu, *Visible Light Communications: Modulation and Signal Processing*. Hoboken, NJ, USA: Wiley, Nov 2017.

[44] J. Armstrong, "OFDM for optical communications," *Journal of Lightwave Technology*, vol. 27, no. 3, pp. 189–204, 2009.

[45] H. Elgala, R. Mesleh, and H. Haas, "Indoor broadcasting via white LEDs and OFDM," *IEEE Trans. Consum. Electron.*, vol. 55, no. 3, pp. 1127–1134, 2009.

[46] X. Li, J. Vucic, V. Jungnickel, and J. Armstrong, "On the capacity of intensity-modulated direct-detection systems and the information rate of ACO-OFDM for indoor optical wireless applications," *IEEE Trans. Commun.*, vol. 60, no. 3, pp. 799–809, 2012.

[47] W. O. Popoola, E. Poves, and H. Haas, "Error performance of generalised space shift keying for indoor visible light communications," *IEEE Trans. Commun.*, vol. 61, no. 5, pp. 1968–1976, 2013.

[48] J. Wang, H. Ge, J. Zhu, J. Wang, J. Dai, and M. Lin, "Adaptive spatial modulation for visible light communications with an arbitrary number of transmitters," *IEEE Access*, vol. 6, pp. 37 108–37 123, 2018.

[49] Q. Gao, J. H. Manton, G. Chen, and Y. Hua, "Constellation design for a multicarrier optical wireless communication channel," *IEEE Trans. Commun.*, vol. 62, no. 1, pp. 214–225, 2014.

[50] M. Beko and R. Dinis, "Systematic method for designing constellations for intensity-modulated optical systems," *J. Opt. Commun. Netw.*, vol. 6, no. 5, pp. 449–458, 2014.

[51] C. Gong, S. Li, Q. Gao, and Z. Xu, "Power and rate optimization for visible light communication system with lighting constraints," *IEEE Trans. Signal Process.*, vol. 63, no. 16, pp. 4245–4256, Aug. 2015.

[52] H. S. Khallaf, A. S. Ghazy, H. M. H. Shalaby, and S. S. A. Obayya, "Performance analysis of visible light communication systems over fading channels," in *19th Int. Conf. Transparent Opt. Netw.(ICTON)*, July 2017, pp. 1–4.

[53] Y. S. Hussein, M. Y. Alias, and A. A. Abdulkafi, "On performance analysis of LS and MMSE for channel estimation in VLC systems," in *2016 IEEE 12th Int. Colloq. Signal Process. & Its Appl. (CSPA)*, 2016, pp. 204–209.

[54] X. Chen and M. Jiang, "Enhanced bayesian MMSE channel estimation for visible light communication," in *2016 IEEE 27th Annual Int. Symp. Pers. Indoor, and Mobile Radio Commun. (PIMRC)*, 2016, pp. 1–6.

[55] H. Dogan, O. Şaylı, and E. Panayirci, "Pilot assisted channel estimation for asymmetrically clipped optical OFDM over visible light channels," in *2016 IEEE Int. Black Sea Conf. Commun. and Netw. (BlackSeaCom)*, 2016, pp. 1–4.

[56] X. Chen and M. Jiang, "Adaptive statistical bayesian MMSE channel estimation for visible light communication," *IEEE Transactions on Signal Processing*, vol. 65, no. 5, pp. 1287–1299, 2017.

[57] A. Yesilkaya, O. Karatalay, A. S. Ogrenci, and E. Panayirci, "Channel estimation for visible light communications using neural networks," in *2016 Int. Joint Conf. Neural Netw (IJCNN)*, 2016, pp. 320–325.

[58] V. B. Manur and L. Ali, "MMSE based compressed sensing algorithms for channel estimation in VLC," in *2019 4th Int. Conf. Elect., Electron., Commun, Comput. Technol. and Optim. Techn. (ICEECCOT)*, 2019, pp. 170–173.

[59] J. C. Estrada-Jiménez, B. G. Guzmán, M. J. Fernández-Getino García, and V. P. G. Jiménez, "Superimposed training-based channel estimation for MISO optical-OFDM VLC," *IEEE Trans. Veh. Technol.*, vol. 68, no. 6, pp. 6161–6166, 2019.

[60] S. Ho, A. A. Saed, L. Lai, and C. W. Sung, "Coding and bounds for channel estimation in visible light communications and positioning," *IEEE J. Sel. Areas in Commun.*, vol. 36, no. 1, pp. 34–44, 2018.

[61] D. R. Ashok and A. Chockalingam, "Compact optimal pilot design for channel estimation in MIMO VLC systems," in *2019 IEEE Wireless Commun. and Netw. Conf. (WCNC)*, 2019, pp. 1–7.

[62] S. M. Moser, "Capacity results of an optical intensity channel with input-dependent gaussian noise," *IEEE Trans Inf. Theory*, vol. 58, no. 1, pp. 207–223, Jan 2012.

[63] S. Hranilovic and F. Kschischang, "A pixelated mimo wireless optical communication system," *IEEE J. Sel. Topics in Quantum Electronics*, vol. 12, no. 4, pp. 859–874, 2006.

[64] M. G. Ulkar, T. Baykas, and A. E. Pusane, "Vlcnet: Deep learning based end-to-end visible light communication system," *J. Lightw. Technol.*, vol. 38, no. 21, pp. 5937–5948, 2020.

[65] L. Z. et al., "High data rate multiple input multiple output (MIMO) optical wireless communications using white led lighting," *IEEE J. Sel. Areas Commun.*, vol. 27, no. 9, pp. 1654–1662, Dec. 2009.

[66] A. Singla, D. Sharma, and S. Vashisth, "Data connectivity in flights using visible light communication," in *2017 Int. Conf. Comput. and Commun. Technologies for Smart Nation (IC3TSN)*, 2017, pp. 71–74.

[67] K. Yan, Z. Li, M. Cheng, and H. C. Wu, "Qos analysis and signal characteristics for short-range visible-light communications," *IEEE Trans. Veh. Technol.*, vol. 70, no. 7, pp. 6726–6734, July 2021.

[68] J. Kahn and J. Barry, "Wireless infrared communications," *Proc. IEEE*, vol. 85, no. 2, p. 265–298, Feb 1997.

[69] L. Zhang, J. Kulon, and Y. Yan, "Accuracy of the frequency and phase measurement concerning different noise sources for phase doppler anemometry," in *2015 IEEE 3rd Int. Conf. on Smart Instrumentation, Measurement and Appl. (ICSIMA)*, 2015, pp. 1–6.

[70] S. Hasinoff, *"Photon Poisson noise" in Computer Vision: A Reference Guide*, 1st ed. Boston, MA, USA: Springer, 01 2014, pp. 608–610.

[71] L. Hua, Y. Zhuang, L. Qi, J. Yang, and L. Shi, "Noise analysis and modeling in visible light communication using allan variance," *IEEE Access*, vol. 6, pp. 74 320–74 327, 2018.

[72] T. Komine and M. Nakagawa, "Fundamental analysis for visible-light communication system using led lights," *IEEE Transactions on Consumer Electronics*, vol. 50, no. 1, pp. 100–107, 2004.

[73] Z. Ahmed, L. Zhang, G. Faulkner, D. O'Brien, and S. Collins, "A shot-noise limited 420 Mbps visible light communication system using commerical off-the-shelf silicon photomultiplier (sipm)," in *2019 IEEE Int. Conf. on Commun. Workshops (ICC Workshops)*, 2019, pp. 1–5.

[74] Z. Gao, Y. Wang, X. Liu, F. Zhou, and K.-K. Wong, "Ffdnet-based channel estimation for massive mimo visible light communication systems," *IEEE Wireless Communications Letters*, vol. 9, no. 3, pp. 340–343, 2020.

[75] Y. S. Hussein, M. Y. Alias, and A. A. Abdulkafi, "On performance analysis of ls and mmse for channel estimation in vlc systems," in *IEEE Int. Colloq. Signal Process. Appl. (CSPA)*, 2016, p. 204–209.

[76] X. Chen and M. Jiang, "Adaptive statistical bayesian mmse channel estimation for visible light communication," *IEEE Trans. Signal Process.*, vol. 65, no. 5, p. 1287–1299, Mar. 2017.

[77] R. K. Pal, S. P. Dash, S. Joshi, and D. Ghose, "Channel estimation and performance analysis of a wide-fov visible light communication system with random receiver orientation and location," *IEEE Trans. on Wireless Commun., early access*, pp. 1–1, 2022.

[78] J. Estrada-Jiménez, B. Guzmán, M. García, and V. Jiménez, "Superimposed training-based channel estimation for miso optical-ofdm vlc," *IEEE Trans. on Veh. Technol.*, vol. 68, no. 6, pp. 6161–6166, 2019.

[79] S. C. G. Gurbilek, M. Koca, "Blind channel estimation for dco-ofdm based vehicular visible light communication," *Physical Communication*, vol. 56, no. 6, pp. 6161–6166, 2022.

[80] Z. Gao, Y. Wang, X. Liu, F. Zhou, and K.-K. Wong, "FFDNet-based channel estimation for massive MIMO visible light communication systems," *IEEE Wireless Commun. Lett.*, vol. 9, no. 3, pp. 340–343, 2020.

[81] M. Hosney, H. A. I. Selmy, A. Srivastava, and K. M. F. Elsayed, "Interference mitigation using angular diversity receiver with efficient channel estimation in MIMO VLC," *IEEE Access*, vol. 8, pp. 54 060–54 073, Mar. 2020.

[82] M. Yaseen, M. Alsmadi, A. E. Canbilen, and S. Ikki, "Visible light communication with input-dependent noise: Channel estimation, optimal receiver design and performance analysis," *Journal of Lightwave Technology*, vol. 39, no. 23, pp. 7406–7416, Dec. 2021.

[83] M. Yuan, X. Sha, X. Liang, M. Jiang, J. Wang, and C. Zhao, "Coding performance for signal dependent channels in visible light communication system," in *Proc. IEEE Global Conf. Signal Inf. Process. (GlobalSIP)*, 2015, pp. 1037–1041.

[84] Y. C. et al., "Optimal resource management for noma-based visible light communication systems with shot noise," *IEEE Trans on Green Commun. and Netw.*, vol. 6, no. 4, pp. 2015–2031, 2022.

[85] M. Jani, P. Garg, and A. Gupta, "Performance analysis of a mixed cooperative PLC–VLC system for indoor communication systems," *IEEE Systems J.*, vol. 14, no. 1, pp. 469–476, May 2019.

[86] H. V. Trees and K. Bell, *Bayesian Bounds for Parameter Estimation and Nonlinear Filtering/Tracking*, 1st ed. Wiley-IEEE Press, Aug. 2007.

[87] S. Kay, *Fundamentals of Statistical Processing, Volume I: Estimation Theory*, 1st ed. Pearson, Mar. 1993.

[88] K. G. Rallis, V. K. Papanikolaou, P. D. Diamantoulakis, S. A. Tegos, A. A. Dowhuszko, M.-A. Khalighi, and G. K. Karagiannidis, "Energy efficient cooperative communications in aggregated VLC/RF networks with NOMA," *IEEE Trans. Commun.*, vol. 71, no. 9, pp. 5408–5419, 2023.

[89] L. Yin and H. Haas, "Physical-layer security in multiuser visible light communication networks," *IEEE J. Sel. Areas Commun.*, vol. 36, no. 1, pp. 162–174, 2018.

[90] Y. Wang, Y. Wang, N. Chi, J. Yu, and H. Shang, "Demonstration of 575-Mb/s downlink and 225-Mb/s uplink bi-directional SCM-WDM visible light communication using RGB LED and phosphor-based LED," *Opt. Express*, vol. 21, no. 1, pp. 1203–1208, Jan. 2013.

[91] M. Shuai, Y. Ruixin, D. Chun, L. Hang, W. Youlong, A.-D. Naofal, and L. Shiyin, "Robust power allocation for integrated visible light positioning and communication networks," *IEEE Trans. Commun.*, vol. 71, no. 8, pp. 4764–4777, 2023.

[92] H. H. T. Z. Gutema and W. O. Popoola, "WDM based 10.8 Gbps visible light communication with probabilistic shaping," *J. Lightw. Technol.*, vol. 40, no. 15, pp. 5062–5069, 2022.

[93] R. Bian, I. Tavakkolnia, and H. Haas, "15.73 Gb/s visible light communication with off-the-shelf LEDs," *J. Lightw. Technol.*, vol. 37, no. 10, p. 2418–2424, 2019.

[94] H. H. D. Milovančev, N. Vokić and B. Schrenk, "Gb/s visible light communication with low-cost receiver based on single-color LED," *J. Lightw. Technol.*, vol. 38, no. 12, pp. 3305–3314, 2020.

[95] W. Yuanquan and C. Nan, "A high-speed bi-directional visible light communication system based on RGB-LED," *China Commun.*, vol. 11, no. 3, pp. 40–44, 2014.

[96] Z. Z. et al., "Embedded electrode Micro-LEDs with high modulation bandwidth for visible light communication," *IEEE Trans. Electron Devices*, vol. 70, no. 2, pp. 588–593, 2023.

[97] S. R. et al, "High-speed integrated visible light communication system: Device constraints and design considerations," *IEEE J. Sel. Areas Commun.*, vol. 33, no. 9, pp. 1750–1757, 2015.

[98] S. L. et al., "Gan-based cascade micro light-emitting diode in parallel and series arrays for visible light communication," *IEEE Photon. J.*, vol. 15, no. 3, pp. 1–4, 2023.

[99] E. X. et al., "High-speed visible light communication based on a III-nitride series-biased Micro-LED array," *J. Lightw. Technol.*, vol. 37, no. 4, pp. 1180–1186, 2019.

[100] Q. H. Pham, J. C. Chen, and H. B. Nguyen, "Three-dimensional numerical study on the efficiency droop in ingan/gan light-emitting diodes," *IEEE Photon. J.*, vol. 11, no. 1, pp. 1–17, 2019.

[101] F. Zafar, M. Bakaul, and R. Parthiban, "Laser-diode-based visible light communication: Toward gigabit class communication," *IEEE Commun. Mag.*, vol. 55, no. 2, pp. 144–151, 2017.

[102] S. Nagabhushana and N. Sathyanarayana, *Lasers and Optical Instrumentation.* I.K. International Publishing House Pvt. Limited, 2010.

[103] L. Issaoui, S. Cho, and H. Chun, "High CRI RGB laser lighting with 11-Gb/s WDM link using off-the-shelf phosphor plate," *IEEE Photon. Technol. Lett.*, vol. 34, no. 2, pp. 97–100, 2022.

[104] T. Wu, Y. Chi, and H. W. et al., "Tricolor R/G/B laser diode based eye-safe white lighting communication beyond 8 Gbit/s," *IEEE Photon. Technol. Lett.*, vol. 7, no. 1, p. 1–10, Dec. 2017.

[105] F. Ahmad, R. N. Sathisha, K. M. Jyothsna, and V. Raghunathan, "Hybrid laser-led transmitter with closed-loop beam-steering control for indoor optical wireless communication," *J. Lightw. Technol.*, vol. 40, no. 12, pp. 3557–3566, 2022.

[106] K. Bera, R. Parthiban, and N. Karmakar, "Coverage improvement of laser diode-based visible light communication systems using an engineered diffuser," *IEEE Access*, vol. 11, pp. 122 833–122 841, 2023.

[107] C. M. Chuang, Y. H. Cheng, and Y. R. Wu, "Electro-optical numerical modeling for the design of UVA nitride-based vertical-cavity surface-emitting laser diodes," *IEEE J. Sel. Top. Quantum Electron.*, vol. 28, no. 1: Semiconductor Lasers, pp. 1–6, 2022.

[108] D. Owen-Newns, J. Robertson, M. Hejda, and A. Hurtado, "GHz rate neuromorphic photonic spiking neural network with a single vertical-cavity surface-emitting laser (VCSEL)," *IEEE J. Sel. Top. Quantum Electron.*, vol. 29, no. 2: Optical Computing, pp. 1–10, 2023.

[109] M. D. S. et al., "Safety analysis for laser-based optical wireless communications: A tutorial," *Proc. IEEE.*, vol. 110, no. 8, pp. 1045–1072, 2022.

[110] Z. Zeng, M. D. Soltani, M. Safari, and H. Haas, "A vcsel array transmission system with novel beam activation mechanisms," *IEEE Trans. Commun.*, vol. 70, no. 3, pp. 1886–1900, 2022.

[111] E. K. B. Turan and S. Coleri, "Vehicular visible light communications noise analysis and autoencoder based denoising," in *2022 Joint European Conference on Networks and Communications 6G Summit (EuCNC/6G Summit)*, 2022, pp. 19–24.

[112] G. Yabre, H. D. Waardt, H. P. A. van den Boom, and G. . D. Khoe, "Noise characteristics of single-mode semiconductor lasers under external light injection," *IEEE J. Sel. Top. Quantum Electron.*, vol. 36, no. 3, pp. 385–393, 2000.

[113] P. Werle and F. Slemr, "Signal-to-noise ratio analysis in laser absorption spectrometers using optical multipass cells," *Appl. Opt.*, vol. 30, no. 4, pp. 430–434, Feb 1991.

[114] T. A. Morris, A. N. Zawada, D. Garcia, J. M. Wheeler, and M. J. F. Digonnet, "Optimization of the angular random walk in laser-driven fiber-optic gyroscopes," *IEEE Sens. J.*, vol. 22, no. 3, pp. 2205–2212, 2022.

[115] J. Wang, J. Wang, and Y. Wang, "Fundamental analysis for visible light communication with input-dependent noise," in *Optical Fiber and Wireless Communications*, R. Roka, Ed. Rijeka: IntechOpen, 2017, ch. 8.

[116] B. Saleh and M. T. Malvin, *Fundamentals of Photonics, 3rd Edition.* Wiley, Feb. 2019.

[117] G. Katz and E. Sonkin, "Level optimization of pam-4 transmission with signal-dependent noise," *IEEE Photon. J.*, vol. 11, no. 1, pp. 1–6, 2019.

[118] N. Dogru, E. Cengiz, and H. S. D. Tunc, "RIN reduction in gain-switched InAs-InP (113) B quantum dot laser based on multi-population rate equations," *IEEE Trans. Electron Devices.*, vol. 70, no. 7, pp. 3695–3703, 2023.

[119] G. Keiser, *Optical Fiber Communications*, 4th ed. McGraw-Hill Education, Sep. 2010.

[120] "Chapter 14 - lightwave analog video transmission," in *Optical Fiber Telecommunications IIIA (Third Edition)*, third edition ed., I. P. Kaminow and T. L. Koch, Eds. Boston: Academic Press, 1997, pp. 523–559.

[121] K. Lau and A. Yariv, "Ultra-high speed semiconductor lasers," *IEEE J. Sel. Top. Quantum Electron.*, vol. 21, no. 2, pp. 121–138, 1985.

[122] S. Vappangi, V. V. Mani, and M. Sellathurai, *Visible Light Communication: Comprehensive Theory and Applications with MATLAB*, 1st ed. CRC Press, Aug. 2021.

[123] P. P. H. H. X. Zhang, Z. Babar and L. Hanzo, "The evolution of optical ofdm," *IEEE Commun. Surv. Tutor.*, vol. 23, no. 3, pp. 1430–1457, 2021.

[124] J. Armstrong and B. J. C. Schmidt, "Comparison of asymmetrically clipped optical ofdm and dc-biased optical ofdm in awgn," *IEEE Trans. Consum. Electron.*, vol. 12, no. 5, pp. 343–345, May 2008.

[125] X. Deng, S. Mardanikorani, G. Zhou, and J. P. M. G. Linnartz, "DC-Bias for optical OFDM in visible light communications," *IEEE Access*, vol. 7, pp. 98 319–98 330, 2019.

[126] K. Aygün and A. Özen, "Ber performance analysis of M-CSK modulated flip-OFDM system in multipath optical channel environment," in *2022 30th Signal Processing and Communications Applications Conference (SIU)*, 2022, pp. 1–4.

[127] J. Lian, Y. Gao, and D. Lian, "Variable pulse width unipolar orthogonal frequency division multiplexing for visible light communication systems," *IEEE Access*, vol. 7, pp. 31 022–31 030, 2019.

[128] D. Tsonev, S. Videv, and H. Haas, "Unlocking spectral efficiency in intensity modulation and direct detection systems," *IEEE J. Sel. Areas Commun.*, vol. 33, no. 9, pp. 1758–1770, 2015.

[129] S. M. et al., "Spectral and energy efficiency of aco-ofdm in visible light communication systems," *IEEE Trans. Wireless Commun.*, vol. 21, no. 4, pp. 2147–2161, 2022.

[130] S. H. R. Bai and Z. Wang, "Low-complexity layered aco-ofdm for power-efficient visible light communications," *IEEE Trans. Green Commun. Netw.*, vol. 6, no. 3, pp. 1780–1792, 2022.

[131] Z. Yang, M. Jiang, L. Zhang, and H. Z. Tan, "Enhanced multiple pulse position modulation aided reverse polarity optical ofdm system with extended dimming control," *IEEE Photon. J.*, vol. 10, no. 3, pp. 1–17, 2018.

[132] C. Z. S. Q. T. Zhang, L. Sun and Z. Ghassemlooy, "Low-complexity receiver for haco-ofdm in optical wireless communications," *IEEE Wireless Communications Letters*, vol. 10, no. 3, pp. 572–575, 2021.

[133] Z. G. X. T. B. L. T. Zhang, H. Ji and S. Qiao, "Spectrum-efficient triple-layer hybrid optical ofdm for im/dd-based optical wireless communications," *IEEE Access*, vol. 8, pp. 10 352–10 362, 2020.

[134] S.-H. L. X. Shi and J. Min, "Adaptive least squares channel estimation for visible light communications based on tap detection," *Optics Communications*, vol. 467, no. 125712, 2020.

[135] Z. Z. J. D. L. Wu, J. Cheng and H. Liu, "Channel estimation for optical-ofdm-based multiuser miso visible light communication," *IEEE Photon. Technol. Lett.*, vol. 29, no. 20, pp. 1727–1730, 2017.

[136] M. Yaseen, A. E. Canbilen, and S. Ikki, "Estimation of random channel gain for siso visible light communications system," *IEEE Can. J. Electr. Comput. Eng*, vol. 46, no. 4, pp. 262–269, 2023.

[137] O. Yazar, M. F. Keskin, and S. Gezici, "Power efficient positioning for visible light systems via chance constrained optimization," *IEEE Trans. Aerospace Electronic Sys.*, vol. -, no. -, pp. –, Mar. 2020.

[138] A. E. C. M. Yaseen and S. Ikki, "Channel estimation in visible light communication systems: The effect of input signal-dependent noise," *IEEE Trans. Veh. Technol.*, pp. 1–11, 2023.

[139] M. A. A. Cheema and S. Ikki, "Distance estimation in visible light communications: The case of imperfect synchronization and signal-dependent noise," *IEEE Trans. Veh. Technol.*, vol. 70, no. 10, pp. 11 044–11 049, 2021.

[140] F. Miramirkhani and M. Uysal, "Channel modeling and characterization for visible light communications," *IEEE Photonics J.*, vol. 7, no. 6, pp. 1–16, 2015.

[141] J. Duan, X. G. Wang, Y. G. Zhou, C. Wang, and F. Grillot, "Carrier-noise-enhanced relative intensity noise of quantum dot lasers," *J. Quantum Electron.*, vol. 54, no. 6, pp. 1–7, 2018.

[142] W. Y. et al., "Performance of Kramers–Kronig receivers in the presence of local oscillator relative intensity noise," *J. Lightwave Technol.*, vol. 37, no. 13, pp. 3035–3043, 2019.

[143] J. Poette, P. Besnard, L. Bramerie, and J. Simon, "Highly-sensitive measurement technique of relative intensity noise and laser characterization," in *Noise and Fluctuations in Photonics, Quantum Optics, and Communications*, L. Cohen, Ed., vol. 6603, International Society for Optics and Photonics. SPIE, 2007, p. 66031R.

[144] S. Kay, *Fundamentals of Statistical Signal Processing: Estimation Theory, Volume I*, 1st ed. Prentice Hall, Mar. 1993.

[145] S. M. Kay, *Fundamentals of Statistical Signal Processing: Estimation Theory*. Prentice Hall, 1997.

[146] S.Kay, *Fundamentals of Statistical Signal Processing: Detection Theory, Volume 2*, 1st ed. Prentice Hall, Jan. 1998.